ELECTRODE EROSION OF AN ELECTRICAL DISCHARGE MACHINING DRILL FOR AEROSPACE FASTENER REMOVAL

By

CONNOR A. MCCAIN

Bachelor of Science in Engineering

Oral Roberts University

Tulsa, Oklahoma

2018

Submitted to the Faculty of the

Graduate College of the
Oklahoma State University
in partial fulfillment of
the requirements for
the Degree of
MASTER OF SCIENCE
May, 2020

ELECTRODE EROSION OF AN ELECTRICAL DISCHARGE MACHINING DRILL USED FOR AEROSPACE FASTENER REMOVAL

Thesis Approved:

Dr. Kurt Rouser

Thesis Adviser

Dr. Sandip Harimkar

Dr. James Kidd

ACKNOWLEDGEMENTS

The author would like to thank Dr. Kurt Rouser, Dr. Sandip Harimkar, and Dr. James Kidd for assistance in the direction of this study. The author would also like to thank research assistants Ryan Platt, Joshua Melvin, Austin Stottlemyre, Lucas Utley, Garner Copher, and Kylar Moody for assistance with testing and data analysis.

Name: CONNOR A. MCCAIN

Date of Degree: MAY, 2020

Title of Study: ELECTRODE EROSION OF AN ELECTRICAL DISCHARGE MACHINING DRILL FOR AEROSPACE FASTENER REMOVAL

Major Field: MECHANICAL AND AEROSPACE ENGINEERING

Abstract: This paper presents an examination of an electrical discharge machining hand drill system for aerospace fastener removal purposes to define secondary level influence of cut depth, electrode diameter, and fastener material type on electrode erosion. In aircraft engine maintenance, repair, and overhaul, even slight process improvements can have a large economic impact. Conventional methods for fastener removal often require use of a mechanical drill, which presents issues with the normal force required, accumulations of small-piece debris, long process times, and damage to parent material. Although the technology of electrical discharge machining has been utilized for decades, it is now being used as a novel solution for removing aerospace fasteners to minimize normal force required, decrease process time, and contain debris. Algorithms have been developed for these systems using mathematical models and experimental testing to estimate the electrode erosion rate during the machining process, but some secondary level variable process influencers are not currently defined. A statistics-based study was performed here to examine electrode erosion rates at varying cut depths from 0.05 to 0.15 inches, relevant electrode diameters from 0.1250 to 0.3300 inches, and workpiece material type (Titanium and Inconel). The experimental data was evaluated using seven parameters: cut time, axial electrode wear, radial electrode wear, electrode wear ratio (a volume change comparison between the fastener material and the electrode), material removal rate (a measure of the mass removed over time), cross-section area difference, and cut depth difference. The most important parameters were found to be axial electrode wear and electrode wear ratio. Results from the study show the rate of axial electrode wear and electrode wear ratio both increase due to cut depth and changing fastener materials from Titanium to Inconel. Axial electrode wear was shown to increase as the electrode diameter was decreased, while electrode wear ratio was shown to increase and then decrease as electrode diameter was increased. Using the data from the study, a rudimentary empirical electrode life prediction was developed, but significant error causes a low confidence level. It is shown that a linear approximation for electrode wear is sufficient for cuts into Inconel fasteners. Analysis of the linear, exponential, weighted polynomial, and geometric volume models of the Titanium cuts show the present data is not sufficient for predicting electrode wear on cuts into Titanium fasteners.

TABLE OF CONTENTS

LIST OF TABLES

LIST OF FIGURES

Figure Page

Figure Page

Figure Page

Figure Page

Figure Page

NOMENCLATURE

A_c	Cut cross-section area
A_e	Electrode cross-section area
ΔA	Cross-section area difference
c	Cut depth
D_i	Inner diameter of the cut
D_o	Outer diameter of the cut
e	Electrode outer diameter
ε_a	Axial electrode wear
ε_r	Radial electrode wear
H_m	Measured cut depth
H_s	Cut Depth selected in E-Drill™
ΔH	Measured hole depth difference
I_a	Electrode inner diameter after cut
I_b	Electrode inner diameter before cut
ΔI	Change in electrode inner diameter
L_a	Length of electrode after cut
L_b	Length of electrode before cut
L_e	Mean length of electrode when E-Drill™ instructs replacement
L_s	Mean electrode length from production
L_u	Useful length of electrode

m_a	Mass after cut
m_b	Mass before cut
$\dot{\mu}$	Material removal rate
N	Number of cuts
n	Number of values recorded for a specific task
O_a	Electrode outer diameter after cut
O_b	Electrode outer diameter before cut
ΔO	Change in Electrode outer diameter
RSD	Sample relative standard deviation
ρ	Material density
s	Sample standard deviation
T	Cut Time
V	Geometric volume
ΔV_e	Electrode volume dissipated during EDM process
ΔV_{fm}	Fastener material volume dissipated during EDM process
W_c	Weighting coefficient
$\dot{\varsigma}$	Electrode wear ratio
$\bar{X}$	Sample mean
x	Value recorded for a parameter of interest

CHAPTER I

INTRODUCTION

1.1 Motivation

Fasteners such as rivets, locking studs/pins, and key-locking inserts (Fig.1), are critical components to achieve mechanical integrity and safety of both commercial and military aerospace structures. There is a wide range of fastener sizes and materials implemented in the aerospace field. According to one estimate, fasteners account for around half of about six million parts of a Boeing 747 [1]. The fasteners, however, undergo fatigue and failures due to a range of mechanisms including static loading (tension, shear, bending and torsion), dynamic/fatigue loading (cyclic stresses or repeated impacts), corrosion, or a combination of mechanisms. Timely inspection and required maintenance of aerospace components also requires removal and replacement of the fasteners in the aerospace maintenance, repair, and overhaul (MRO) industry. Conventional methods for removing rivets, key-locking studs, and other fasteners typically involve mechanical drilling or cutting tools that have long process times, excessive amounts of debris, elevated noise levels, high drill speeds and normal force requirements, frequent in-process misalignment, and significant environmental, health and safety (EH&S) concerns. Thus, there is a demand in the aerospace MRO industry to develop tools and practices to avoid these drawbacks especially for hard metal applications such as titanium and Inconel [1].

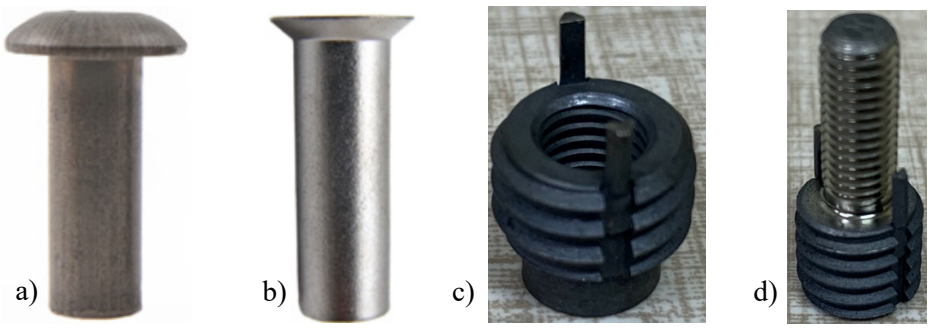

Figure 1: Examples of Aerospace Fasteners: a) Button, b) Countersunk, c) Key-Locking Insert, d) Key-Locking Stud (Photos a) and b) courtesy of Cherry Aerospace)

Electrical Discharge Machining (EDM) is a well-established method [2, 3] and has emerged as a fast, portable means for aerospace fastener removal with minimal debris, noise, misalignment and normal force [4]. The EDM procedure uses electrical arcs from an electrode to remove a specific amount and shape of metallic material. During the material removal process, the electrode also wears, and all of the dissipated material is dispersed into the dielectric fluid surrounding the electrode and piece being machined (Fig. 2). Use of EDM hand drills has been shown to reduce fastener removal times from over 5 minutes to under 10 seconds. Furthermore, it prevents debris/burrs and hole drift that are common with mechanical drilling and cutting.

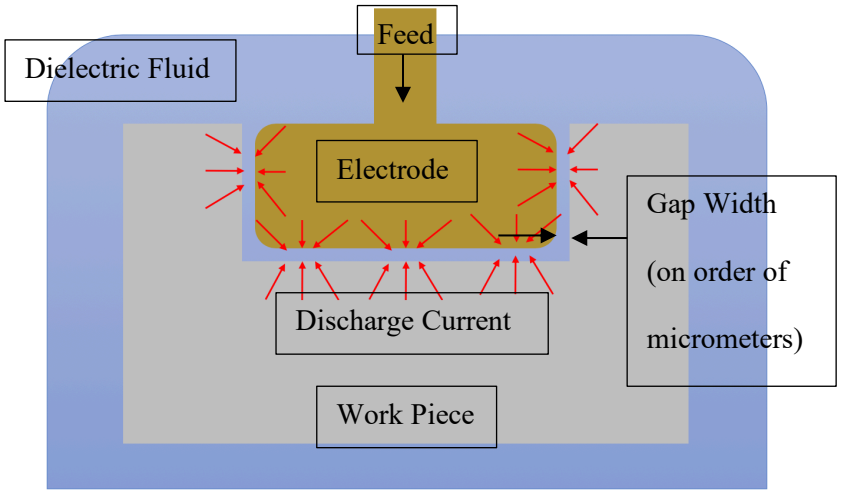

Figure 2: EDM General Concept

While there are several equipment manufacturers of EDM technologies, the Perfect Point EDM (PPE) E-Drill™ (Fig. 3) has emerged as a potential technology in the aerospace MRO industry for fastener removal [4-6]. Perfect Point EDM utilized mathematical models and experimental tests to create an electrode erosion rate algorithm that is implemented by the E-Drill™ user interface to predict electrode life for supply chain forecasts. With this model, the user is able to find an estimate for cut time and number of cuts per electrode based on input parameters such as fastener type, cut method, fastener head diameter, and fastener shank diameter. The PPE algorithm accounts for many different parameters such as system current and voltage as well as electrode thermal conductivity. Such parameters are considered to be primary-level variable process parameters. There are; however, some secondary-level variable process parameters that have not been evaluated. The effects of depth of cut, electrode diameter, and fastener material on electrode wear have not been examined in the current hand-held EDM algorithm. While the primary-level parameters are vital to provide an estimate of electrode life, accounting for secondary-level parameters increases the accuracy of the algorithm. Due to the costs associated with aerospace fastener and fastener removal, any improvement in the accuracy of the hand-held EDM algorithm will see a significant economic impact.

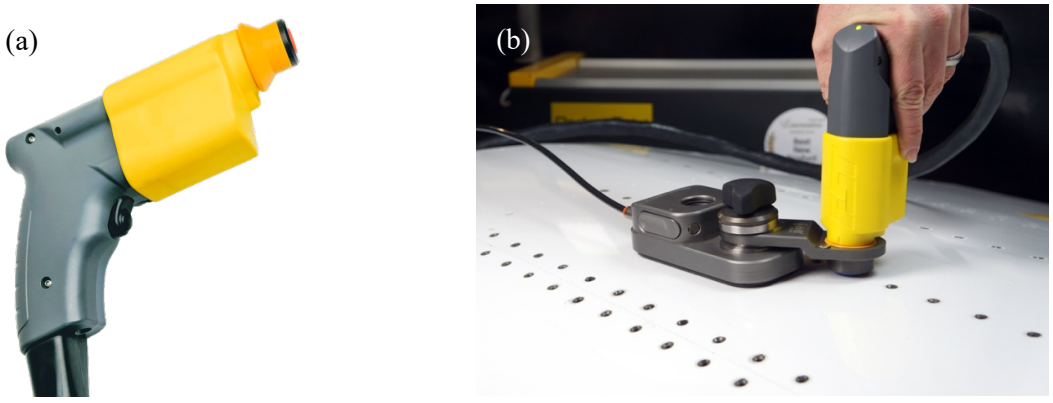

Figure 3: (a.) PP E-Drill™ small hole EDM Machine hand tool and (b.) an example of operation of E-DrillTM with gas turbine engine combustor (photos courtesy of PPedm)

1.2 Goals and Objectives

The goal of the current study is to examine the effects of secondary-level variable process parameters on electrode wear for hand-held EDM applications. Experimental cuts will be performed at three cut depths with three electrode diameters on two typical aerospace fastener materials. Measurements of the electrode properties before and after the cuts will be taken, and that data will be analyzed by seven unique parameters. The results of the study will provide preliminary electrode wear ratio and axial electrode wear prediction models dependent on the secondary-level variable process parameters. Specific objectives include: 1) evaluation of electrode wear through determination of cut time, axial electrode wear, radial electrode wear, material removal rate, cross-section area difference, and selected and measured hole depth difference, 2) developing empirical electrode life predictions, and 3) modeling predictive functions to predict electrode wear.

1.3 Thesis Outline

Background for general EDM processes and the hand-held EDM application are provided with a literature review and analytical theory section in Chapter 2. Chapter 3 discusses the experimental setup, design of experiment, and data recording for the experimental cuts. Results are examined in Chapter 4, with sections for all seven of the parameters used to analyze the data from the experimental cuts. Chapter 5 shows the analytical study performed to provide an estimation of cuts per electrode for the experimental variables as well as the prediction of axial electrode wear and electrode wear ratio using data analysis. An uncertainty analysis is also discussed in Chapter 5, and Chapter 6 provides conclusions and recommendations for further work.

CHAPTER II

BACKGROUND

This chapter reviews the different types of EDM processes, and the theory used to evaluate and compare the variances in electrode erosion between processes. The EDM method for this study is presented with an explanation for how it differs from other approaches. Previous studies on electrode erosion are examined, and the current study is shown to be novel.

2.1 Electrical Discharge Machining

Mechanical drilling methods, typically with the use of manual drilling and/or milling cutting tools, have been traditionally used for the removal of rivets, key-locking inserts, and other fasteners (Fig. 4). These methods have some inherent disadvantages, including setup accuracy, drill speed, normal force requirements, operator skill, in-process misalignment, and environmental, health, and safety (EH&S) concerns (ergonomic risk exposure to eyes, hands; potential exposure to hazardous material/debris). The methods are very slow on hard materials and produce large quantities of sharp metallic foreign object debris (FOD). The workpiece damage due to drill "wander" is also a major concern due to fastener removals with these traditional machining methods [4-6].

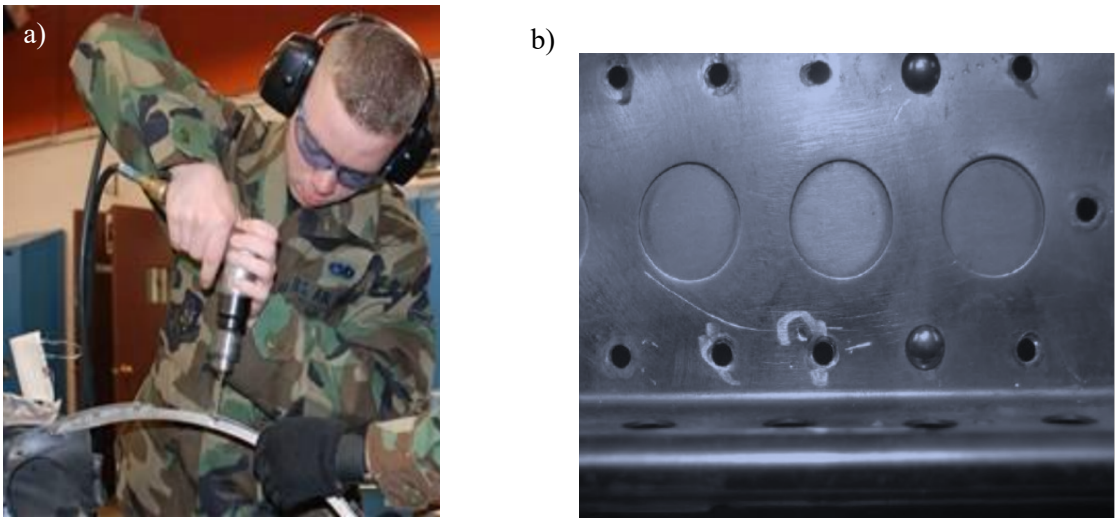

Figure 4: Mechanical drilling for fastener removal illustrating the operation, (a.) debris generated during operation, and (b.) damage to the workpiece (Photos courtesy of PPedm)

EDM was discovered in 1770, but the common application of EDM for material removal began in the 1940's. The main mechanisms behind EDM are: an electrical current passes between an electrode (tool) and a metal workpiece, being separated by a dielectric fluid; the fluid serves as an electrical insulator until sufficient voltage is applied to achieve its ionization point; and, the fluid then behaves as an electrical conductor, such that a resulting spark discharge melts or vaporizes a specific portion of the workpiece (the tool also undergoes some erosion). The dielectric fluid also serves as a means to flush away particles of the eroded material away from the workpiece and electrode. The process is sustained by pulsing and maintaining a consistent gap between the electrode and work piece [7, 8]. Three main variations of the EDM processes are: ram/die-sinking EDM, wire EDM, and hole drilling/micro-EDM. The schematics of these processes are shown in Figs. 5-7.

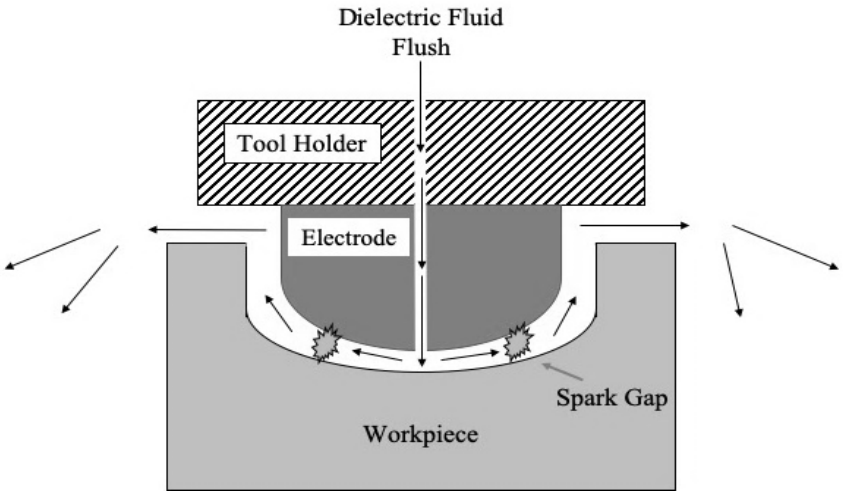

Figure 5: Schematic of ram/die-sinking EDM

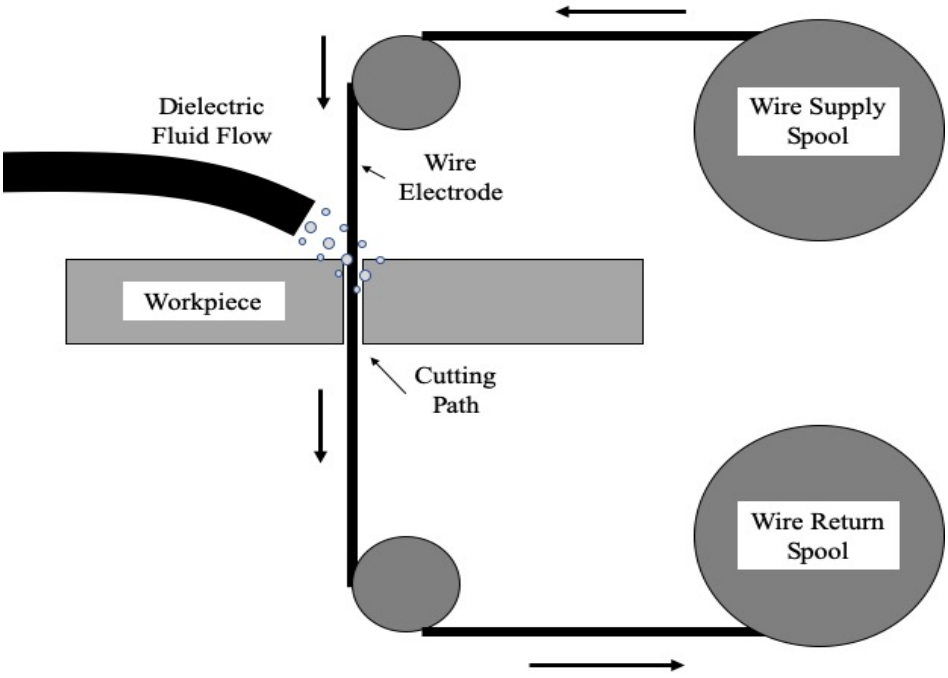

Figure 6: Schematic of wire EDM

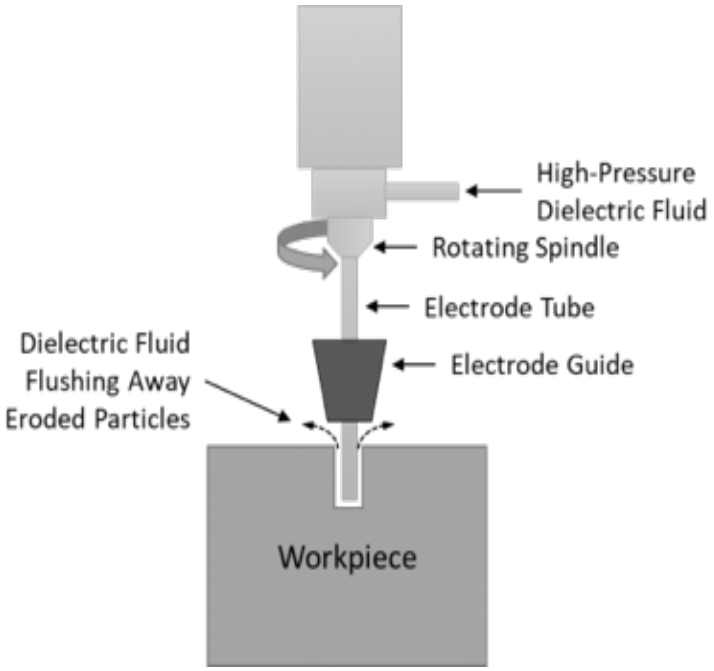

Figure 7: Schematic of hole-drilling/micro EDM

Ram EDM involves plunging a custom electrode shape to effectively stamp the shape into the workpiece (Fig. 5) [3, 9]. It is often used to form customized cavity shapes in a parent material. Wire EDM uses a thin wire for an electrode, moving and cutting a path through the workpiece (Fig. 6) [3, 8, 10]. It is often used to cut material when minimal material removal is necessary. In Hole Drilling EDM process, a cylindrical electrode plunges into the workpiece to form a hole (Fig. 7) [3, 7, 8, 10]. A guide ensures the desired hole path is maintained. This process has been used with aircraft gas turbines to drill cooling holes into hard, metal alloy blades and vanes with highly complex geometries. All of the EDM processes have electrode wear, but the amount and rate all depend input parameters such as cut depth, electrode diameter, and parent material type.

2.2 Hand-held Electrical Discharge Machining

While the established EDM processes have been very well developed and implemented in industry, these processes are not suitable for aerospace fastener removals because these they involve heavy machinery, require complex tooling (CNC), and are unhandy (bulky and cumbersome). The ideal EDM system for fastener removal needs to be handheld (similar to

mechanical drill) but with additional advantages related to process efficiency, ease of operation, and human/environmental safety. Recently, PP EDM Corporation, a privately funded corporation founded in 2005 (Huntington Beach, CA), patented a hand-held EDM drill (E-Drill™) for fastener removal [4-6]. Fig. 3 shows the PP E-Drill™ machine hand-held tool and an example operation of E-Drill™ with gas turbine engine combustor. The schematics of the EDM hand tool, and cross-sectional view of the tool design, and actual cross section of a fastener with electrode are shown in Fig. 8 and 9.

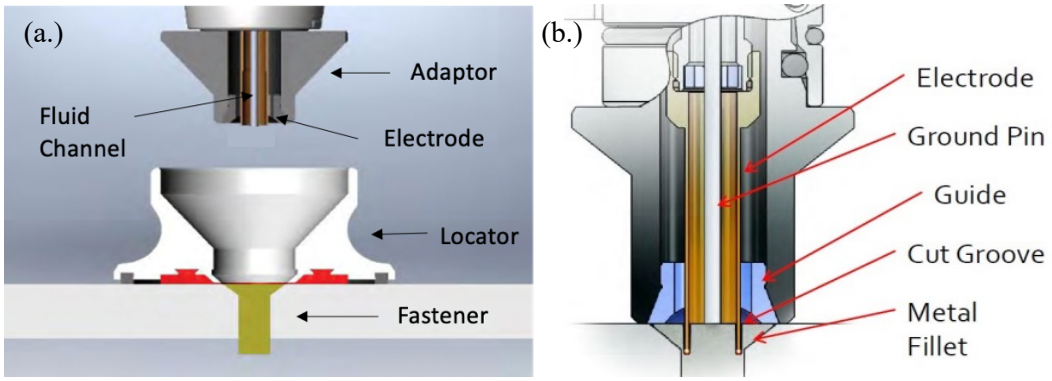

Figure 8: Schematics of a) external grounding and b.) center grounding application PP E-Drill™ tool and design (Photos courtesy of PPedm)

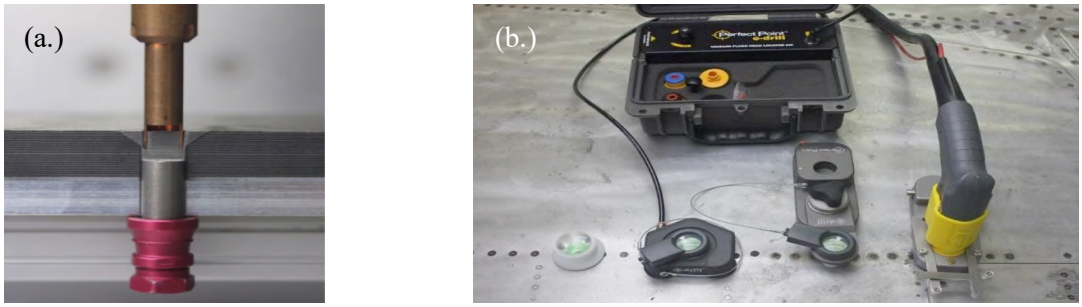

Figure 9: (a) Cross section of fastener and electrode showing cut groove in the fastener head; (b) locator tools for alignment of E-Drill™ for external grounding application (Photos courtesy of PPedm)

The E-Drill™ tool works on the principle of EDM and is operated with simple steps: (a) align the tool with the target fastener; the center ground pin makes contact with the fastener head (center

grounding application shown in Figure 8), or the electrode tip contacts the fastener head (external grounding application shown in Figure 9); (b) cutting electrode advances and spark-erodes a circular cut groove into the fastener head; the cut diameter is within that of the fastener head and shaft so that the electrode does not come in contact with the skin, fastener hole or substructure; (c) de-ionized water flushes cut zone, keeping part cool and removing cut debris; and (d) once cut is complete, remaining metal fillet is punched out (Fig. 8-9). To set cut parameters, the E-Drill™ system is completely programmable for the fastener type, size, and material. A key step in the operation involves carefully placing the locator to center the tool on the fastener; several location tools have also been designed to locate the E-Drill™ over the center of the fastener (Fig 9 (b.)). Some of the advantages of the E-Drill™ over mechanical/twist drilling are: closed-loop system flushes, vacuums, and captures debris while operating (no FOD); minimal pressure required reducing the risk if injury; precision locator and fixed head minimizes the damage to the surrounding structure; and minimal noise pollution [4-6].

2.3 Existing Knowledge and Gaps

There is a wealth of previous literature about EDM covering topics such as applications, performance measures, process parameters, and electrode design and manufacture. Abbas et al. examined the current state of EDM research and found general research trends focus on ultrasonic vibration, dielectric fluid comparisons, dry EDM, and predictive modeling techniques [10]. Ho and Newman found the research trends in die-sinking EDM focus on include process variable optimization, process monitoring, improvement of performance measures, and predictive modeling [7]. Mahendran et al. studied the current research into wire and micro EDM and found focuses in peak current levels, power supply generation, material removal rate, and electrode wear rate [3].

Theoretical models have been previously proposed, including anode (positively charged workpiece) and cathode (negatively charged workpiece) erosion models to provide a general model to apply across the different types of EDM. DiBitonto et al. examined the cathode portion

of the erosion model, and they found it differed from typical conduction models because the cathode accepts power at the boundary condition instead of temperature. They were able to develop a universal, dimensionless model in terms of the cathode material's thermophysical properties to solve for an optimum pulse time factor and erodibility [11]. Patel et al. examined the anode portion of the erosion model, and they found the anode also accepts power at the boundary condition rather than temperature, as is common in most point heat-source models. By determining the melt fronts between the anode and the plasma, they found the anode melts rapidly during on-times and then resolidifies. From this, they were able to determine that ram/die-sinking EDM should be operated with longer on-times, while wire EDM should be operated with short on-times [12]. This EDM cathode and anode modeling study was the precursor for many further studies into the modeling of the EDM process for specific applications. Hewidy et al. examined the modeling of machining Inconel 601 with a wire EDM system by utilizing response surface methodology. They found the material removal rate for the Inconel 601 increased with increases in peak current and dielectric fluid pressure. Their modeling techniques allowed them to see the impact of changes to any input parameter on the resultant response parameter [13].

Other studies have researched process parameter impact on EDM systems through experimental measures. Hasçalik and Çaydas examined the effects of changing electrode material types (graphite, copper, and aluminum) and process parameters (pulse current and duration) on the ram EDM of Titanium alloy, Ti-6Al, 4V. They found that increasing the pulse durations above 200 μs saw a decrease in material removal rate and surface roughness. Also, graphite electrodes had the highest material removal rate with the least amount of workpiece cracking[14]. Thoe et al. studied the use of ultrasonic vibration and peck cycles to increase the material removal rate during the EDM of small diameter (less than 1 mm diameter) cooling holes into a nickel alloy. They found the use of ultrasonic vibration during the EDM process saw an increase in material removal rate, and a peck cycle was necessary to maintain a consistent rate of penetration [15]. Wang and Yan performed the rotary EDM of blind holes into composite aluminum (Al2O3/6061Al) in order to

optimize the system operating parameters. They recorded and compared material removal rate, electrode wear ratio, and rotation rate. From this, they were able to determine the increase of rotational speed or dielectric flushing pressure cause increases in material removal rate and electrode wear ratio. They also found changing electrical based parameters (e.g. peak current, polarity, pulse duration, and power supply voltage) had a more significant effect on the process than changing the non-electrical based parameters (e.g. electrode rotational speed, dielectric fluid pressure, and the number of through holes in the electrode) [16]. The current study uses this understanding to say examining non-electrical based parameters is a secondary-level impact on the overall prediction modeling. Kahn analyzed the difference between wear along the cross-section of an electrode to the wear along the length of the electrode during a ram EDM procedure. The study was conducted with brass and copper electrodes machining into aluminum and mild steel. Kahn found wear along the cross-section was greater than wear along the length for the solid electrodes. The study also showed brass electrodes had a greater wear rate due to a lower material thermal conductivity and melting points. Also, it showed materials being machined that have lower thermal conductivity result in a decreased material removal rate; therefore, causing a higher wear ratio [17].

There are gaps of knowledge regarding the electrode wear rate for the hand-held EDM applications due to the difference in duty cycle and electrode design. Duty cycle is the percentage of time a machine can safely operate within a specified window of time. Regarding differences in duty cycle, conventional EDM systems have a maximum duty cycle of 30%, while the E-Drill^{TM} has a duty cycle around 90%. Regarding the electrode design, the hand-held EDM system requires a hollow copper electrode with dielectric fluid flowing through the central channel (Figure 8). Conventional EDM electrodes either do not have fluid channels or have small diameter fluid channels to the electrode cross-section. Therefore, there is a need to study the electrode wear caused by the hand-held EDM system to provide second-level effects contributing to electrode life prediction models.

2.4 Theory for Analysis

For this study, seven unique parameters were selected to examine the electrode wear data collected from the performed EDM cuts with the E-Drill™. The chosen parameters are cut time (T), axial electrode wear (ε_a), radial electrode wear (ε_r), electrode wear ratio ($\dot{\varsigma}$), material removal rate ($\dot{\mu}$), cross-section area difference (ΔA), and selected and measured hole depth difference (ΔH). T is the time for the entire EDM cut, and it is provided by the E-Drill™ system in seconds. This is an important parameter because it can be used to directly compare machining time for any setting combination on the machine. It is also used in other parameters to nominalize by time. ε_a examines the change in length (axial direction) for the electrode during a single cut as shown in Eq. 1 where L_b is the electrode length before the cut and L_a is the electrode length after the cut. ε_a can be used to observe the wear rate of the electrode, but it can also be affected by the amount of fastener material that attaches to the end of the electrode. Also, if the electrode is not wearing evenly, the length can be difficult to measure correctly.

$$\varepsilon_a = L_b - L_a \ [in.] \tag{1}$$

ε_r examines the change in electrode diameter (radial direction) during a single cut as shown in Eqs. 2-4 where O_b is the electrode outer diameter before the cut, O_a is the electrode outer diameter after the cut, ΔO is the change in electrode outer diameter, I_b is the electrode inner diameter before the cut, I_a is the electrode inner diameter after the cut, and ΔI is the change in electrode inner diameter. ε_r is an important factor to consider because any change in electrode diameter could affect the precision of the next cut. All ε_r results should be much smaller than the electrode diameter, or the next hole size could be larger than desired.

$$\Delta O \ = O_b - O_a \ [in.] \tag{2}$$

$$\Delta I \ = I_b - I_a \ [in.] \tag{3}$$

$$\varepsilon_r = \Delta O \ + \ \Delta I \ [\text{in.}] \tag{4}$$

$\dot{\varsigma}$ provides a volume comparison between the fastener material and the electrode to eliminate length measurements. The volume loss due to the cutting process is calculated for the fastener material and the electrode using Eq. 5, where ΔV is the volume lost during the EDM process (by either the electrode or the fastener material), m_b is the mass before the cut, m_a is the mass after the cut, and ρ is the material density.

$$\Delta V = \frac{m_b - m_a}{\rho} \left[in.^3\right] \tag{5}$$

$\dot{\varsigma}$ is then calculated using Eq. 6 by dividing the volume lost for the electrode (ΔV_e) by the volume lost for the fastener material (ΔV_{fm}). This is a standard measurement for electrode wear calculations in the field of EDM.

$$\dot{\varsigma} = \frac{\Delta V_e}{\Delta V_{fm}} \tag{6}$$

$\dot{\mu}$ is a ratio of the material volume removed to the time of the cut as seen in Eq. 7 and 8, where A_c is the cut cross section area, D_o is the outer diameter of the cut, D_i is the inner diameter of the cut, H is the depth of the cut, and T is the cut time. Unlike electrode wear ratio, the volume removed is calculated by multiplying the cut cross section area by the depth of the cut. $\dot{\mu}$ is a comparison used across different EDM types and EDM machines because it is nominalized by time [18].

$$A_c = \pi * \left[\left(\frac{D_o}{2}\right)^2 - \left(\frac{D_i}{2}\right)^2\right] \left[in.^2\right] \tag{7}$$

$$\dot{\mu}\left[\frac{in^3}{hr}\right] = \frac{A_c\left[in^2\right] * H[in]}{T\,[s]} * 60\left[\frac{s}{min}\right] * 60\left[\frac{min}{hr}\right] \tag{8}$$

ΔA examines the difference in cross-section area between the hole after the cut has been performed and the electrode. This parameter shows the extent to which the electrode cuts larger than its own cross section and is calculated using Eqs. 7, 8, and 9 where A_e is the electrode cross section area. The sparks from the EDM process remove more material than just the size of the

electrode, so it is important to understand how much larger the cut cross-section is than the electrode cross section.

$$A_e = \pi * [\left(\frac{D_O}{2}\right)^2 - \left(\frac{D_i}{2}\right)^2] \tag{9}$$

$$\Delta A = A_c - A_e \tag{10}$$

ΔH is a parameter designed to observe the difference between the selected cut depth on the EDM machine and the measured depth after the cut, and it is calculated using Eq. 11 where H_s is the selected cut depth that is entered into the E-Drill™, and H_m is the measured cut depth. When removing aerospace fasteners, any variation in the cut depth could result in damage to the parent material if the cut is too deep or an inability to properly remove the fastener if the cut is too shallow. Understanding the possible variation in the machine provides important information for the selection of an aerospace fastener cut depth.

$$\Delta H = H_s - H_m \tag{11}$$

Along with the formulas required to solve for the seven parameters, the equations for sample mean ($\bar{X}$), sample standard deviation (*s*), and sample relative standard deviation (*RSD*) are required for the statistical analysis. These equations are shown respectively in Eqs. 12, 13, and 14 where *x* is a value recorded for a parameter of interest, *n* is the number of values recorded for the specific task.

$$\bar{X} = \frac{\sum x}{n} \tag{12}$$

$$s = \frac{\sum (x - \bar{X})^2}{n-1} \tag{13}$$

$$RSD = \frac{s}{\bar{X}} \tag{14}$$

CHAPTER III

EXPERIMENTAL METHODOLOGY

This chapter reviews experimental setup, design of experiment, and the data recording process.

3.1 Experimental Setup

The setup for the study first involves taking measurements of the material coupons and the electrodes. For the cut depth study, the chosen depths were selected to model depths in the range of those utilized for typical aerospace fasteners (0.05 in., 0.10 in., and 0.15 in.). For the electrode diameter study, the selected electrodes (Fig. 10) are relevant sizes for typical aerospace fasteners and provide a significant difference in diameter (0.125 in., 0.1875 in., and 0.33 in.). The E-Drill™ serial number for the base unit is MSU100114 and the serial number for the hand tool is 305145002.

Figure 10: Electrodes Used in Study with Diameters of 0.125 in., 0.1875 in., and 0.33 in. From Left to Right

For the fastener material study, the selected material coupons are made of Titanium (Ti-6Al-4V) and Inconel 718 to represent typical aerospace fastener materials, and they are 2.5 in. squares with a thickness of 0.5 in. The Titanium fastener material would typically be used in the cold section of the aerospace turbine engine, while the Inconel fastener material would be used in the hot section. To ensure the cuts were not performed too close to each other or to an edge, a jig, as seen in Fig. 11, was 3D printed out of polylactic acid (PLA). Two sides of the jig extend past the main platform to slide over the fastener material coupon. The top platform has a central hole that aligns the cut in the center of the quadrant. This jig was designed with a slot on the material side for an O-ring to keep the dielectric fluid from escaping. After a cut is made, the jig is moved to the next quadrant on the fastener material coupon.

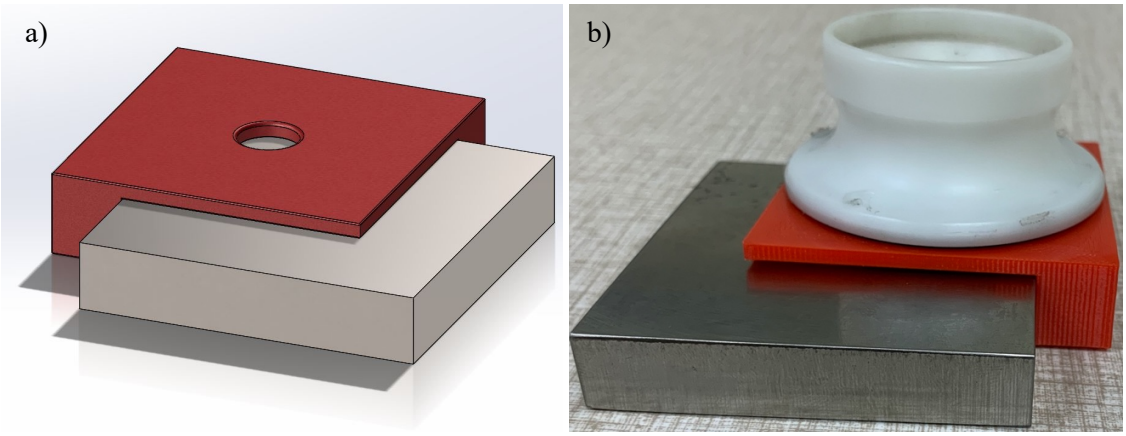

Figure 11: a) CAD Design for Experimental Jig and b) Experimental Jig on Workpiece with E-Drill Locator

Once the fastener material coupon and jig are secured in a vice (Fig. 12), the external-grounding clamp for the E-Drill™ is secured onto the specimen. Then, the specimen is ready for cutting. After the specimen setup is complete, the machine parameters are set using the handheld terminal. The parameters for "Type" are set to "Hole:, "Method" is set to "Flush Head", "Material" is set to the fastener material type being investigated, "Cut Depth" is set to the experimental cut depth, and the fastener diameter parameters are set to match the experimental electrode. Finally, the

operator is able to make the cut into the fastener material coupon. Figure 13 shows one of the cuts from the study with labels for the inner diameter, outer diameter, areas of heat affect, and splatter. The splatter is small spheres of material that were removed from the parent material but reattached to the surface of the parent material before they could be sucked back up the E-Drill™ hand tool. Also shown is the dielectric fluid containment area where the O-ring in the bottom of the experimental jig keeps the fluid from escaping out the sides of the jig.

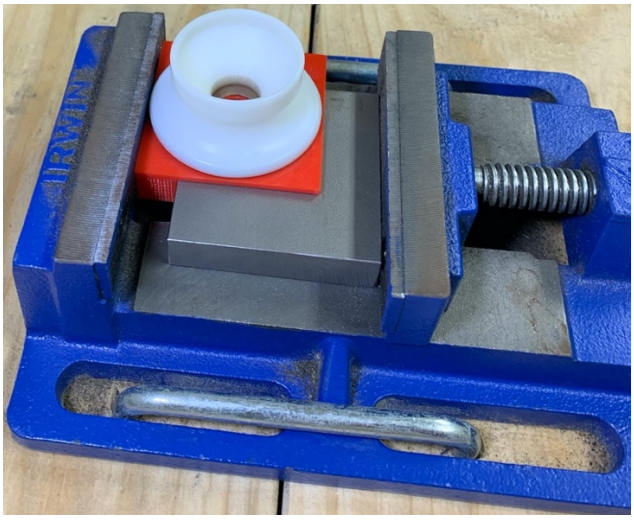

Figure 12: Experimental Setup in Vice

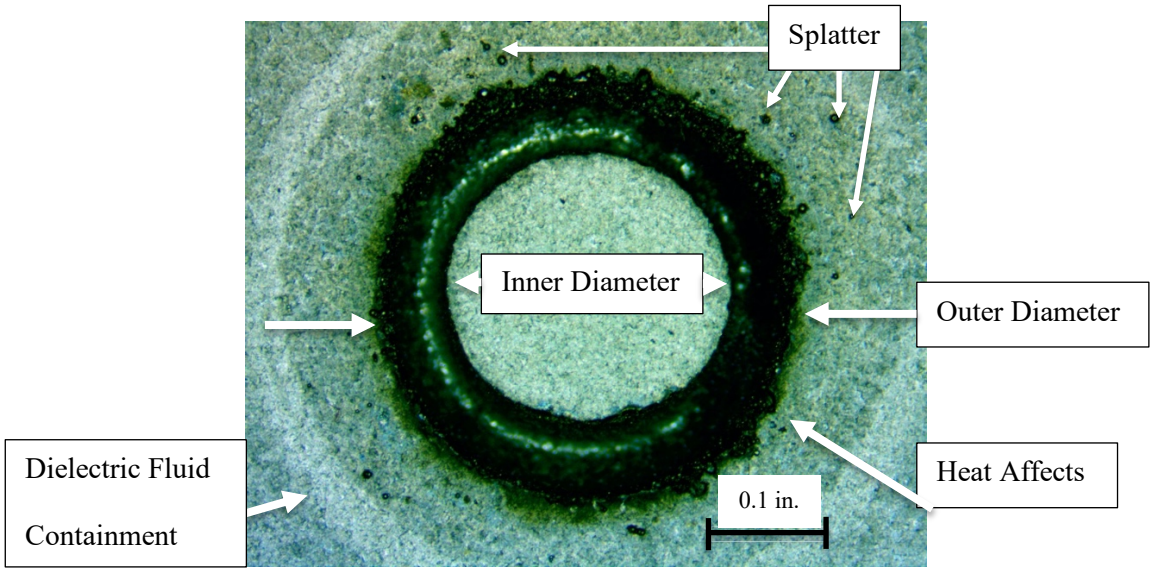

Figure 13: E-Drill™ Cut into Inconel 718 using 0.33 in. Diameter Electrode to a cut depth of 0.15 in.

3.2 Design of Experiment

With the focus of evaluating the electrode wear due to cut depth, electrode diameter, and fastener material, the experiment was designed with 8 parameter tests with 3 cuts per test for a total of 24 cuts. The electrode diameters used in the study were chosen because they are consistent with different types of aerospace fasteners, are readily available through the supplier (PPedm), and they provide a wide range of size for examining the effects of changing electrode diameter. The fastener materials used in the study were chosen because they are common to gas turbine engine fastener and were readily available at the time of the study. The design of experiments can be seen in Table 1 below. Each chosen depth was tested three times into both of the selected fastener materials. For these cuts, the electrode was only changed when required by the E-Drill™, so as to simulate a practical application. The system alerted the operators of the need to change the electrode after the first cut on the Titanium (Ti-6AL-4V) fastener material. After those tests were completed, the electrode was changed to the 0.125 in. electrode for three cuts and then to the 0.1875 in. electrode for three cuts. Both of these tests were performed with new electrodes and a cut depth of 0.1 in. to allow for comparison to the cuts of the same depth with the 0.33 in. electrode. The complete study was performed by the same individual to reduce effects caused by differences in operators.

After ensuring the machine and hand tool were ready for EDM operation, the operator would enter the following settings into the handheld terminal: “Hole” was selected for “Type”, “Flush Head” was selected for “Method”, either “Titanium” or “Inconel” were selected under “Material, and correct dimensions for the electrode were selected under the “Head ∅” and “Shank ∅”. The cut depth was then adjusted in the “Advanced Mode” selection window. Then, the experimental jig would be secured on the specimen and both would be clamped together in the vise so the specimen and jig would not move during the EDM process. The external grounding clamp was secured on the specimens. Then, E-Drill™ hand tool was removed from the holster and connected to the external grounding clamp. Preparations for the cut were finalized by inserting the electrode

side of the gun into the locator on top of the experimental jig. While applying pressure on the hand tool perpendicular to the fastener material surface, the trigger on the hand tool was squeezed until the machine finished the cut. To see the full setup and procedure, see Appendix A and B.

Table 1: Design Experiment for Study

Task	Cut Depth (in.)	Electrode Diameter (in.)	Material	Number of Cuts
1.1	0.05	0.3300	Inconel 718	3
1.2	0.10	0.3300	Inconel 718	3
1.3	0.15	0.3300	Inconel 718	3
2.1	0.05	0.3300	Ti-6Al-4V	3
2.2	0.10	0.3300	Ti-6Al-4V	3
2.3	0.15	0.3300	Ti-6Al-4V	3
3	0.10	0.1875	Ti-6Al-4V	3
4	0.10	0.1250	Ti-6Al-4V	3
Total Number of Cuts:				**24**

3.3 Data Recording

To ensure the most accurate data possible, all measurements were performed immediately before and after the cuts were performed. This reduced any likelihood of damage occurring between the cut and the measurement, which would cause significant changes in data. All distance measurements were taken with a Fowler High Precision 52-008 Series dial caliper, which has a range of 6.5 in. and a resolution of 0.001 in. All weight measurements were taken with an OHAUS Model TS4KD Precision Standard balance, which has a range of 4000 grams with a resolution of 0.1 grams or a range of 400 grams with a resolution of 0.01 grams. Before the cut was made, the electrode would be measured for weight, length, outer diameter, and inner diameter, and the fastener material coupon would be measured for weight. After the cut was completed, the cut time would be recorded, the electrode would again be measured for weight, length, outer diameter, and inner diameter, and the fastener material coupon would be weighed again. Along with those measurements, hole depth, outer diameter, and inner diameter were also recorded. The hole created by the EDM process is not perfectly clean or perfectly symmetrical, so

the measurements of the hole have error. Some of this is due to bias error of the instrumentation, which is 0.0005 in. for the caliper. Most of the error; however, is due to precision error due to randomness associated with imperfect symmetry of the cuts. Regarding error in the weight measurements, some is due to the bias error of the balance, which is 0.005 grams for the electrodes and Titanium specimens (under 400 grams) and 0.05 grams for the Inconel specimens (over 400 grams). Some of the error is also due to slag from the fastener material and electrode either attaching to the remaining electrode or to the surface of the fastener material rather than being removed into the E-Drill^{TM} system.

CHAPTER IV

RESULTS

This chapter discusses the results from the experimentation as interpreted by seven parameters to examine electrode wear from the E-Drill™ cuts into aerospace fastener material. The seven parameters used to evaluate the electrode wear are: cut time (T), axial electrode wear (ε_a), radial electrode wear (ε_r), electrode wear ratio ($\dot{\varsigma}$) material removal rate ($\dot{\mu}$), cross-section area difference (ΔA), and selected and measured hole depth difference (ΔH). Statistical analysis was performed on the data and is shown in the form of tables. Results from the parameter calculations were put into graphs for ease of visual comparison. Means were used for the comparisons because there was considerable variability between cuts of the same parameters. The measurements of the electrode that exhibit change from the EDM process are the length and the mass, but those values are easily affected by the splatter from the fastener material attaching to the tip of the electrode (Fig. 14). When removing an actual fastener, the outer diameter of the E-Drill™ cut would occur within the outer radius of the fastener, so most of the splatter would be removed when the fastener is removed. Two electrodes were used for the Tasks 1 and 2 because a single electrode is not able to make all of those cuts. The electrode was replaced based on the E-Drill™'s suggestion after the first cut of Task 2.1. Also, the jig described in section 4.1 was used to allow the cuts to be made on the material specimens available. Without the jig, the E-Drill™ locator would overhang the material coupon, but it does provide an additional error in the testing. It was decided

that due to this variability, the mean for each experimental parameter would provide the most accurate representation of the available data. Figures 15-18 show representative cuts in order to exhibit the variation between cuts of the same parameters and variation caused by changing cut depth, electrode diameter, and fastener material. To view the photos of all 24 cuts, see Appendix C. Also, the raw data from the measurements of the electrode and fastener material before and after the cut can be seen in Appendix D.

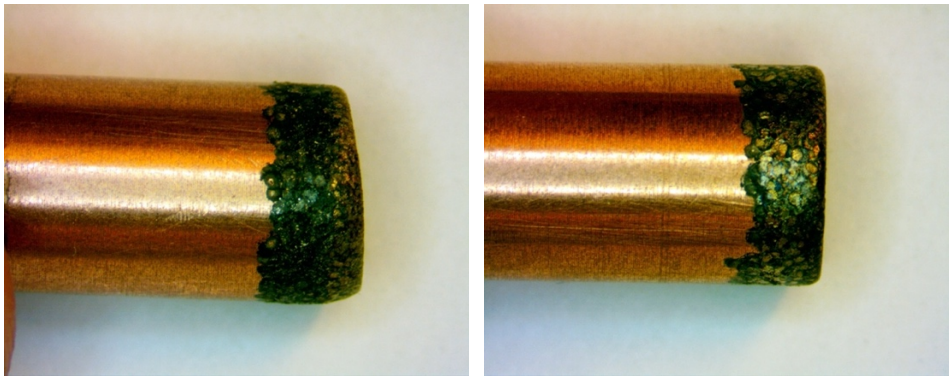

Figure 14: a) Electrode 1 tip after Task 2.11 and b) Electrode 2 after Task 2.33

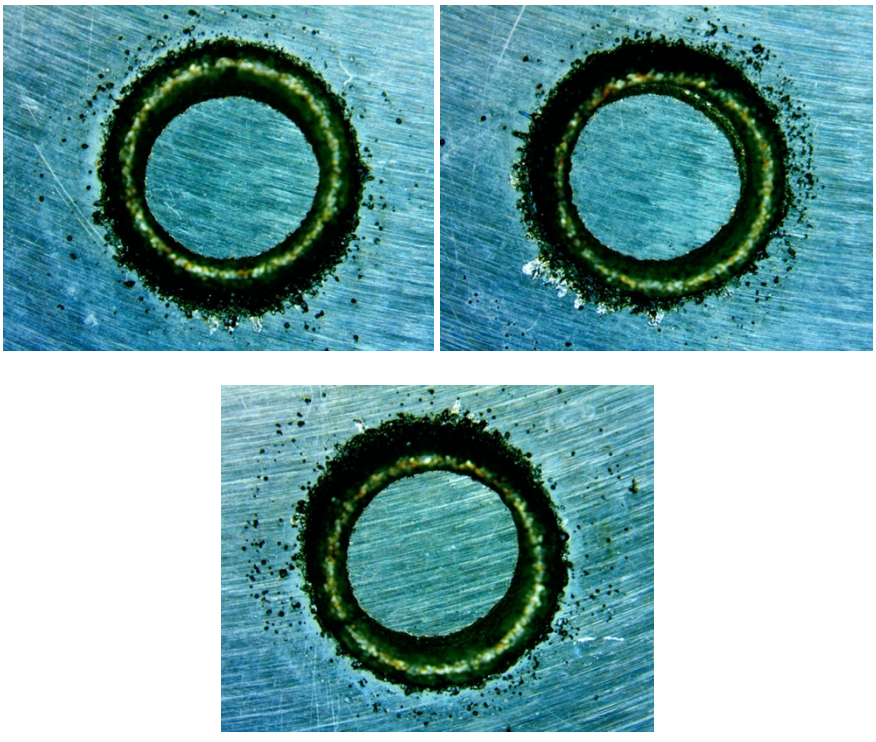

Figure 15: Variation between three cuts with no change to parameters (Task 2.3 cuts)

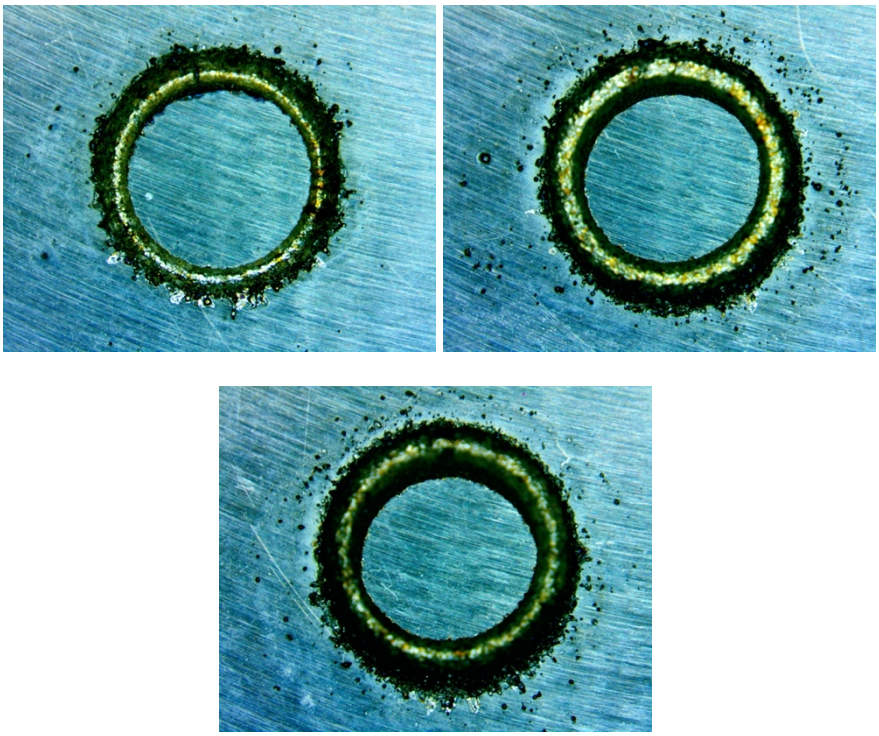

Figure 16: Variation due to changes in cut depth (Task 2.1 Cut 1, Task 2.2 Cut 1, Task 2.3 Cut 3)

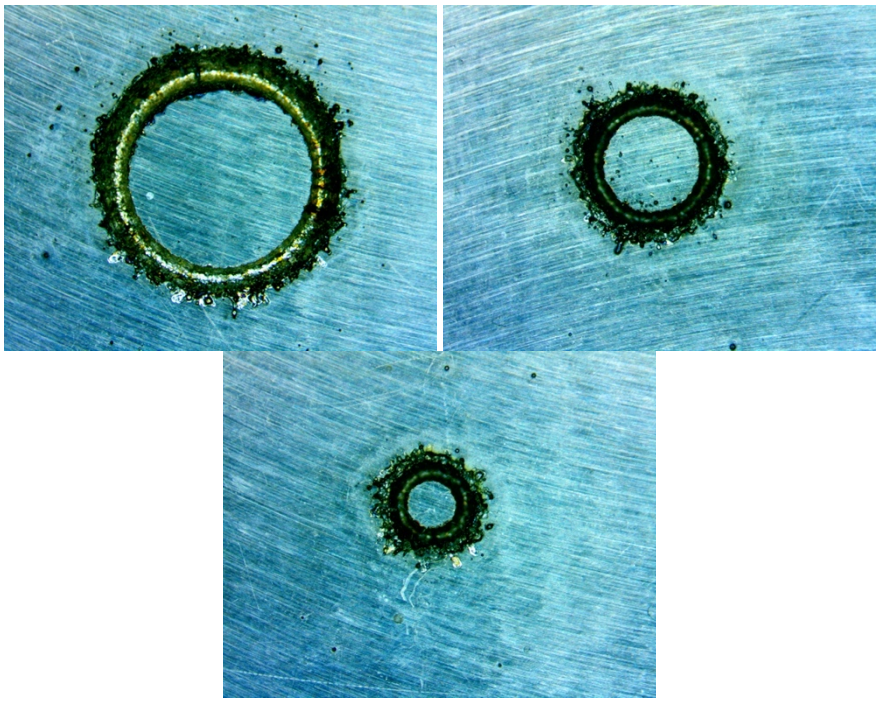

Figure 17: Variation due to changes in electrode diameter (Task 2.1 Cut 1, Task 3 Cut 1, Task 4 Cut 1)

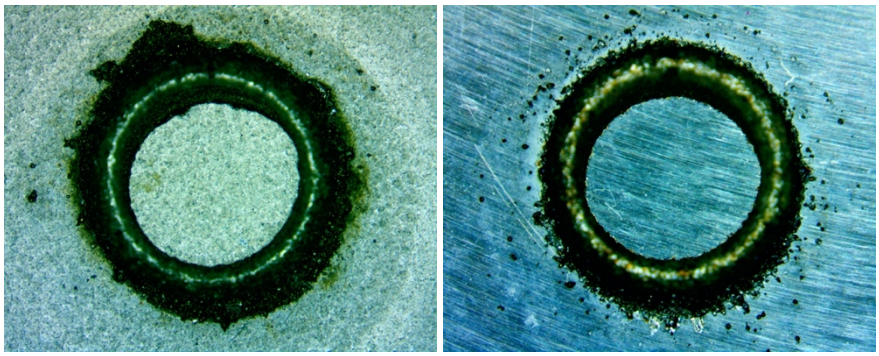

Figure 18: Variation due to changes in fastener material (Task 1.3 Cut 1, Task 2.3 Cut 1)

4.1 Cut Time (*T*)

Displayed in Table 2 is the *T* mean, sample standard deviation, and relative sample standard deviation for each of the tasks described in Table 1. Though the relative standard deviation reaches above 10% in three different tasks, generally, the cut times have a small standard deviation (especially compared to the other parameters). Because the electrode retracts to the same place before each cut, as the electrode wears, the time to cut will increase slightly.

Table 2: *T* Statistical Analysis

Task	Mean (s)	Standard Deviation (s)	Relative Standard Deviation
1.1	9.00	0.75	8%
1.2	21.17	0.96	5%
1.3	35.17	3.19	9%
2.1	9.40	0.90	10%
2.2	28.27	0.90	3%
2.3	48.33	9.95	21%
3	6.20	0.36	6%
4	5.20	1.00	19%

Figures 19 and 20 show the mean *T* due to cut depth in Inconel and Titanium. Cuts into the Titanium required a longer cut time for the same depth of cut into Inconel. The difference between the cut times increases as the cut depth is increased. While the cut time increase for cuts into Inconel shows small changes in the rate of increase as cut depth increases, the cut time

increase for cuts into Titanium shows an almost exponential rate of increase as cut depth increases. The *T* data over cut depth for both Inconel and Titanium fit both a linear and an exponential approximation with R^2 values close to 1. The linear and exponential approximations for both are shown in Figures 19 and 20 along with the 2nd order polynomial function to show the true data curve.

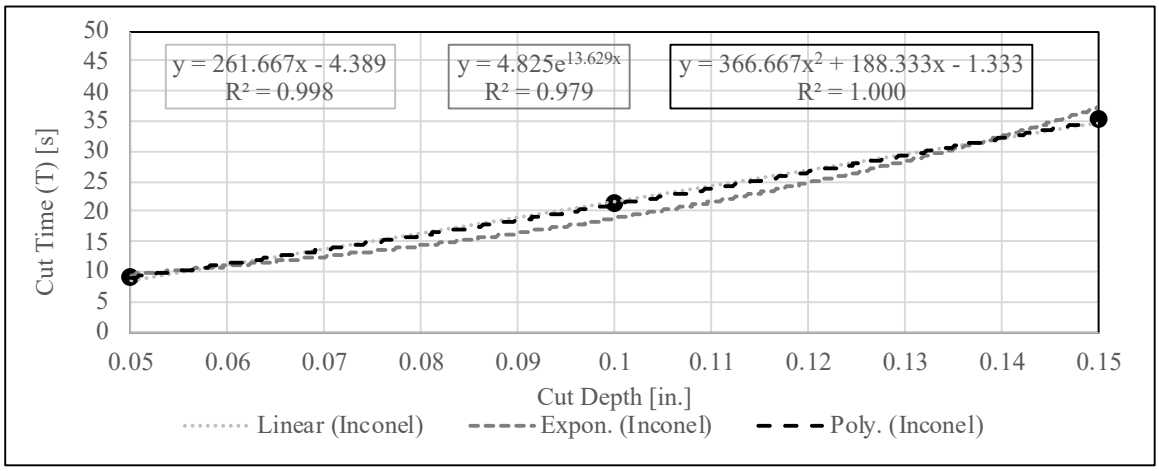

Figure 19: Mean *T* Due to Cut Depth in Inconel

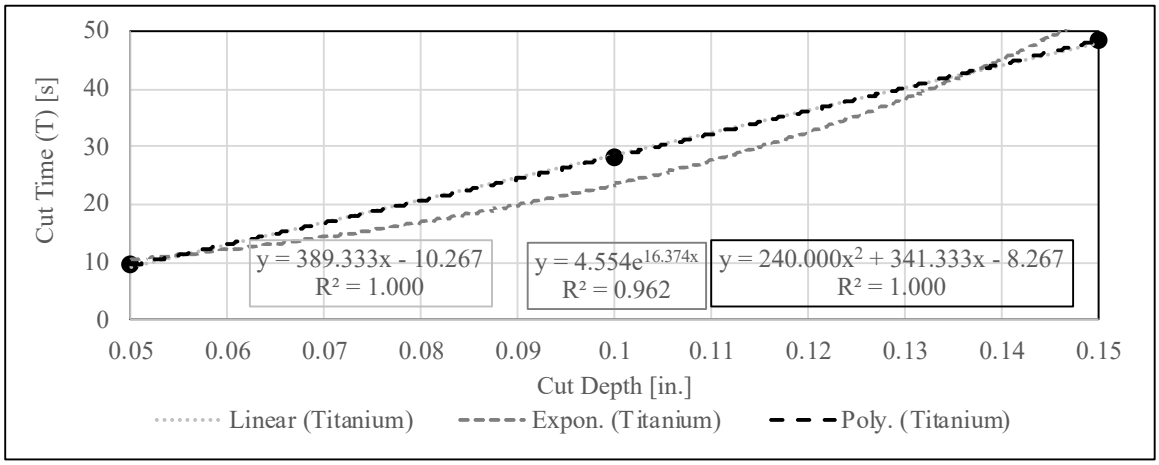

Figure 20: Mean *T* Due to Cut Depth in Titanium

Figure 21 shows the mean *T* of the three different electrode sizes for a cut depth of 0.1 in. into Titanium specimens. The 0.33 in. electrode has a significantly longer *T* than either the 0.1875 in. electrode or the 0.125 in. electrode. There is a 128% difference between the 0.33 in. and 0.1875

in. electrodes' cut time and a 17.5% difference between the 0.1875 in. and 0.125 in. electrodes' cut time. This shows the increase in cut time due to an increase in cut depth is not linear and is more similar to an exponential plot (as seen in the approximations). The 0.1875 in. electrode is closer in size to the 0.125 in. electrode than the 0.33 in. electrode, but the difference in mean cut time is significantly more than the ratio of diameters would show for a linear relation. The *T* data over electrode diameter for Titanium fits both a linear and an exponential approximation with R^2 values close to 1. The linear and exponential approximations for both are shown in Figure 21 along with the 2nd order polynomial function to show the true data curve.

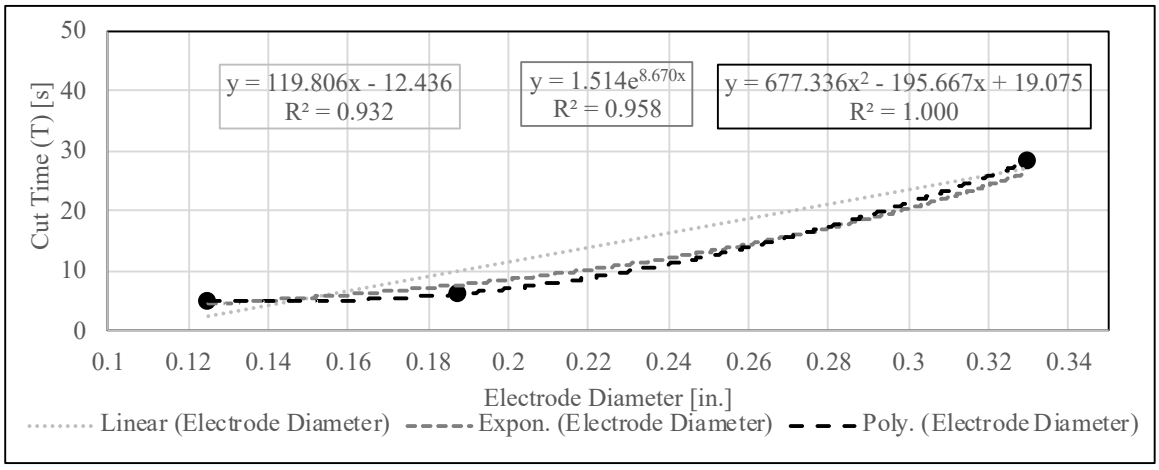

Figure 21: Mean *T* of Three Different Electrode Sizes with a Cut Depth of 0.1 in. into Titanium

4.2 Axial Electrode Wear (ε_a)

Displayed in Table 3 is the ε_a average, sample standard deviation, and relative sample standard deviation for each of the tasks described in Table 1. All ε_a data tested did result in high relative standard deviations. The relative standard deviation for Tasks 2.1 and 2.2 being over 100% is likely due to only having small changes in the electrode axial length. Any slag or measurement error will have a relatively large impact with the smaller values.

Table 3: ε_a Statistical Analysis

Task	Mean (in.)	Standard Deviation (in.)	Relative Standard Deviation
1.1	4.00E-03	1.00E-03	25%
1.2	7.67E-03	5.77E-04	8%
1.3	1.47E-02	7.09E-03	48%
2.1	8.33E-04	1.26E-03	151%
2.2	3.33E-04	1.15E-03	346%
2.3	1.67E-03	5.77E-04	35%
3	3.00E-03	1.00E-03	33%
4	4.33E-03	1.53E-03	35%

Figures 22 and 23 show the mean ε_a due to cut depth in both Inconel and Titanium using the E-Drill™. As can be seen in the figures, the mean ε_a from cuts into the Inconel was significantly higher than from cuts into the Titanium. It is believed this is due to Inconel having a higher thermal conductivity. Although there is minimal change in mean axial electrode wear across the three cut depths for the Titanium pieces, there is a steady increase in mean ε_a as the cuts increase in depth for the Inconel specimens. It is believed that with more data, a similar trend would be seen in the Titanium specimen. The ε_a data over cut depth for Inconel fits both a linear and an exponential approximation with R^2 values close to or exactly 1, but the approximations for Titanium have low R^2 values. The linear and exponential approximations for both are shown in Figures 22 and 23 along with the 2nd order polynomial function to show the true data curve. Because ε_a is the most important factor for electrode life, this shows a linear approximation is sufficient for prediction of electrode supply chain when using the E-Drill to remove Inconel (hot section) fasteners. For the Titanium, it was determined that further analysis would be required for a prediction model.

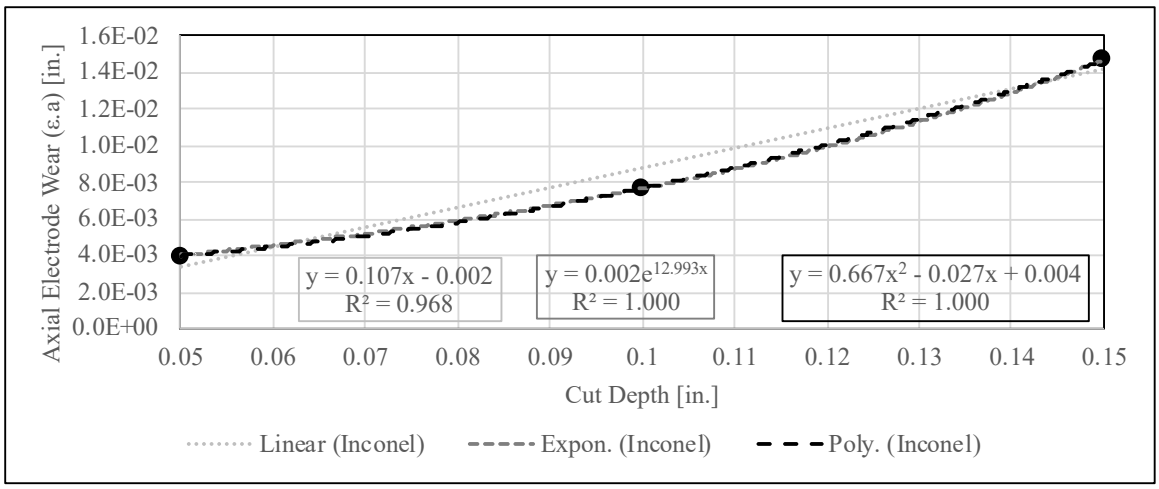

Figure 22: Mean ε_a Due to Cut Depth in Inconel

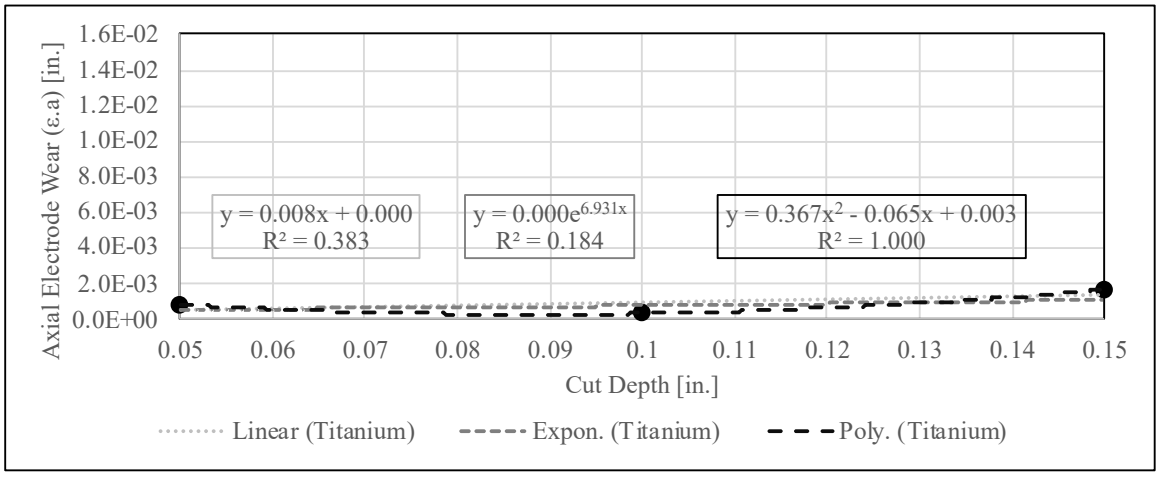

Figure 23: Mean ε_a Due to Cut Depth in Titanium

A comparison of the mean ε_a for a 0.1 in. cut depth into a Titanium specimen with electrodes of three different diameters (0.33 in., 0.1875 in., and 0.125 in.) using the E-Drill™ is shown in Fig. 24. It can be seen there is a significant increase in ε_a as the diameter of the electrode decreases. The mean for the 0.1875 in. diameter electrode is 9 times more than the mean for the 0.33 in. diameter electrode, and the mean for the 0.125 in. diameter electrode is 13 times more than the mean for the 0.33 in. diameter electrode. Since the change in electrode diameter is greater from the 0.33 in. diameter electrode to the 0.1875 in. diameter electrode than from the 0.1875 in. diameter electrode to the 0.125 in. diameter electrode, the axial electrode wear difference between

the 0.33 in. diameter electrode and the 0.1875 in. diameter electrode is significantly greater than the axial electrode wear difference between the 0.1875 in. diameter electrode and the 0.125 in. diameter electrode. The ε_a data over electrode diameter for Titanium fits both a linear and an exponential approximation with R^2 values close to or exactly 1. The linear and exponential approximations for both are shown in Figure 22 along with the 2nd order polynomial function to show the true data curve.

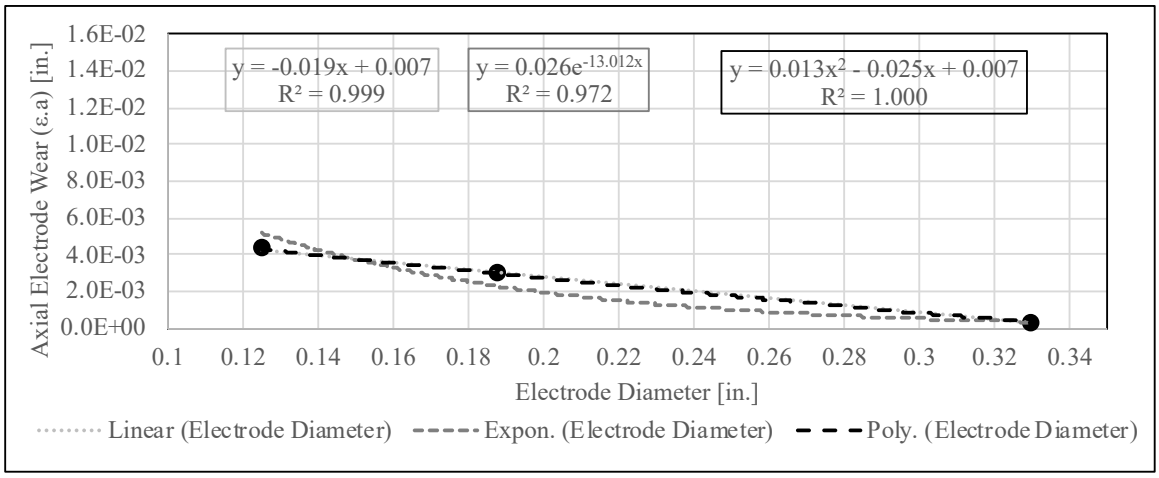

Figure 24: Mean ε_a of Three Different Electrode Sizes with a Cut Depth of 0.1 in. into Titanium

4.3 Radial Electrode Wear (ε_r)

Table 4 shows the ε_r average, sample standard deviation, and relative sample standard deviation for each of the tasks described in Table 1. Mean values for the ε_r are all under 6.66E-04 in., which is below the resolution level for the caliper. The relative standard deviations are all over 200% because the standard deviations are much larger than the mean values. This data represents a minimal radial electrode change occurring during the cutting process.

Table 4: ε_r Statistical Analysis

Task	Mean (in.)	Standard Deviation (in.)	Relative Standard Deviation
1.1	6.67E-04	1.53E-03	229%
1.2	0.00E+00	0.00E+00	N.A.
1.3	6.67E-04	3.79E-03	568%
2.1	-6.67E-04	2.31E-03	346%
2.2	-3.33E-04	2.08E-03	624%
2.3	-3.33E-04	2.08E-03	624%
3	6.67E-04	3.21E-03	482%
4	3.33E-04	2.08E-03	624%

Figures 25 and 26 show the mean ε_r due to cut depth in both Inconel and Titanium using the E-Drill™, and Fig. 27 shows the mean ε_r of the three different electrode sizes with a cut depth of 0.1 in. into Titanium. While the charts appear to show significant differences between the ε_r values for the different cut depths, fastener materials, and electrode diameters, the actual mean values are an order of magnitude (sometimes two orders of magnitude) smaller than the values for ε_a. The values are also smaller than the resolution level of the caliper with large standard deviations. This shows the main focus for electrode wear with the E-Drill™ should be placed on ε_a rather than ε_r. Due to the shape of the curve fit, only the linear approximation was able to be made for the ε_r data. The linear approximations have low values for R^2 for both cut depth studies and the electrode diameter study. The linear approximations and 2nd order polynomial curves are shown in Figures 25-27.

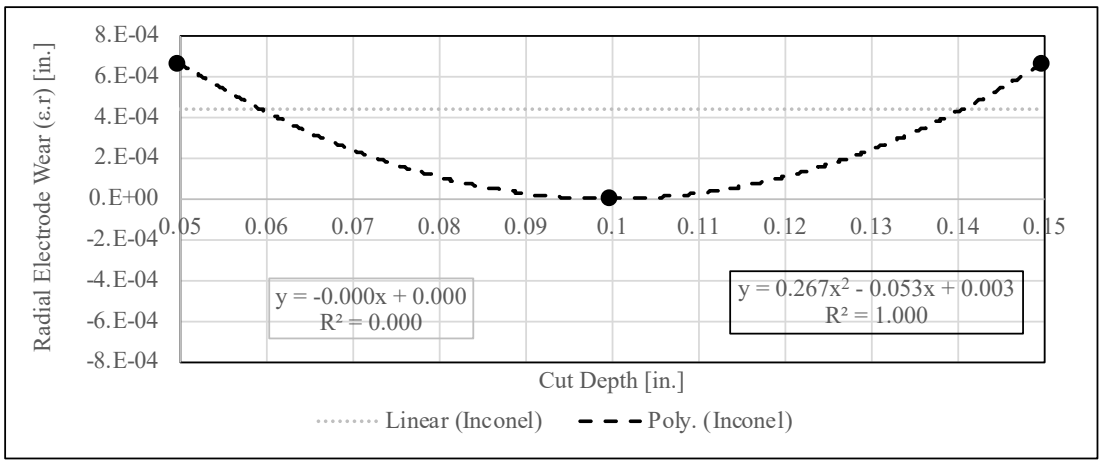

Figure 25: Mean ε_r Due to Cut Depth in Inconel

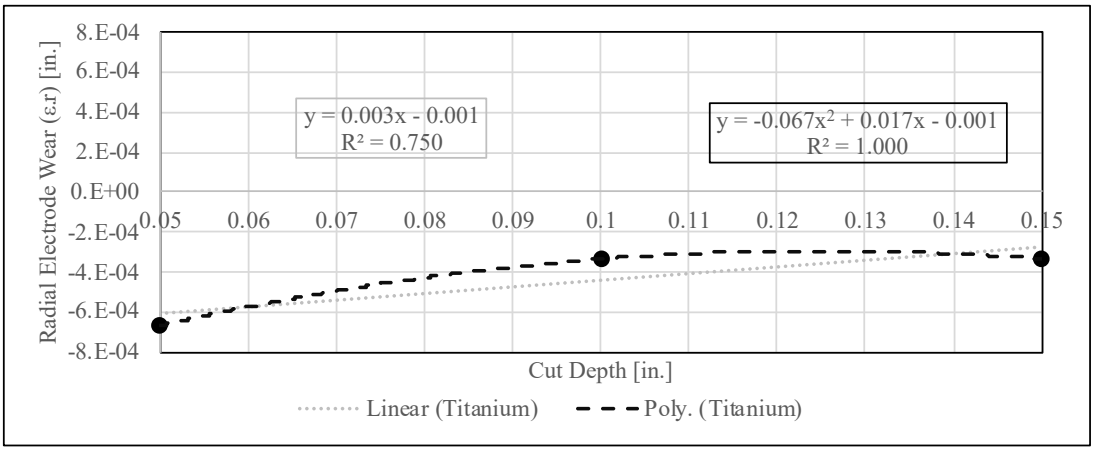

Figure 26: Mean ε_r Due to Cut Depth in Titanium

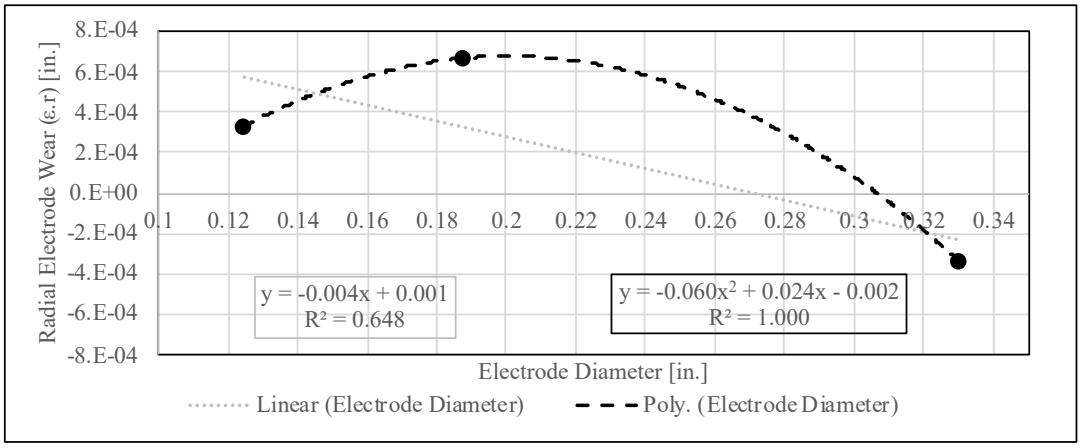

Figure 27: Mean ε_r of Three Different Electrode Sizes with a Cut Depth of 0.1 in. into Titanium

4.4 Electrode Wear Ratio ($\dot{\varsigma}$)

As previously explained, $\dot{\varsigma}$ is a commonly used metric for electrode wear in EDM literature as it focused on the volume removed from the electrode compared to the volume removed from the material being cut. Displayed in Table 5 is the $\dot{\varsigma}$ average, sample standard deviation, and relative sample standard deviation for each of the tasks described in Table 1. Only one task (2.2) did not result in a high relative standard deviation. The negative average value and relative standard deviation for Task 2.1 comes from an increase of mass for the electrode from before the cut to after the cut. This occurs when the cut is not very deep so the added slag from the parent material outweighs the electrode material lost during the cutting process. The relative standard deviation for Task 4 being over 1000% is due to small values with a single value that was negative likely because of the aforementioned slag. This parameter should be re-examined in further studies.

Table 5: $\dot{\varsigma}$ Statistical Analysis

Task	Mean	Standard Deviation	Relative Standard Deviation
1.1	7.11E-02	2.07E-01	292%
1.2	7.61E-02	1.52E-02	20%
1.3	9.98E-02	2.49E-02	25%
2.1	-4.98E-02	1.16E-01	233%
2.2	1.72E-02	5.94E-04	3%
2.3	7.40E-03	6.43E-03	87%
3	5.17E-02	4.99E-02	97%
4	8.31E-03	1.12E-01	1353%

Figures 28 and 29 show the mean $\dot{\varsigma}$ due to cut depth in both Inconel and Titanium using the E-Drill™. As shown by the 0.05 in. cut depth into titanium, the $\dot{\varsigma}$ can result in a negative value especially for shallow cut depths. This is because the volume of the electrode can increase due to slag from the material being cut attaching to the electrode. The Inconel is significantly denser than the copper electrode, so even though the length of the electrode has decreased (as seen in Fig. 22), when slag attaches to the electrode, the electrode has gained mass. From the graphs, it

can be seen the $\dot{\varsigma}$ for cuts into Inconel is significantly higher than for cuts into titanium. Although the $\dot{\varsigma}$ for the titanium cuts do not show a consistent increase or decrease, the $\dot{\varsigma}$ for the Inconel cuts show a gradual increase over the three cut depths. The $\dot{\varsigma}$ data over cut depth for Inconel fits both a linear and an exponential approximation with R^2 values close to 1, but the linear approximation for Titanium has a low R^2 value. The linear and exponential approximations for both are shown in Figures 28 and 29 along with the 2nd order polynomial function to show the true data curve.

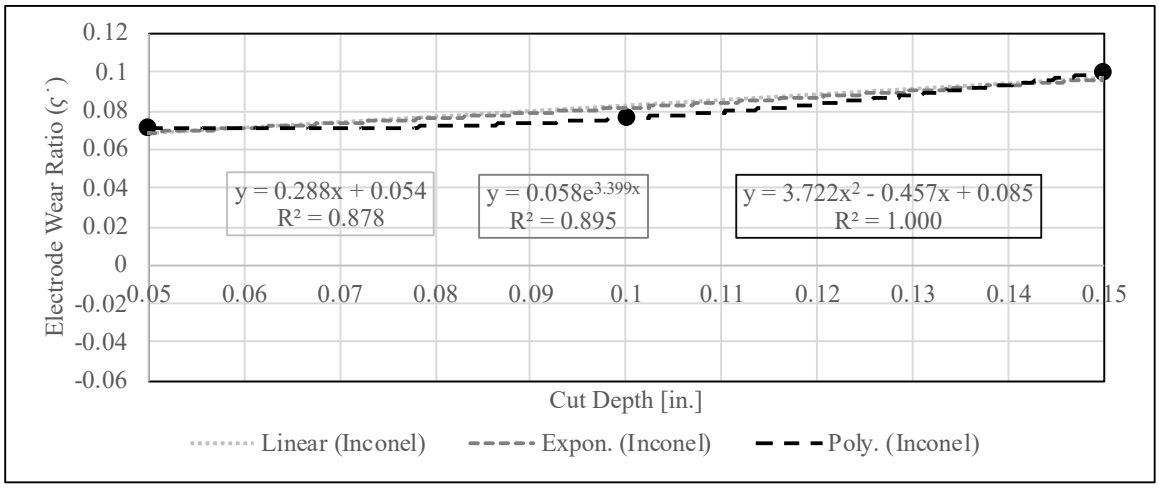

Figure 28: Mean $\dot{\varsigma}$ Due to Cut Depth in Inconel

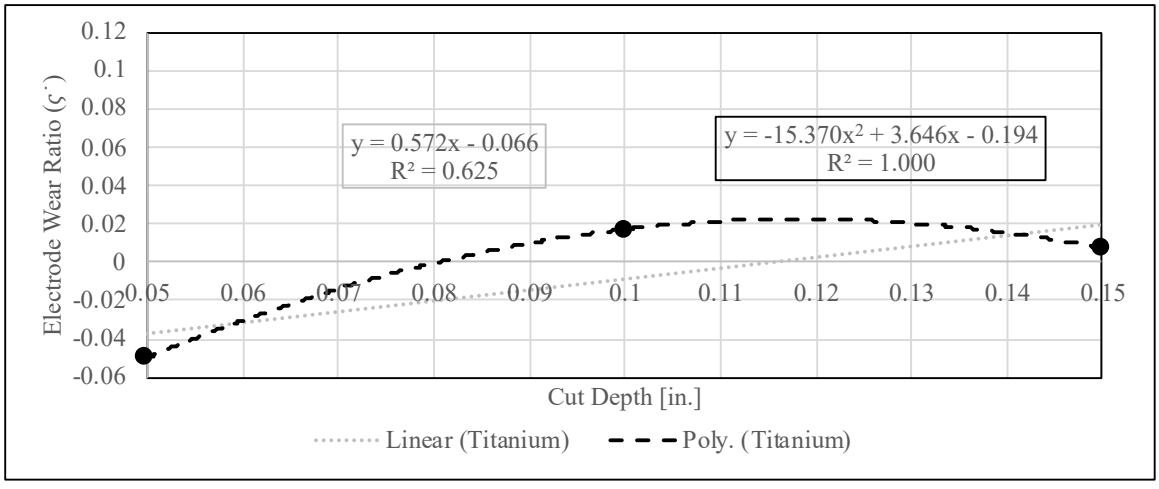

Figure 29: Mean $\dot{\varsigma}$ Due to Cut Depth in Titanium

A comparison of the mean $\dot{\varsigma}$ for a 0.1 in. cut depth into a Titanium specimen with electrodes of three different diameters (0.33 in., 0.1875 in., and 0.125 in.) using the E-Drill™ is shown in Fig.

30. The results of the comparison show a significantly higher $\dot{\varsigma}$ for the 0.1875 in. diameter electrode than the 0.33 in. diameter electrode and the 0.125 in. diameter electrode. This result was not expected due to the axial electrode wear continuing to increase as the diameter of the electrode decreased. There is a high likelihood of error with the 0.125 in. and 0.1875 in. diameter electrode results for $\dot{\varsigma}$ due to the sensitivity of the of the scale only measuring to 2 decimal places. Since the decreases in mass were on the order of 0.01 grams, some of the cuts showed a decrease in length but no decrease in mass. The $\dot{\varsigma}$ data over electrode diameter for Titanium has a poor fit for both a linear and an exponential approximation. The linear and exponential approximations for both are shown in Figure 33 along with the 2nd order polynomial function to show the true data curve.

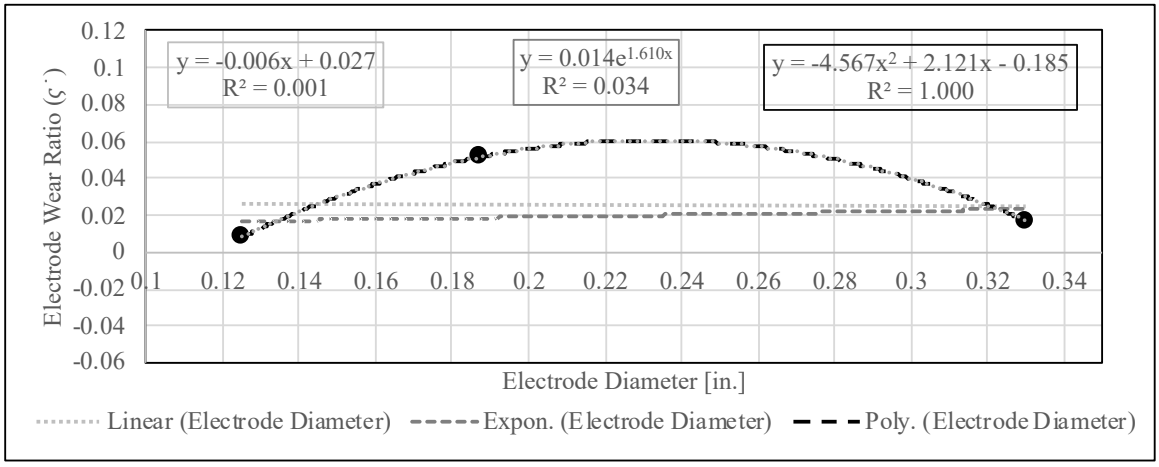

Figure 30: Mean $\dot{\varsigma}$ of Three Different Electrode Sizes with a Cut Depth of 0.1 in. into Titanium

4.5 Material Removal Rate ($\dot{\mu}$)

Table 6 shows the $\dot{\mu}$ mean, sample standard deviation, and relative sample standard deviation for each of the tasks described in Table 1. Four of the tasks had relative standard deviations over 10%, and Task 2.1 had a relative standard deviation of 44%. This large value for Task 2.1 is also seen in Table 7 dealing with the cross-section area difference. A further investigation of the raw data shows one of the cuts in Task 2.1 has significantly different values for fastener material hole

depth, hole OD, and mass change than the other cuts in Task 2.1. After this cut, the E-Drill™ notified the operator the electrode needed to be changed, so Electrode 2 was introduced into the experiment. Comparing to the study done by Sultan et al., the $\dot{\mu}$ rates found for the E-Drill™ are an order of magnitude larger than $\dot{\mu}$ rates for a die sinking EDM [18].

Table 6: $\dot{\mu}$ Statistical Analysis

Task	Mean (in^3/hr)	Standard Deviation (in^3/hr)	Relative Standard Deviation
1.1	0.721	1.26E-02	2%
1.2	0.659	1.73E-02	3%
1.3	0.581	1.28E-02	2%
2.1	0.475	2.09E-01	44%
2.2	0.519	3.43E-02	7%
2.3	0.442	1.00E-01	23%
3	0.774	9.28E-02	12%
4	0.647	1.45E-01	22%

Figures 31 and 32 show the mean $\dot{\mu}$ due to cut depth in both Inconel and Titanium using the E-Drill™. At each cut depth, the mean value for $\dot{\mu}$ was greater with cuts into Inconel than into Titanium. Even though Task 2.1 had a large standard deviation, at the high end of the results, it was still less than the results of Task 1.1. This matches well with Kahn's study because it found materials with a lower thermal conductivity led to lower $\dot{\mu}$ values. The mean $\dot{\mu}$ value for cuts into Inconel decreased as the cut depth increased. The mean $\dot{\mu}$ value for cuts into Titanium remain relatively consistent across the three cut depths. The $\dot{\mu}$ data over cut depth for Inconel fits both a linear and an exponential approximation with R^2 values close to 1, but the approximations for Titanium have low R^2 values. The linear and exponential approximations for both are shown in Figures 31 and 32 along with the 2nd order polynomial function to show the true data curve.

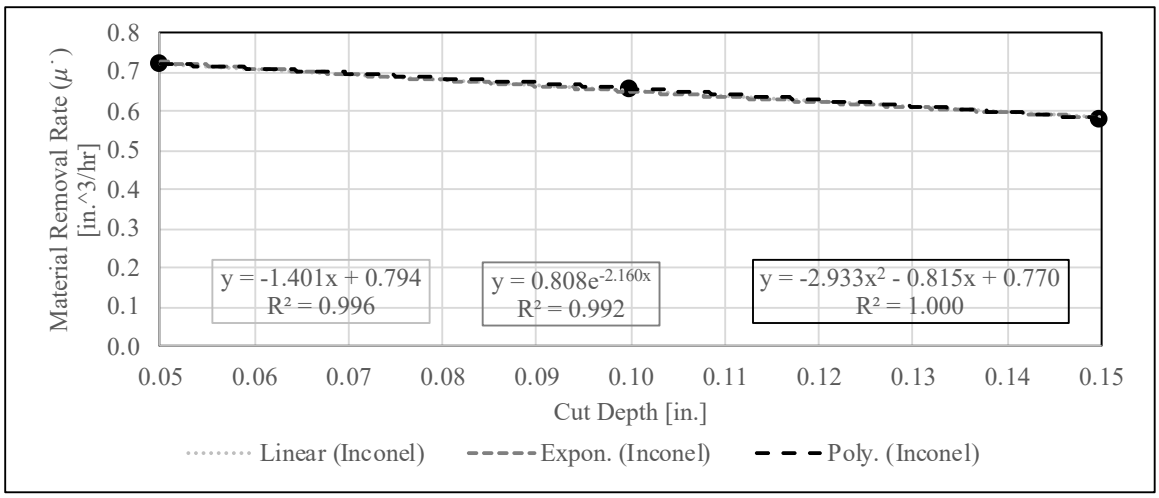

Figure 31: Mean $\dot{\mu}$ Due to Cut Depth in Inconel

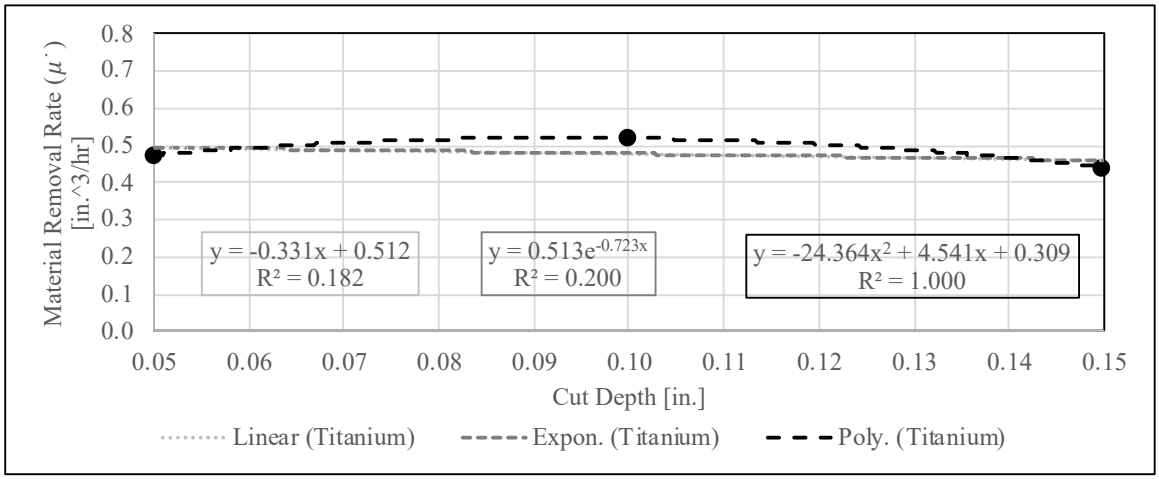

Figure 32: Mean $\dot{\mu}$ Due to Cut Depth in Titanium

Figure 33 shows the mean $\dot{\mu}$ values of the testing for three different electrode sizes with a cut depth of 0.1 in. into Titanium. As the diameter of the selected diameter decreases, there is an increase in the mean value of $\dot{\mu}$ from the 0.33 in. diameter electrode to the 0.1875 in. diameter electrode and a decrease in the mean value of $\dot{\mu}$ from the 0.1875 in. diameter electrode to the 0.125 in. diameter electrode. The difference between the 0.33 in. diameter electrode and the 0.1875 in. diameter electrode is greater than the difference between the 0.1875 in. diameter electrode and the 0.1875 in. diameter electrode by 80.1%. If the standard deviation of Task 4 was

added to the mean $\dot{\mu}$ value for the 0.125 in. diameter electrode (Task 4), the value would be larger than the 0.1875 in. diameter electrode. The $\dot{\mu}$ data over electrode diameter for Titanium has a poor fit for both a linear and an exponential approximation. The linear and exponential approximations for both are shown in Figure 33 along with the 2nd order polynomial function to show the true data curve.

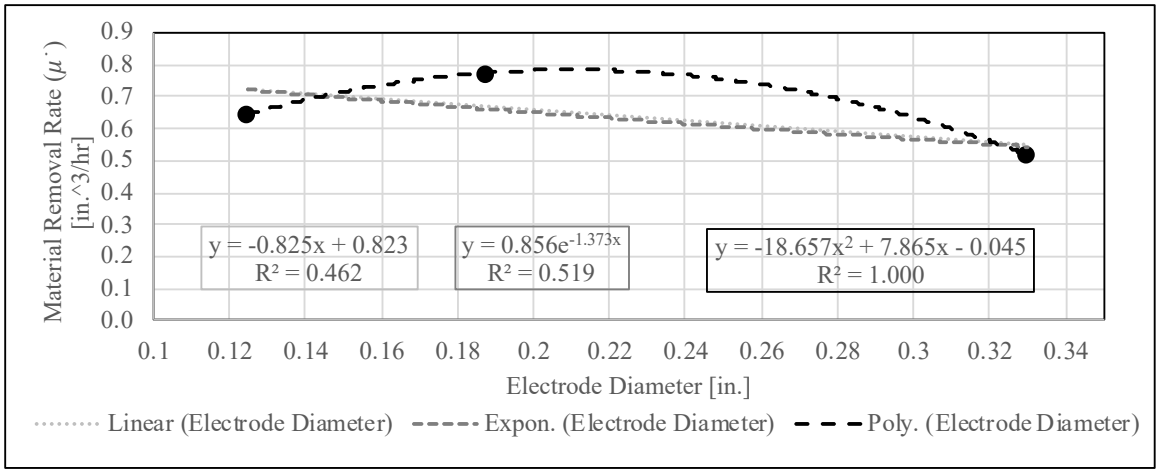

Figure 33: Mean $\dot{\mu}$ of Three Different Electrode Sizes with a Cut Depth of 0.1 in. into Titanium

4.6 Cross-section Area Difference (ΔA)

Table 7 shows the ΔA mean, sample standard deviation, and relative sample standard deviation for each of the tasks described in Table 1. This parameter looks at the difference between the cut cross section area and the electrode cross section area after the cut. One task had a relative standard deviation over 25%, and the rest ranged from 8% to 25%. The one task that had a relative standard deviation of 145% was Task 2.1. This has been a theme through most of the examined parameters with the change of electrode between cuts in Task 2.1 being the most likely explanation.

Table 7: *ΔA* Statistical Analysis

Task	Mean (in.^2)	Standard Deviation (in.^2)	Relative Standard Deviation
1.1	3.07E-02	6.51E-03	21%
1.2	4.23E-02	3.44E-03	8%
1.3	6.48E-02	1.24E-02	19%
2.1	2.86E-02	4.15E-02	145%
2.2	5.62E-02	1.43E-02	25%
2.3	4.59E-02	9.40E-03	20%
3	2.25E-02	4.55E-03	20%
4	1.22E-02	2.12E-03	17%

Figures 34 and 35 show the mean *ΔA* due to cut depth in both Inconel and Titanium using the E-Drill™. Unlike the other parameters discussed so far, *ΔA* theoretically should not increase with increased cut depth as long as the same diameter electrode is being used. Figure 34 shows there is an increase in the mean *ΔA* as cut depth is increased for cuts into Inconel. For cuts into Titanium, there is an increase and then a decrease in mean *ΔA* as the cut depth is increased. It also should be noted that the large standard deviation for the shortest cut depth into Titanium (Task 2.1) makes the comparison difficult for the Titanium cuts. The mean *ΔA* is greater for the cuts into Inconel at the cut depths of 0.05 in. and 0.15 in., and the mean *ΔA* is greater for cuts into Titanium at the cut depth of 0.1 in. The *ΔA* data over cut depth for Inconel fits both a linear and an exponential approximation with R^2 values close to 1, but the approximations for Titanium have low R^2 values. The linear and exponential approximations for both are shown in Figures 34 and 35 along with the 2nd order polynomial function to show the true data curve.

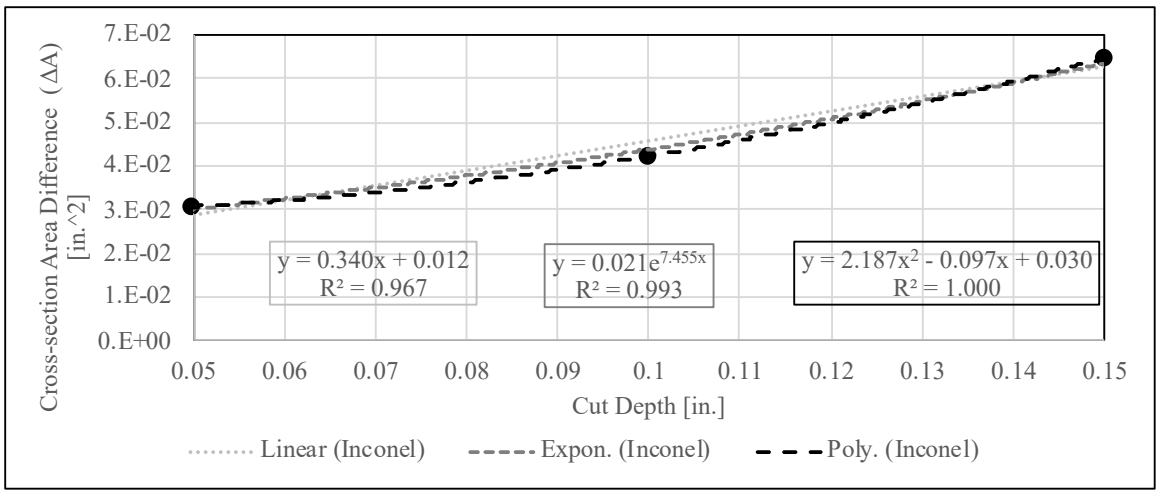

Figure 34: Mean *ΔA* Due to Cut Depth in Inconel

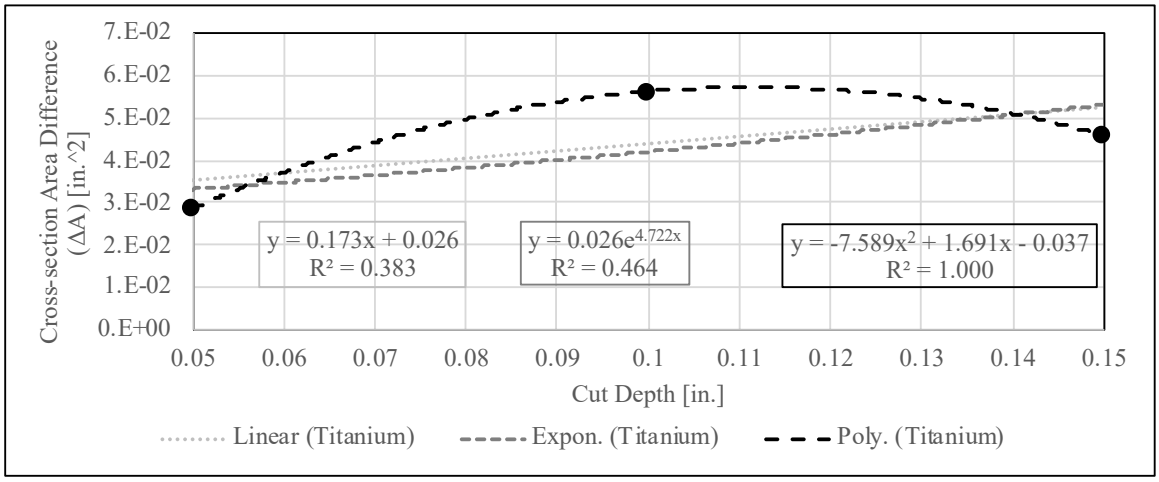

Figure 35: Mean *ΔA* Due to Cut Depth in Titanium

Figure 36 shows the mean *ΔA* values from the testing for three different electrode sizes with a cut depth of 0.1 in. into Titanium. As expected, as the diameter of the electrode decreases, the *ΔA* also decreases. Between the 0.33 in. and 0.1875 in. diameter electrodes, the ratio of the two diameters (smaller diameter over larger diameter) is 0.568 while the ratio of the mean *ΔA* values is 0.400. Between the 0.1875 in. and 0.125 in. diameter electrodes, the ratio of the two diameters is 0.667 while the ratio of the mean *ΔA* values is 0.542. According to those ratios, as the diameter of the electrode increases, the ratio of *ΔA* to electrode diameter also increases. A larger diameter electrode will affect proportionally more fastener material than a smaller diameter electrode for

the same cut depth and fastener material. The *ΔA* data over electrode diameter for Titanium fits both a linear and an exponential approximation with R^2 values close to 1. The linear and exponential approximations for both are shown in Figure 36 along with the 2nd order polynomial function to show the true data curve.

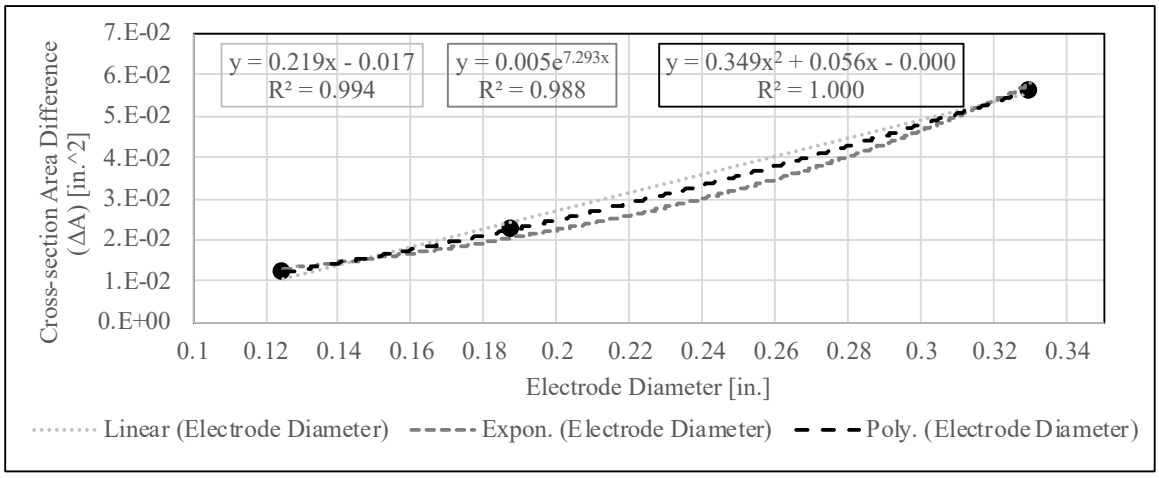

Figure 36: Mean *ΔA* of Three Different Electrode Sizes with a Cut Depth of 0.1 in. into Titanium

4.7 Cut Depth Difference (*ΔH*)

Table 8 shows the *ΔH* mean, sample standard deviation, and relative sample standard deviation for each of the tasks described in Table 1. The parameter looks at the difference between the cut depth entered into the E-Drill™ and the cut depth measured after the cut was performed. Measuring the cut depth was difficult due to the uneven wear around the end of the electrode as can be seen in Figs 15-18 and slag remaining in the bottom of the cut. This is the most likely reason for the absolute values of the relative standard deviations to be over 20% for all but two tasks.

Table 8: *ΔH* Statistical Analysis

Task	Mean (in.)	Standard Deviation (in.)	Relative Standard Deviation
1.1	6.33E-03	3.79E-03	60%
1.2	1.27E-02	4.04E-03	32%
1.3	3.50E-02	8.19E-03	23%
2.1	2.10E-02	7.94E-03	38%
2.2	1.60E-02	1.00E-03	6%
2.3	2.37E-02	1.01E-02	43%
3	7.67E-03	1.15E-03	15%
4	-1.50E-02	7.00E-03	47%

Figures 37 and 38 show the mean *ΔH* due to cut depth in both Inconel and Titanium using the E-Drill™. For the 0.05 in. and 0.1 in. cut depth tasks, the mean value of *ΔH* is greater for the Titanium cuts than the Inconel cuts. For the 0.15 in. cut depth tasks, the mean value of *ΔH* is greater for the Inconel cuts than the Titanium cuts. Mean values of *ΔH* for the cuts into Inconel increases as the depth of cut increases. The trend for the Inconel cuts functions more exponentially than linearly. Mean values of *ΔH* for the cuts into Titanium decrease from the 0.05 in. cut depth to the 0.1 in. cut depth and then increase from the 0.1 in. cut depth to the 0.15 in. cut depth. There is a 97.4% difference between the range of the mean values of *ΔH* for the Titanium cut tasks (0.01 in.) and of the *ΔH* mean values for the Inconel cuts (0.029 in.). The *ΔH* data over cut depth for Inconel fits both a linear and an exponential approximation with R^2 values close to 1, but the approximations for Titanium have low R^2 values. The linear and exponential approximations for both are shown in Figs. 37 and 38 along with the 2nd order polynomial function to show the true data curve.

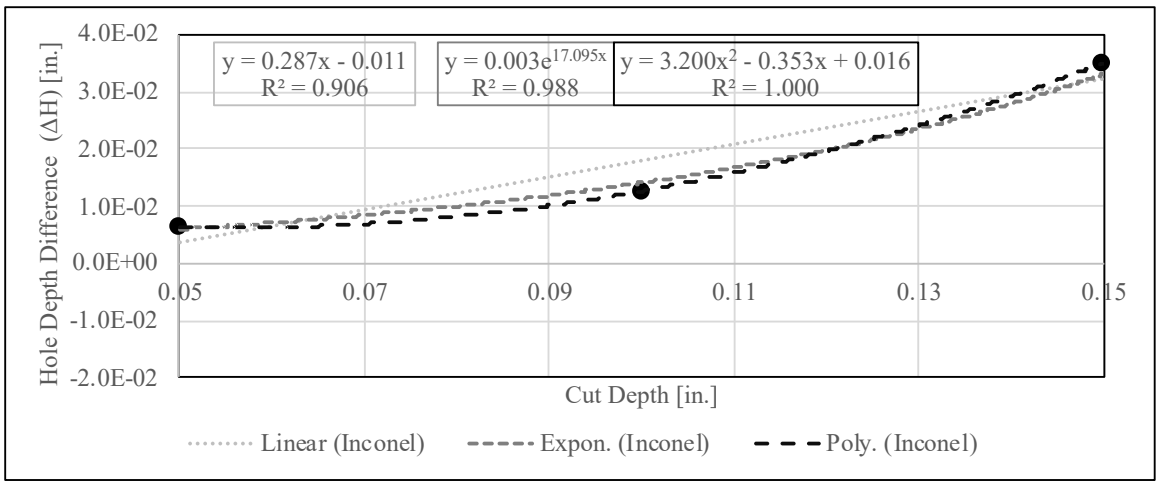

Figure 37: Mean *ΔH* Due to Cut Depth in Inconel

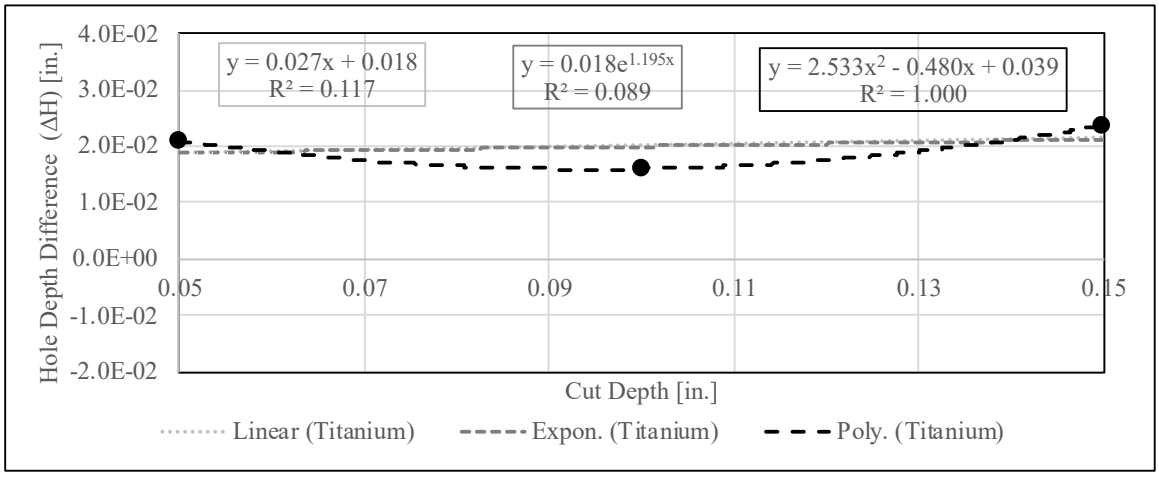

Figure 38: Mean *ΔH* Due to Cut Depth in Titanium

Figure 39 shows the mean *ΔH* values from the testing for three different electrode sizes with a cut depth of 0.1 in. into Titanium. Mean values for *ΔH* decrease as the diameter of the electrode decreases. The negative *ΔH* mean value for the 0.125 in. diameter electrode means the electrode cut deeper into the fastener material than the depth that was entered into the E-Drill™. When removing aerospace fasteners, if the cut is deeper than the input depth, the parent material becomes susceptible to damage. All three cuts in Task 4 (0.125 in. diameter electrode) were measured to be deeper than the input cut depth (0.1 in.). The *ΔH* data over electrode diameter for Titanium has a poor fit for both a linear approximation, and an exponential function was unable

to be plotted due to the shape of the data. The linear and exponential approximations for both are shown in Figure 39 along with the 2nd order polynomial function to show the true data curve.

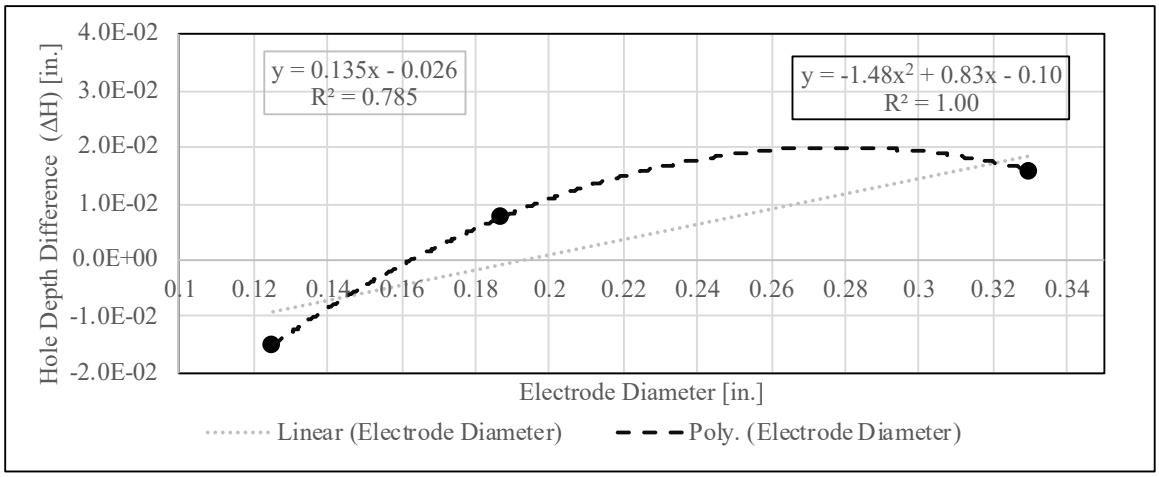

Figure 39: Mean *ΔH* of Three Different Electrode Sizes with a Cut Depth of 0.1 in. into Titanium

CHAPTER V

ANALYTICAL STUDY

This chapter examines the utilization of the data from this study to provide two different prediction models of electrode wear when using the E-Drill™. An empirical model of electrode life was designed using the data recorded during this study and knowledge acquired during the use of the E-Drill™ in similar studies. Next, preliminary, predictive models of electrode wear ratio ($\dot{\varsigma}$) and axial electrode wear (ε_a) were found using polynomial fit lines on the experimental data graphs and weighting functions for cut depth and electrode diameter. Finally, an uncertainty analyses was performed on the models.

5.1 Design of Empirical Electrode Life Prediction Model

From discussions with the E-Drill™ manufacturer (PPedm) and through operation of the machine in this study and previous studies, the main parameter that determines electrode life is the axial length of the electrode. The machine alerts the operator of the need to change electrodes when the E-Drill™ hand tool is no longer able to extend the tip of the electrode to the necessary depth due to the axial wear of the electrode. While this determination process does have significant variance (as seen in section 4.2), a general prediction of cuts per electrode provides the operator with an estimation of the number of electrodes to purchase. It can also be an indication of any machine operation issues if the actual number of cuts does not match the estimated number. The empirical prediction model from this study results directly from the data recorded for ε_a and electrode

dimensions. As previously discussed, the data for ε_a had significant variance, so a more rigorous model would require significantly more testing, which was out of the scope of the current project. The model was developed by solving for the number of cuts required to reduce the electrode axial length from the mean starting length (L_s) to the mean length of electrode when E-Drill instructs replacement of the electrode (L_e). Equation 15 shows the useful length of the electrode (L_u) as the difference between the two mean values. Equation 16 then shows the method for calculating the number of cuts (N) using the mean axial electrode wear (ε_a) for each of the different cut depth (x), electrode diameter (y), and fastener material (z) combinations tested in this study. Because the number of cuts per electrode must be a whole number when considering E-Drill™ operation, all values of N are rounded down to the nearest integer.

$$L_u = L_s - L_e \tag{15}$$

$$N = \frac{L_u}{\varepsilon_{a\ x,y,z}} \tag{16}$$

5.2 Empirical Electrode Life Predictions

By utilizing Eqs. 15 and 16, the empirical electrode life prediction was calculated as number of cuts per electrode (N) for each of the different combinations of cut depth, electrode diameter, and fastener material examined in the study. Table 9 shows the calculated N values for each of the examined factor selections along with the ε_a values (from Section 4.2) and the L_a values measured during the study. Looking at the table, the prediction values for N follow an expected decrease as cut depth increases (with electrode diameter and fastener material). The rate of decrease for the N value as cut depth increases follows a more exponential than linear path for the Inconel cuts. As electrode diameter decreases (with cut depth and fastener material held constant), the prediction values of N also decrease. The rate of decrease of N again follows a more exponential path as the electrode diameter decreases. The Titanium cuts produce a predicted N value at least five times greater than the predicted N values for the Inconel Cuts. There is one predicted N value that is an

outlier from the other values. $N_{0.10,\ 0.33,\ Titanium}$ is significantly higher than the predicted N values at the cut depths above and below the value. The reason for the difference is the value of ε_a for the outlying N value is smaller than the other two N values. There was minimal change in the axial length of the electrodes during the Titanium cuts, so an accurate determination of the ε_a was difficult. Based on results from the Inconel cuts and the other two Titanium cuts, the $N_{0.10,\ 0.33,\ Titanium}$ value was expected to be in the range of 45 to 90, so the author recommends further investigation to determine if this outlier is due to uncertainty error or if it is an anomaly.

Table 9: Empirical Electrode Life Prediction Model

Cut Depth (x) [in.]	Electrode Diameter (y) [in.]	Fastener Material (z)	εa [in.]	L.a [in.]	N.x,y,z
0.05	0.3300	Inconel	4.00E-03	7.50E-02	18
0.10	0.3300	Inconel	7.67E-03	7.50E-02	9
0.15	0.3300	Inconel	1.47E-02	7.50E-02	5
0.05	0.3300	Titanium	8.33E-04	7.50E-02	90
0.10	0.3300	Titanium	3.33E-04	7.50E-02	225
0.15	0.3300	Titanium	1.67E-03	7.50E-02	45
0.10	0.1875	Titanium	3.00E-03	7.55E-02	25
0.10	0.1250	Titanium	4.33E-03	8.05E-02	18

5.3 Method for Preliminary Predictive Models

After examining the linear, exponential (when applicable), and 2nd order polynomial functions for the experimental data in the Results section, it was determined the Titanium cuts required further analysis to develop preliminary, predictive models, unlike the Inconel cuts that are sufficiently modeled by a linear approximation for ε_a. The two parameters that provide the most assistance to initial supply chain prediction are electrode wear ratio and axial electrode wear, so those were the focus of this study. The word "preliminary" is used because to provide a truly predictive model, more cuts would need to be examined due to decrease the random error in the data. The results of these predictive models only apply to cuts into Titanium and should be further iterated as will be discussed in Section 5.7 and in the Conclusion.

The method employed to design these preliminary, predictive models was combining the 2nd order polynomial functions from the data (shown in the Results section) of the cut depth variation and electrode diameter variation studies. Rather than merely adding the data together, weighting coefficients (W_c), which added up to 1, were multiplied on each of the polynomial function. The weighting coefficients were varied from 0 to 1 in increments of 0.2. The inclusion of the weighting factor displays if either cut depth or electrode diameter has more of an impact on the predicted variable (either electrode wear ratio or axial electrode wear) than the other (Eq. 17).

$$\dot{\varsigma} \text{ or } \varepsilon_a = W_{c1} * [Cut\ Depth\ Function] + W_{c2} * [Electrode\ Diameter\ Function] \quad (17)$$

The resulting functions were all plotted on two separate graphs, one with cut depth as the x-axis for one and electrode diameter as the x-axis for the other. The predicted variable was on the y-axis. Because the study included 3 mean values at a cut depth of 0.1 in. and 3 mean values at an electrode diameter of 0.33 in., the values for the functions at each of the cut depths or electrode diameters were averaged to provide the value that was plotted on the graph. Then, mean value data from the Results section was plotted on the graphs. Each weighted function's proximity to the data points (and standard deviations) and to the general shape of the data was examined for both cut depth and electrode diameter graphs in order to determine the weighted function that best described the data trend.

5.4 Electrode Wear Ratio ($\dot{\varsigma}$) Preliminary Predictive Model

Although electrode wear ratio does not appear to be directly correlated to the E-Drill™ determination of electrode life, it is an important overall consideration for electrode life. As previously discussed, the splatter from the cutting process could cause the volume of the electrode to exhibit wear while there is no change in axial wear. This shows the importance of analyzing electrode wear ratio along with axial electrode wear.

Shown in Equation 18 is the base equation for the $\dot{\varsigma}$ preliminary predictive model with c as the cut depth, e as the electrode diameter, and W_{c1} and W_{c2} as the weighting functions. The cut depth and electrode diameter functions were taken from the figures in Section 4.4.

$$\dot{\varsigma} = W_{c1}[15.37c^2 + 3.6465c - 0.1937] + W_{c2}[-4.5667e^2 + 2.1213e - 0.1855] \quad (18)$$

Using Equation 18, the range of weighted $\dot{\varsigma}$ functions were plotted in Fig. 40 against cut depth and in Fig. 41 against electrode diameter. From the plot in Fig. 40, the standard deviation of the cuts reduces significantly as the cut depth increases. This is likely due to the difference between the low range of instrumentation and the high range of the instrumentation. At the low range, a small difference due to random error has a larger effect on the result than at the higher range of instrumentation. The plot in Fig. 41 appears to show the standard deviation increases as electrode diameter increases, but it must be noted that the final cut data point is a mean and standard deviation of 9 cuts rather than 3 cuts like the other two points. As previously stated in Section 5.3, the weighted functions combined the resultant functions from both the cut depth and electrode diameter studies. This means the data for all the 0.1 in. cut depth cuts were averaged in the cut depth plot, and the data for all the 0.33 in. electrode diameters were averaged in the electrode diameter plot.

The functions were then compared to see which weighting function combination was closest to the cut data and took the general shape of the cut data for both plots. From an examination of both plots, the prediction model that appears to best fit the cut data points and the overall shape of the cut data for both plots occurs when W_{c1} is 0.4 and W_{c2} is 0.6. This results in the function shown in Equation 19, which provides the preliminary predictive model for $\dot{\varsigma}$. This model is proposed as an initial step in classifying the $\dot{\varsigma}$ for the E-Drill™ electrodes, but further study should be performed to reduce the random error associated with this function. The uncertainty of this function will be analyzed in Section 5.6.

$$\dot{\varsigma} = 0.4[15.37c^2 + 3.6465c - 0.1937] + 0.6[-4.5667e^2 + 2.1213e - 0.1855] \quad (19)$$

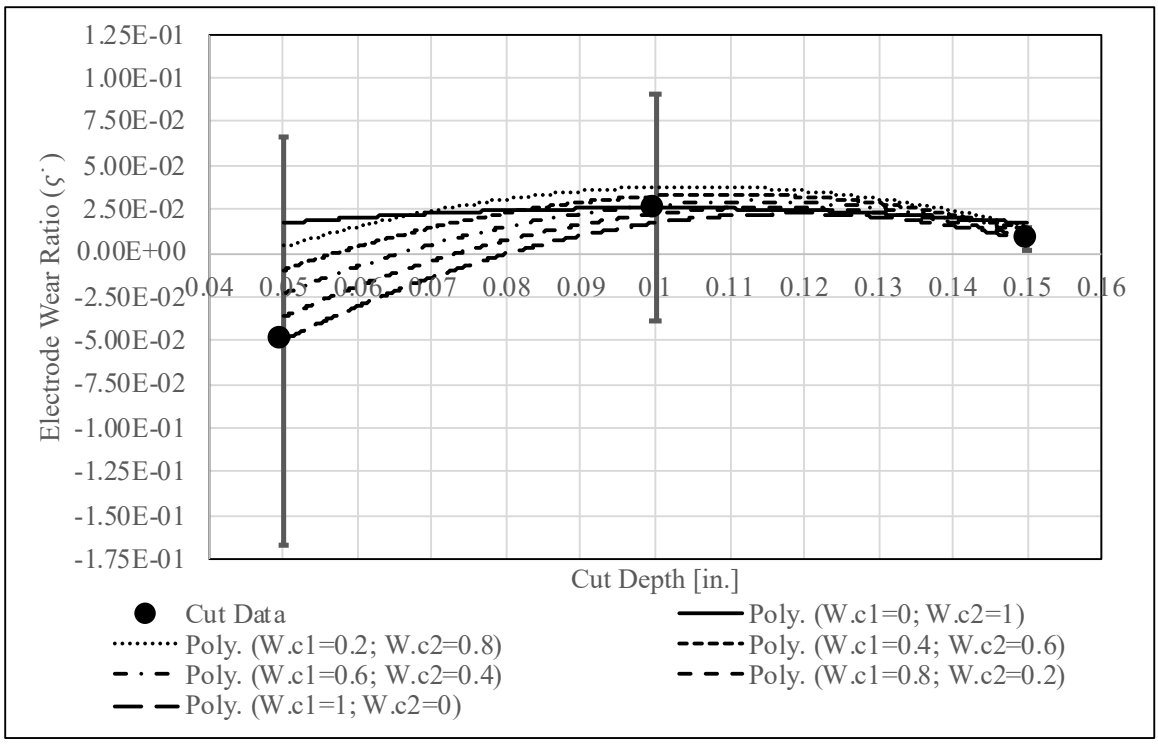

Figure 40: ς̇ Weighted Functions Plotted Over Cut Depth

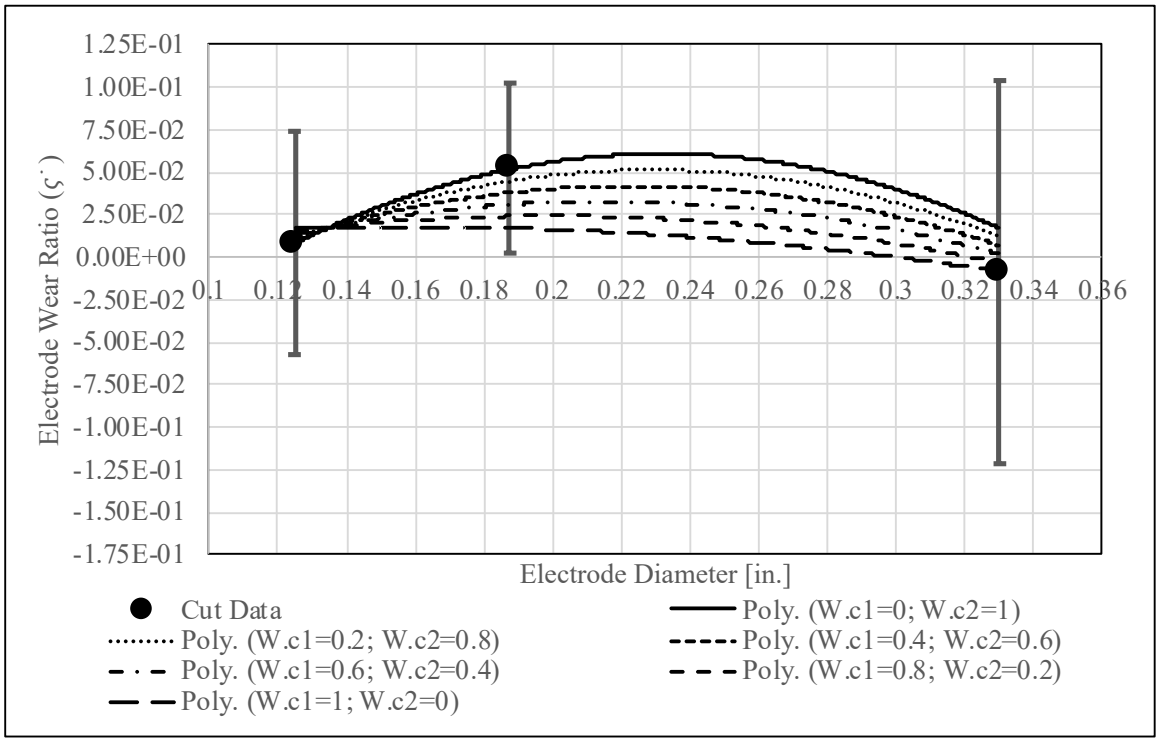

Figure 41: ς̇ Weighted Functions Plotted Over Electrode Diameter

5.5 Axial Electrode Wear (ε_a) Preliminary Predictive Model

Axial electrode wear is the most important parameter in the study, because it provides a direct correlation for electrode life. With ε_a, initial supply chain predictions can be made more accurately. The current E-Drill™ ε_a model does not consider secondary-level influencers such as cut depth and electrode diameter, so this study investigated those effects by developing a preliminary predictive model. This is the most important result from the study because the E-Drill™ electrode life relies on a predictive model of ε_a to determine when the electrode needs to be replaced. Improving that model by considering cut depth and electrode diameter will improve the accuracy of the electrode life prediction model.

Shown in Equation 20 is the base equation for the ε_a preliminary predictive model with c as the cut depth, e as the electrode diameter, and W_{c1} and W_{c2} as the weighting functions. The cut depth and electrode diameter functions were taken from the figures in Section 4.2.

$$\varepsilon_a = W_{c1}[0.3667c^2 - 0.065c + 0.0032] + W_{c2}[0.0128e^2 - 0.0253e + 0.0073] \quad (20)$$

Using Equation 20, the range of weighted ε_a functions were plotted in Fig. 42 against cut depth and in Fig. 43 against electrode diameter. From the plot in Fig. 42, the standard deviation increases and then decreases as the cut depth increases. The large standard deviation for the cut data at 0.1 in. is likely due to that point including the cuts at different electrode diameters. As discussed in the previous section, the cut data points at 0.1 in. in the cut depth plot (Fig. 42) and 0.33 in. in the electrode diameter plot (Fig. 43) are a mean value for 3 tasks (9 cuts) while the other two points on those plots are only mean values for a 1 task (3 cuts). This was done to allow the preliminary models to be functions of both cut depth and electrode diameter. There is; however, a decrease in standard deviation in Fig. 42 between the first cut data point (0.05 in.) and the last cut data point (0.15 in.). The reason for this change is likely due to the instrumentation range being higher at the last point, meaning random errors has smaller effects on the results.

While the standard deviation in Fig. 43 does decrease as the electrode diameter increases, the amount of decrease is small. No clear trend is presented in the standard deviations of Fig. 43. The functions in Figs. 42 and 43 were then compared to see which weighting function combination was closest to the cut data and took the general shape of the cut data for both plots. On both plots, some of the weighted functions appeared to match the general shape of the data, but those functions did not align with the cut data points. To resolve this issue, an offset of 0.001 in. was added to the weighted functions, and new plots were made with the new functions (Figs. 44 and 45). From an examination of both plots, the prediction model that appears to best fit the cut data points and the overall shape of the cut data for both plots occurs when W_{c1} is 0.2 and W_{c2} is 0.8. This results in the function shown in Equation 21, which provides the preliminary predictive model for ε_a. This model is proposed as an initial step in classifying the ε_a for the E-Drill™ electrodes, but further study should be performed to reduce the random error associated with this function. The uncertainty of this function will be analyzed in Section 5.6.

$$\varepsilon_a = 0.2[0.3667c^2 - 0.065c + 0.0032] + 0.8[0.0128e^2 - 0.0253e + 0.0073] + 0.001 \quad (21)$$

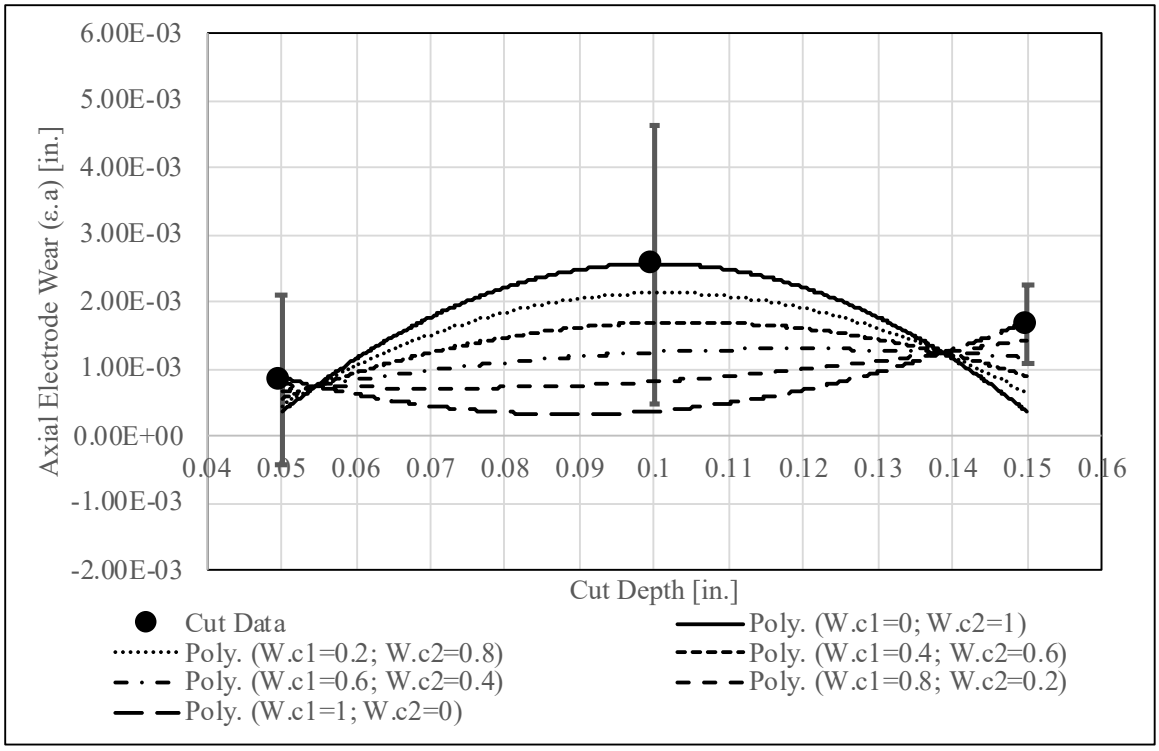

Figure 42: ε_a Weighted Functions Plotted Over Cut Depth

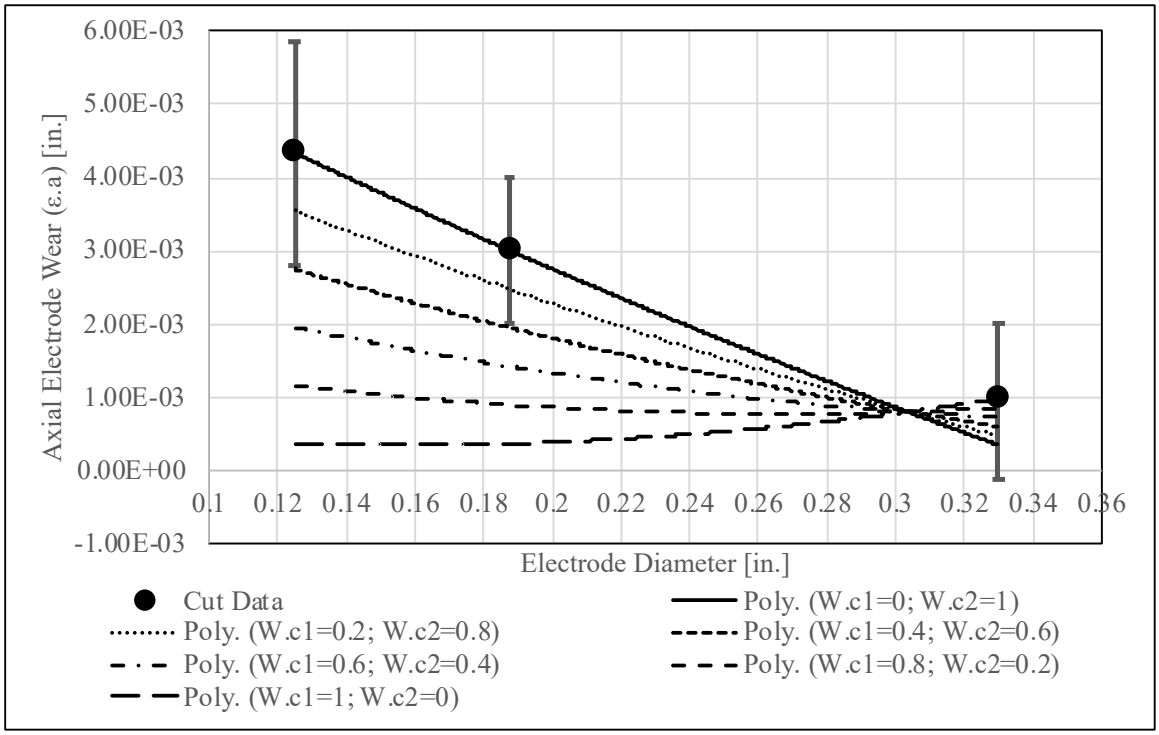

Figure 43: ε_a Weighted Functions Plotted Over Electrode Diameter

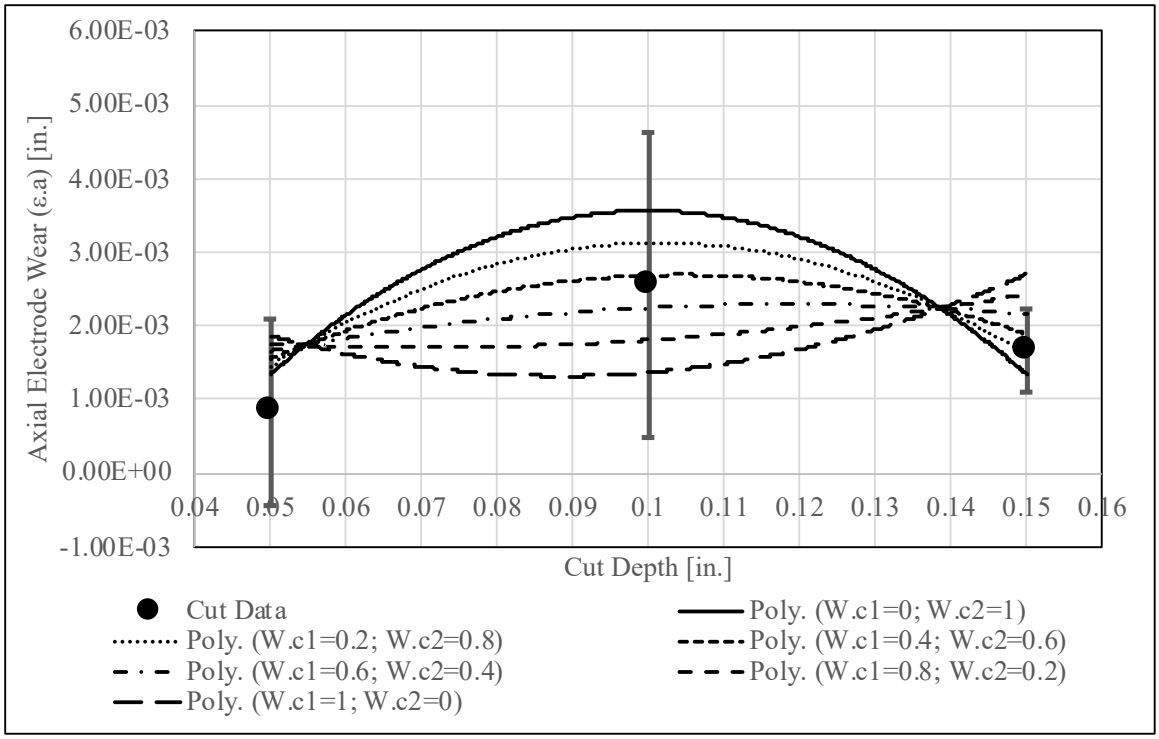

Figure 44: ε_a Weighted Functions Plotted Over Cut Depth with an Offset of 0.001 in.

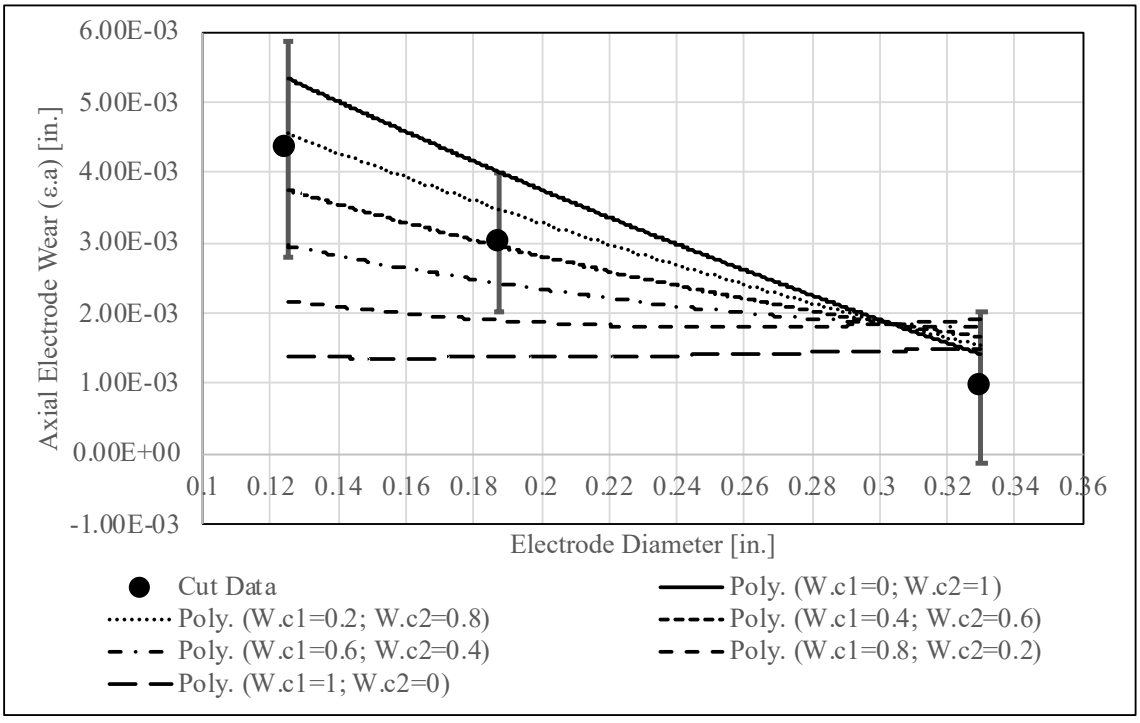

Figure 45: ε_a Weighted Functions Plotted Over Electrode Diameter with an Offset of 0.001 in.

5.6 Geometric Volume Models

Because there was significant variance between the $\dot{\varsigma}$ and ε_a predictive models using weighted functions plotted against cut depth and against electrode diameter, further analysis was performed for the Titanium cuts as an attempt to design an electrode wear prediction model for supply chain management. By examining the geometric volume (V) of the electrode portion that machines into the fastener material, a parameter is developed that combines the cut depth and electrode diameter into a single variable (Eq. 22). This method displays a purely mechanical correlation as it does not account for the electrical properties (e.g. voltage, current, or material thermal conductivity). The correlation is similar to examining the wear on a drill, and the purpose is to compare the volume of material removed from the workpiece due the electrode to the wear of the electrode.

$$V = \pi H_s[\left(\frac{O_a}{2}\right)^2 - \left(\frac{I_a}{2}\right)^2] \tag{22}$$

Plots of $\dot{\varsigma}$ and ε_a over geometric volume are shown in Figs. 46 and 47, respectively. Looking at the $\dot{\varsigma}$ plot, there is a general trend upwards for $\dot{\varsigma}$ as V into the workpiece increases. For the ε_a plot, there is a general trend downwards for ε_a as V into the workpiece increases. Regarding uncertainty, 2nd and 3rd order approximations may have greater values for R^2, but they do not represent the data trend (going up and down between points). The linear approximations do appear to follow the general data trend, but the R^2 values are very low. The cause of this error is likely due to splatter and not accounting for the electrical properties, which were not published at the time of this study. From this uncertainty analysis, it can be determined that models from geometric volume consideration do not adequately represent the wear of an electrode for cuts into Titanium fasteners.

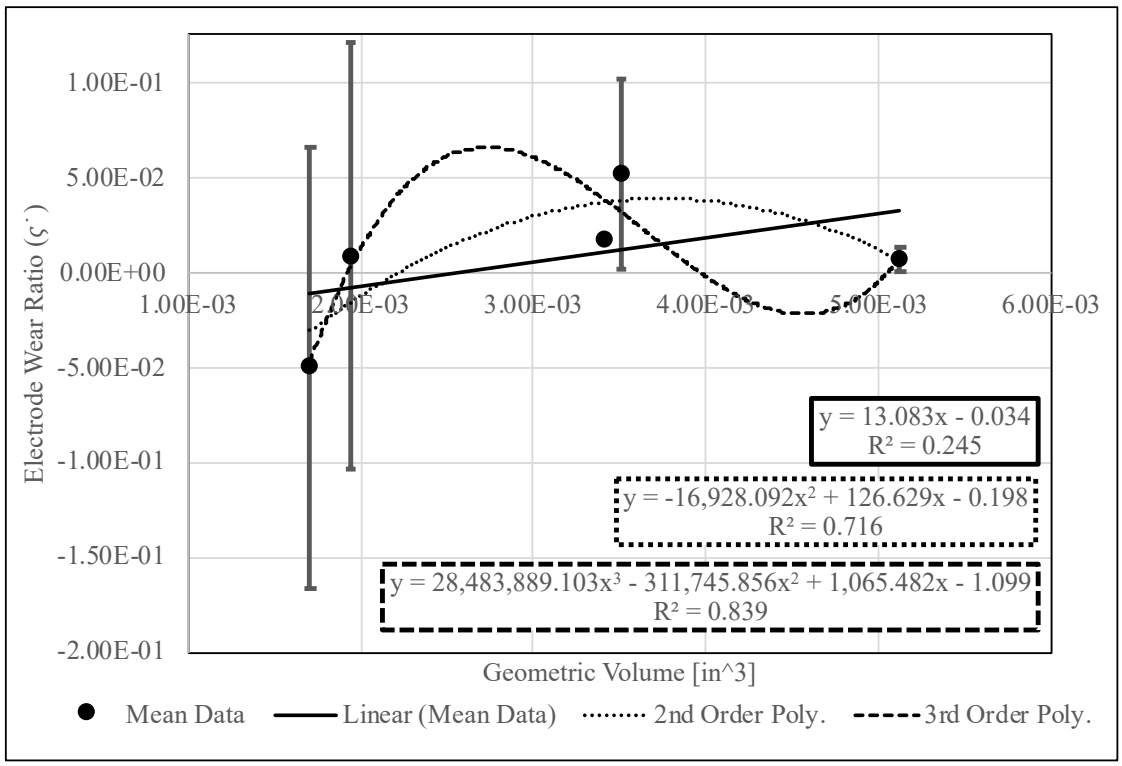

Figure 46: Mean $\dot{\varsigma}$ correlated to geometric volume for Titanium cuts

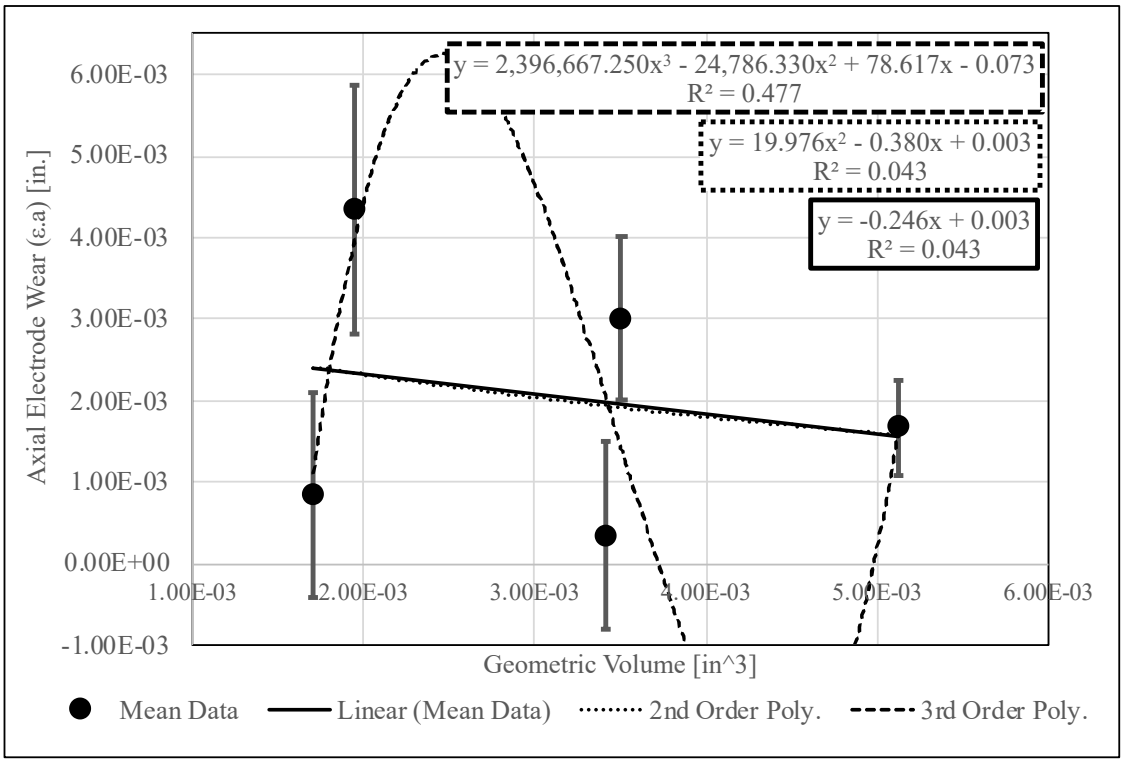

Figure 47: Mean ε_a correlated to geometric volume for Titanium cuts

5.7 Uncertainty Analysis

Although some uncertainty analysis has been previously noted in the analytical study, this section focuses on an uncertainty analysis for the $\dot{\varsigma}$ and ε_a weighted prediction models for the Titanium cuts as well as the $\dot{\varsigma}$ and ε_a linear approximations for the Inconel cuts.

Regarding the $\dot{\varsigma}$ weighted polynomial models for cut depth and electrode diameter, the percent error calculations can be seen in Table 10. The electrode diameter model has less error than the cut depth model, but with a plot average of 19%, this error is still too high to say this is a reliable model for $\dot{\varsigma}$. This error for both the cut depth and electrode diameter weighted models along with the linear and exponential approximations from the Results section show the current data is not capable of modeling $\dot{\varsigma}$ for cuts into Titanium. Figures 48 and 49 show the final weighting function plotted against cut depth and electrode diameter respectively. On those figures, the error bars indicate the standard deviation at the from the mean value. This error agrees with the percent error calculations that the $\dot{\varsigma}$ for Titanium cuts cannot be accurately modeled using this data set.

Table 10: Percent error calculations for $\dot{\varsigma}$ weighted polynomial models

Cut Depth Study	Cut Data Point	0.05 in.	0.1 in.	0.15 in.	Plot Average
	Experimental Value	-4.98E-02	2.57E-02	7.40E-03	N.A.
	Theoretical Value	-9.59E-03	3.25E-02	1.33E-02	N.A.
	Percent Error	420%	21%	44%	162%
Electrode Diameter Study	Cut Data Point	0.125 in.	0.1875 in.	0.33 in.	Plot Average
	Experimental Value	8.31E-03	5.17E-02	-8.41E-03	N.A.
	Theoretical Value	6.98E-03	3.79E-02	1.19E-02	N.A.
	Percent Error	19%	36%	1%	19%

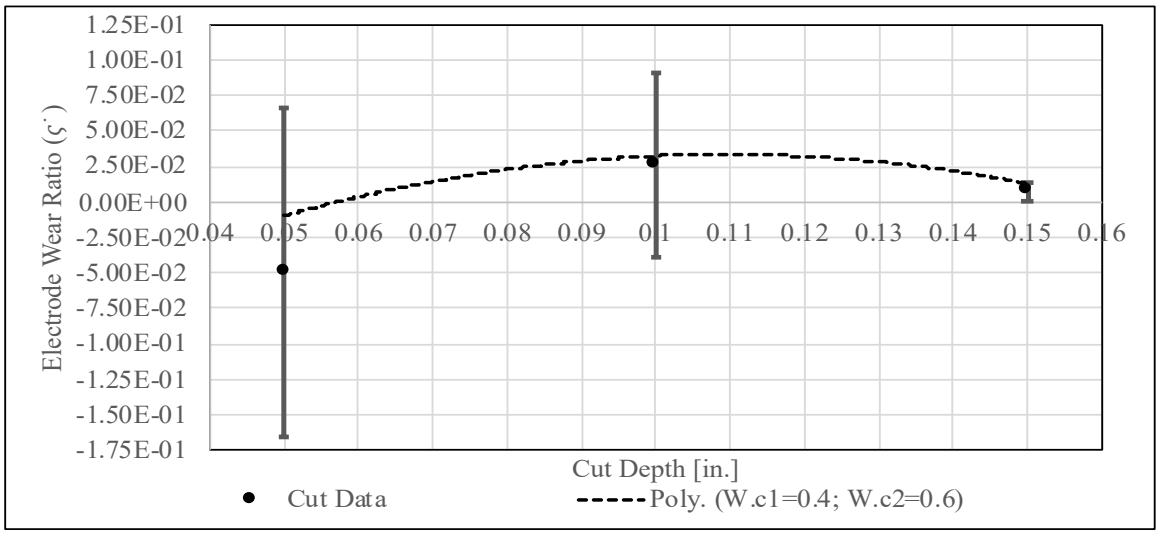

Figure 48: $\dot{\varsigma}$ weighted polynomial model plotted over cut depth with standard deviation bars

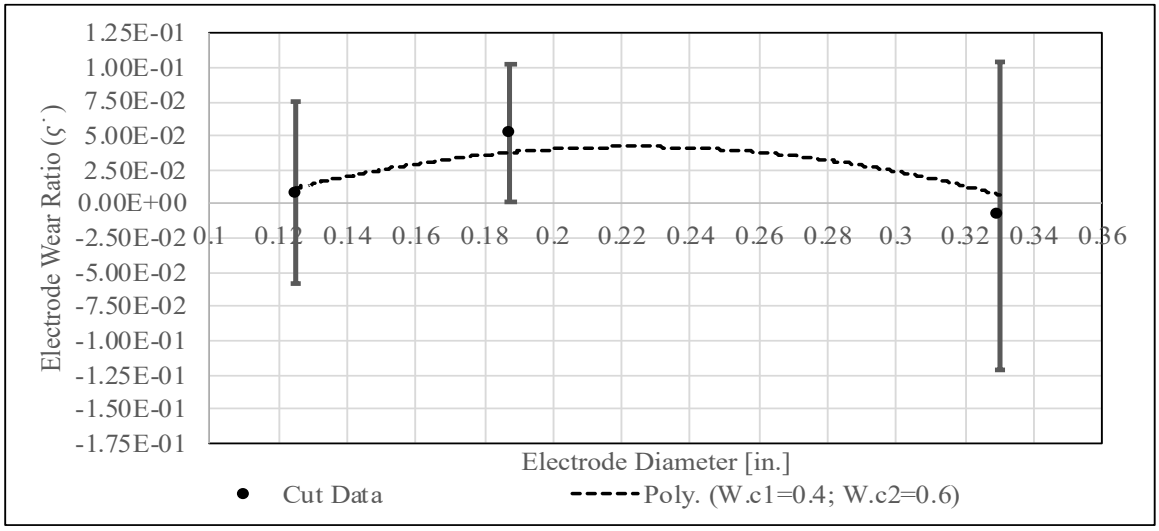

Figure 49: $\dot{\varsigma}$ weighted polynomial model plotted over electrode diameter with standard deviation bars

Regarding the ε_a weighted polynomial models for cut depth and electrode diameter, the percent error calculations can be seen in Table 11. The electrode diameter model again has less error than the cut depth model. At 7% error for the plot average, the electrode diameter model initially shows potential for application, but that is a comparison with the mean value that has high

standard deviation. Figures 50 and 51 show the final weighting function plotted against cut depth and electrode diameter respectively. On those figures, the error bars indicate the standard deviation at the from the mean value. Considering these factors, the error for both the cut depth and electrode diameter weighted models along with the linear and exponential approximations from the Results section show the current data is not capable of modeling ε_a for cuts into Titanium.

Table 11: Percent error calculations for $\varepsilon_a$weighted polynomial models

Cut Depth Study	Cut Data Point	0.05 in.	0.1 in.	0.15 in.	Plot Average
	Experimental Value [in.]	8.33E-04	2.56E-03	1.67E-03	N.A.
	Theoretical Value [in.]	1.45E-03	3.12E-03	1.62E-03	N.A.
	Percent Error	43%	18%	3%	21%
Electrode Diameter Study	Cut Data Point	0.125 in.	0.1875 in.	0.33 in.	Plot Average
	Experimental Value [in.]	4.33E-03	3.00E-03	9.44E-04	N.A.
	Theoretical Value [in.]	4.54E-03	3.48E-03	1.53E-03	N.A.
	Percent Error	5%	14%	1%	7%

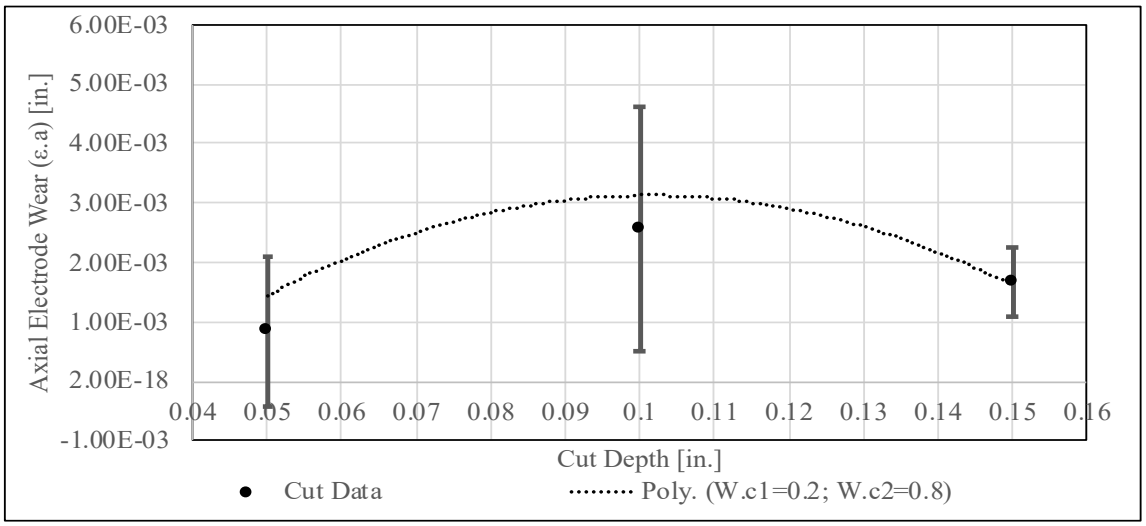

Figure 50: ε_a weighted polynomial model plotted over cut depth with standard deviation bars

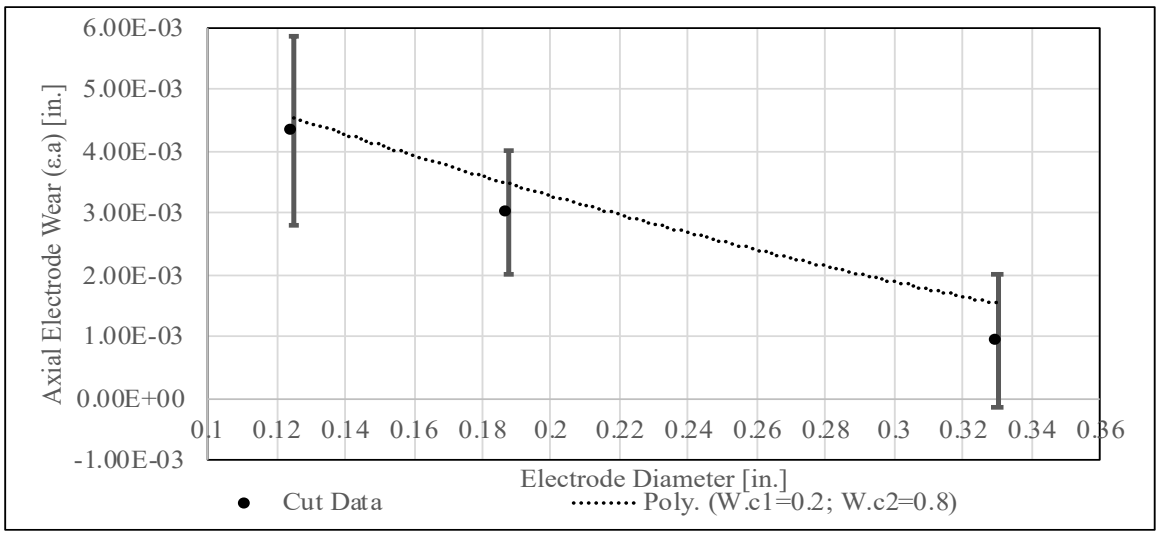

Figure 51: ε_a weighted polynomial model plotted over electrode diameter with standard deviation bars

Regarding the $\dot{\varsigma}$ and ε_a linear approximations for the cuts into Inconel, Figs. 52 and 53 show the mean $\dot{\varsigma}$ and ε_a values plotted against cut depth with standard deviation bars. From Fig. 52, it can be seen there is significant error at 0.05 in. cut depth for $\dot{\varsigma}$. This is due to the ratio being more affected by the balance resolution for smaller mass changes. Looking at the error bars for $\dot{\varsigma}$, the confidence in the linear approximation is low for shallow cut depths but increases as cut depth increases. From Fig. 53, it can be seen there is significant error at 0.15 in. cut depth for ε_a. This is due to increased splatter and variation in cut as the cut depth increases. Looking at the error bars for ε_a, there is confidence in the linear approximation for shallow cut depths, but the confidence decreases as the cut depth increases past 0.1 in.

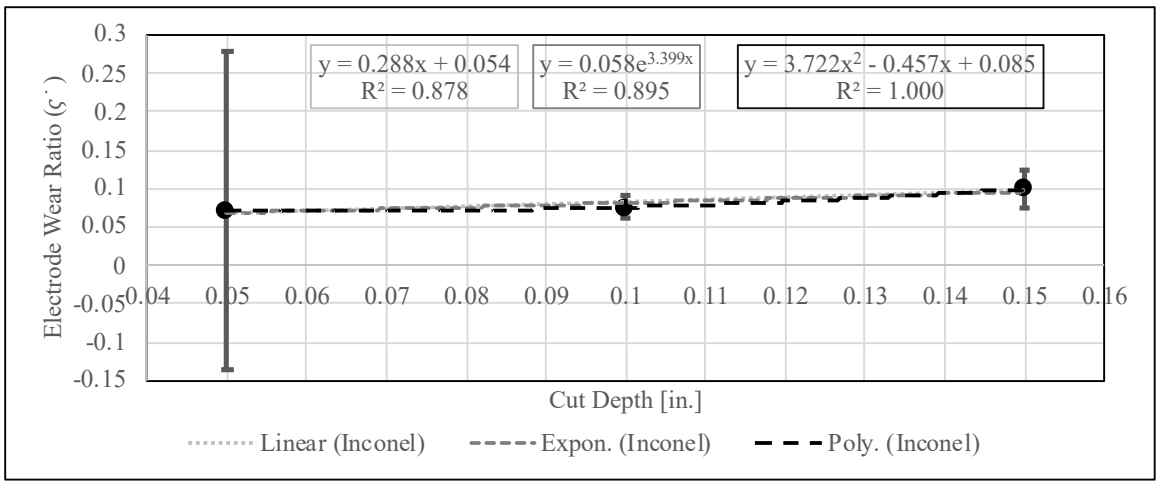

Figure 52: Mean $\dot{\varsigma}$ due to cut depth in Inconel with standard deviation bars

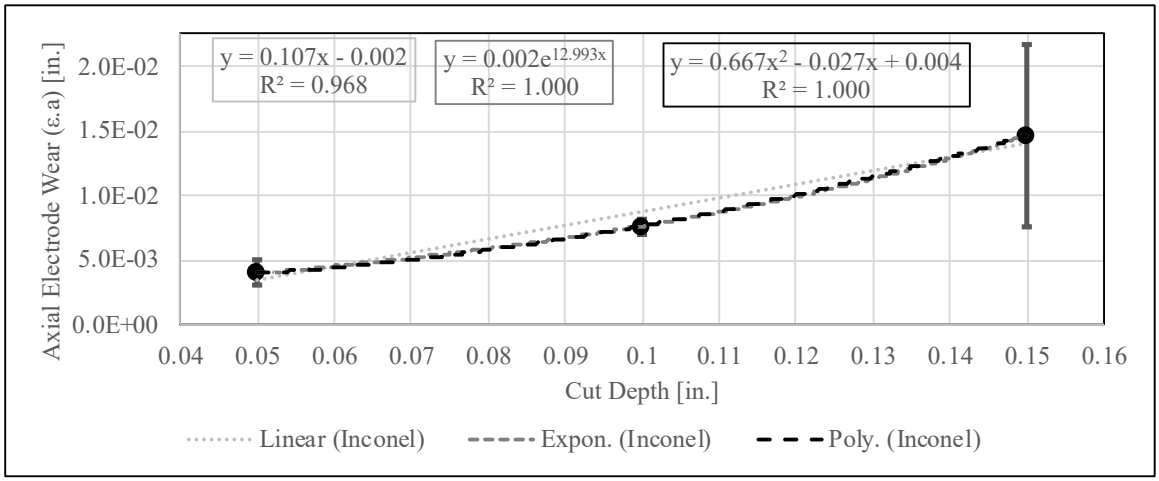

Figure 53: Mean ε_a due to cut depth in Inconel with standard deviation bars

CHAPTER VI

CONCLUSION

This chapter presents a summary of the electrode wear study using the E-Drill™ EDM machine as well as recommendations for future studies.

6.1 Summary

Results from this study show multiple aspects of electrode wear during the EDM process of the PPedm E-Drill™ for aerospace fastener removal. While primary process factors such as current and voltage have been considered in the determination of electrode life prediction models, several secondary-level process factors have not been factored into the models. The secondary-level process factors for the E-Drill™ examined in the study were cut depth, electrode diameter, and fastener material, and the experimental data clearly exhibited the electrode wear was affected by all three process factors. Seven parameters were used to investigate the wear of the electrodes and examine the differences due to the secondary-level process factors. The mean cut time increases a cut depth increases and as electrode diameter increases. Cuts into Titanium had a greater mean cut time than cuts into Inconel. The mean axial electrode wear increases as cut depth increases and as electrode diameter decreases. Cuts into Inconel had greater mean axial electrode wear than cuts into Titanium. The radial electrode wear values were smaller than the accuracy level of the caliper, causing large standard deviations. Because of this, the effects of secondary-level process factors on radial electrode wear was not able to be accurately shown. The mean electrode wear

ratio increases as cut depth increases for cuts into Inconel, but the data was unclear for the Titanium cut trend. Also, the mean electrode wear increased then decreased as electrode diameter was increased. Cuts into Inconel had a greater mean electrode wear ratio than cuts into Titanium. The mean material removal rate increases as cut depth decreases, and as electrode diameter increases, the mean material removal rate decreases and then increases. Cuts into Inconel have a greater material removal rate than cuts into Titanium. The mean cross-section area difference increases as cut depth increases for cuts into Inconel, but the data is unclear for a trend on cuts into Titanium. As the electrode diameter increases, the mean cross-section area difference increases. Results from the tests do not show cuts into either fastener material consistently having a larger cross-section area difference. The mean cut depth difference increases as cut depth increases and as electrode diameter increases. Results from the tests do not show cuts into either fastener material consistently having a larger cut depth difference.

From the study data, an empirical electrode life prediction model was calculated. The results of the model show the estimated number of cuts per electrode for E-Drill^{TM} use with the process factors examined in the study, but the model has significant error due to large deviations in axial electrode wear and minimal data on the minimum usable length of the electrode. After performing an uncertainty analysis for the most important electrode life parameters, axial electrode wear and electrode wear ratio, the linear approximations for cuts into Inconel provide a sufficient model for electrode wear. Because the linear and exponential approximations for cuts into Titanium did not provide a sufficient electrode wear prediction, models were developed for electrode wear ratio and axial electrode wear using the weighted polynomial functions from the cut depth and electrode diameter studies on cuts into Titanium. To combine the cut depth and electrode diameter into a single parameter, the geometric volume was also used to provide another model for electrode wear ratio and axial electrode wear. Analysis of the linear, exponential, weighted polynomial, and geometric volume models of the Titanium cuts show the present data is not sufficient for predicting electrode wear on cuts into Titanium fasteners.

6.2 Future Recommendations

As addressed several times in this study, a valuable future study would begin with more testing for the current process factors. The number of cuts made for this study resulted in large standard deviations for multiple factors. Increasing the number of cuts at the specified parameters would show if the variability was due to only having a small number of data points or inconsistency with the E-Drill™ EDM process. Another method for reducing variability would be the addition of splatter removal techniques before measurement is performed. This would assist in error reduction for the Titanium specimens. Finally, it would be beneficial to examine the impact of material properties such as thermal conductivity, melting point, density, and hardness on electrode wear for the E-Drill™. This would be performed by testing a larger variety of fastener material types.

REFERENCES

[1] “Automatic Fastener Hole Inspection in Aircraft.” Olympus Industrial Resources, URL: https://www.olympus-ims.com/en/applications/automatic-fastener-hole-inspection-in-aircraft/ [Retrieved August 2018].

[2] Abbas, Norliana Mohd, Darius G. Solomon, and Md Fuad Bahari. “A Review on Current Research Trends in Electrical Discharge Machining (EDM).” *International Journal of machine tools and Manufacture* 47, no. 7-8 (2007): 1214-1228.

[3] Mahendran, S., R. Devarajan, T. Nagarajan, and A. Majdi. “A review of micro-EDM.” *Proceedings of the international multi conference of engineers and computer scientists*, vol. 2. 2010.

[4] Gibbons, M. T., “Improved Fastener Removal: Handheld EDM.” *Department of Defense Maintenance Symposium Great Ideas Competition,* 2012.

[5] Becker, J., “Perfect Point Fastener Separation Technology- The 21st Century Solution to Removing ‘Hard-Metal’ Fasteners.” Perfect Point EDM Corp., 2017.

[6] Harrell, L., “Reducing the Cost of Ownership through Technology.” *Tinker and the Primes*, 2018.

[7] K. Ho and S. Newman, “State of the Art Electrical Discharge Machining (EDM),” International Journal of Machine Tools & Manufacture, Vol. 43, pp. 1287-1300, 2003.

[8] Bisaria, H., and P. Shandilya. “Machining of Metal Matrix Composites by EDM and Its Variants: A Review.” *DAAAM International Scientific Book* (2015).

[9] “Conventional or RAM EDM (Die Sinker EDM).” Header Die & Tool, Inc., URL: https://www.header.com/capabilities/conventional-edm [Retrieved August 2018]

[10] N. Abbas, D. Solomon and F. Bahari, “A Review on Current Research Trends in Electrical Discharge Machining (EDM),” International Journal of Machine Tools & Manufacture, Vol. 47, pp. 1214-1228, 2005.

[11] D. DiBitonto, P. Eubank, M. Patel and M. Barrufet, “Theoretical Models of the Electrical Discharge Machining Process. I. A Simple Cathode Erosion Model,” Journal of Applied Physics, Vol. 66, pp. 4095-4103, 1989.

[12] M. Patel, M. Barrufet, P. Eubank, and D. DiBitonto, “Theoretical Models of the Electrical Discharge Machining Process. II. The Anode Erosion Model,” Journal of Applied Physics, Vol. 66, pp. 4104-4111, 1989.

[13] M. Hewidy, T. El-Taweel, and M. El-Safty, “Modelling the Machining Parameters of Wire Electrical Discharge Machining of Inconel 601 Using RSM,” Journal of Materials Processing Technology, Vol. 169, pp. 328-336, 2005.

[14] A. Hasçalik and U. Çaydas, “Electrical Discharge Machining of Titanium Alloy (Ti-6Al-4V),” Journal of Applied Surface Science, Vol. 253, pp. 9007-9016, 2007.

[15] T. Thoe, D. Aspinwall, and N. Killey, “Combined Ultrasonic and Electrical Discharge Machining of Ceramic Coated Nickel Alloy,” Journal of Materials Processing Technology, Vols. 92-93, pp. 323-328, 1999.

[16] C. Wang and B. Yan, “Blind-Hole Drilling of AL2O3/6061Al Composite Using Rotary Electro-Discharge Machining,” Journal of Materials Processing Technology, Vol. 102, pp. 90-102, 2000.

[17] A.A. Khan, “Electrode wear and material removal rate during EDM of aluminum and mild steel using copper and brass electrodes,” The International Journey of Advanced Manufacturing Technology, Vol. 39, pp. 482-487, 2008.

[18] T. Sultan, A. Kumar, R. Dev Gupta, “Material Removal Rate, Electrode Wear Rate, and Surface Roughness Evaluation in Die Sinking EDM with Hollow Tool Through Response Surface Methodology,” International Journal of Manufacturing Engineering, Vol. 2014, Article ID 259129, 2014.

APPENDICES

APPENDIX A: EXPERIMENTAL SETUP

1. Acquire all tools needed for this experiment, according to the supply list provided below, before beginning any setup.

    1.1. Perfect Point EDM E-Drill ™ Mobile Service Unit (MSU) in Richmond Hill 165CA

    1.2. Proper breaker box and outlet, 30A and 240V

    1.3. Work bench

    1.4. Tap water

    1.5. E-Drill ™ Electrode

    1.6. E-Drill ™ Hand-Held Terminal (HHT)

    1.7. E-Drill ™ gun

    1.8. E-Drill ™ locator

    1.9. E-Drill ™ adaptor

    1.10. E-Drill ™ guide

    1.11. E-Drill ™ grounding clamp

    1.12. E-Drill ™ torque-ring wrench

    1.13. E-Drill ™ Plastic Fill/Drain container

    1.14. E-Drill ™ Drain/Fill Tubing

    1.15. Transportation containers for specimens

1.16. Marker for labeling all electrodes and fastener material coupons

1.17. 4-inch vise (attached to work bench) with flat surface for specimens

1.18. Desk lamp

1.19. Paper towels

1.20. Safety glasses for all individuals in room

1.21. Gloves for Operator and Assistant Operator

1.22. Trash can

1.23. Needle-nose pliers

1.24. Small chisel set

1.25. Hammer

1.26. Scale

1.27. Fowler High Precision 52-008 Series Dial Caliper

1.28. OHAUS Model TS4KD Precision Standard Balance

1.29. Computer for inputting data

1.30. AMscope for pictures before and after E-Drill ™ operation

2. A minimum of two people will be needed to complete this experiment.

2.1. An operator to run the machine, position the E-Drill ™ gun, hold the gun during cutting, report the cut time, remove the electrode, report the weight on the scale, and prepare the next cut. This individual will select the settings for the cut and take all necessary pictures. They will also document the cut in a specified laboratory notes document.

2.2. Another person to verify the operator's selection of settings, the positioning of the gun, and the vacuum seal throughout the cutting process. This individual will also use paper towels to wipe away any excess water during and after the operation of the E-Drill ™ and position the light in the optimal position during the removal process. Between cuts, this person will enter the data from the cut (e.g. cut time, electrode weight, etc.) into the data spreadsheet.

2.2.1. One person is required to have a charged cell phone in case of emergencies and is required to call emergency services if necessary.

2.2.2. If instead they are the injured party, then know that it is possible to call emergency services without knowing a phone's unlocking code.

2.3. The operator individual must have current EDM training certificates posted on the wall.

2.4. Any other people present must remain a minimum of five feet from the machine and wear eye protection.

2.4.1. Mark sure all individuals who are not operating the machine recognize and stay behind the marked 5-foot line around the machine and workbench.

3. Prepare E-Drill ™ for operation. (From "Perfect Point E-Drill ™ Quick Start & Maintenance Guide")

3.1. With the E-Drill ™ MSU and HHT installed, and power connected to the Mobile Service Unit (MSU), locate the power switch on the back service panel of the MSU and turn it to the "ON" (up) position.

3.2. If indicated the DI water system tank is empty, follow the procedures below from "Perfect Point Fill System Before Use" document.

3.2.1. Unpack the system and locate the joined clear Drain/Fill Tubing and Plastic Fill/Drain container included with the shipment.

3.2.2. Connect the MSU Power Cord and HHT prior to proceeding.

3.2.3. Insert the ends of the Fill/Drain tube in the VACUUM and PRESSURE Ports in the back of the MSU. Fill the Plastic Container with approximately 2 Gal. of clean tap water. Submerge the opposite end of the tubing in the water. Ensure the end the tubing will remain submerged throughout the following procedures or air will be introduced into the system and bleeding procedures will take longer than necessary.

3.2.4. Power up the system. It will take approximately 30 seconds for the HHT to load the system program. Once the terminal screen is lit and menus appear, proceed to Step v.

3.2.5. Use the HHT to access the system Maintenance screen. Run the “Top Off” procedure to charge the dielectric system. The vacuum pump will start, drawing water into the system until the HHT indicates the tank is full and the pump shuts off automatically.

3.2.6. Next, run “Empty Sediment Tank” routine to purge the system of air, while taking care to hold the end of the fill drain tube submerged in the container. The pressure pump will start, expelling water from the system until the HHT indicates the tank is empty and the pump shuts off automatically. A popup screen will appear on the HHT asking if the Sediment Tank is being cleaned. Select “NO”. Run the “Top Off” procedure once more to fully fill the system. If you have reason to believe that all the air has not been bled from the fluid system, repeat Step vi.

3.2.7. When connecting an E-Drill ™ gun to the system, it is good practice to bleed the E-Drill ™ umbilical before use. Connect the E-Drill ™ Umbilical Cable to the MSU. Be sure the umbilical VACUUM and PRESSURE lines are installed in their proper locations. Turn the MSU Circuit Breaker “ON”. When the HHT has booted up, navigate to the Maintenance screen. Install an Electrode and its matching Adapter in the E-Drill ™, and completely retract the Electrode using the Retract button.

3.2.8. Press the “Empty Sediment Tank” button on the HHT Maintenance screen; the pressure pump will start. Next; using the empty Plastic Fill/Drain container, depress the E-Drill ™ ground pin against the floor of the container. Allow entrapped air and water flow to escape from the E-Drill ™ tip until a steady flow of water is achieved, then stop the pump by pressing the “Empty Sediment Tank” button again.

3.3. The system will power up and after a few seconds the Hand Held Terminal touch screen will illuminate and display the last fastener entry.

3.4. If the screen of the Handheld Terminal is not illuminated, touch the screen to awaken it. Go to bottom right tab on screen and touch the tab for “Select: Visual”.

3.4.1. Under “Type”, scroll down to and select “Hole” option.

3.4.2. Under “Method”, select the “Flush Head” option.

3.4.3. Under “Material”, select the “Titanium” or “Inconel” options.

3.4.4. For “Head ∅”, select the proper electrode diameter value.

3.4.5. Under “Shank ∅”, select the “13/65 (0.203)” option.

3.5. If the cut depth needs to be adjusted in smaller increments than allowed by “Select: Visual”, then the operator needs to open the “Advanced Mode”.

3.5.1. Begin by pressing the top left corner of the screen followed by the top right corner, within 2 seconds.

3.5.2. Enter the password provided to those who have completed the proper training.

3.5.3. Press the tab titled “Advanced” at the bottom middle of the screen.

3.5.4. Tap the box next to “Cut Depth:” and enter the desired cut depth. Press the “Save” tab at the bottom of the screen.

3.6. Install the proper electrode into the E-Drill ™ and the correct adaptor for the fastener type to be removed.

3.7. E-Drill ™ grounding clamp should be attached to the parent material and connected to the wire hanging from the gun.

3.8. Electrode replacement is when the current electrode is consumed and should be replaced when indicated by a flashing green light on the hand-tool and a message on the Hand Held Terminal. The replacement process is provided below.

3.8.1. Unlock the installed Adapter Tip by gripping and twisting it counter-clockwise (when viewed from the front of the e drill). Then pull the Adapter tip straight out.

3.8.2. Unthread the existing Electrode using the Torque-Ring Wrench by inserting it over the Electrode until it engages the Electrode detents. Remove the Electrode by turning it counter-clockwise. It may be necessary to advance the electrode: in which case, with system power on, advance the installed electrode completely forward by depressing gun trigger until the Electrode advances fully. When you have reached the forward limit the LED at the top of the E-Drill ™ will illuminate Red and the E-Drill ™ mechanism will stop automatically. If the electrode wont advance, and the system is indicating that the electrode should be replaced, press the green retract button briefly before attempting to advance the electrode.

3.8.3. Hand-thread the replacement Electrode onto the E-Drill ™. Install the Torque-Ring Wrench by slipping it over the Electrode until it engages the Electrode detents. Tighten the replacement Electrode with the Torque -Ring until it in.breaks in. (or skips) when the required torque is reached. Remove the Torque-Ring and replace the required Adapter Tip over the Electrode.

3.8.4. Retract the Electrode by pressing and holding down the green retract button in the base of the E-Drill ™ grip until the LED in the back of the E-Drill ™ handle illuminates Green indicating the Electrode is fully retracted.

4. Prepare the specimens for operation.

4.1. Measure the height, outer diameter (OD), inner diameter (ID), and weight of the electrode. Then, input all data into the computer.

4.2. Measure the length, width, height, and weight of the fastener material coupon. Then, input the data into the computer.

APPENDICES

APPENDIX B: EXPERIMENTAL PROCEDURE

1. Ensure all participants are wearing PPE per safety instructions before starting any part of the experimental procedures.
2. Record both users and any maintenance procedures performed, including both date and time.
3. Before operating further, consult the checklist to ensure no errors occur during experimentation.
4. Next, place the jig on the specimen and clamp them together in the vise, tightening down to ensure the specimen and jig will not move while drilling.
5. To prepare the E-Drill™ gun, place the corresponding adapter for the locator onto the end of the gun.
6. To start the drilling process, grab the E-Drill™ gun in your dominant hand. The pointer finger should lay along the side of the gun and the middle finger should hold the trigger, with the rest holding the handle.
7. Insert the electrode side of the gun into the locator perpendicular to the parent material.
8. Check to make sure there is a green light on the E-Drill™ showing that it is ready to cut. If the light is not green, refer to the Perfect Point E-Drill™ Quick Start and Maintenance Guide.
9. Place your non-dominant hand on top of the gun and apply light pressure, this is to properly seal the end and to ensure a nice, clean cut.

10. Keeping pressure applied, squeeze the trigger with your middle finger to start drilling. Keep holding the trigger until the machine stops cutting.

11. After the EDM is done drilling, leave the gun pressed down for a few seconds then tilt it at a slight angle to allow excess liquid to be vacuumed into the machine

12. Place the gun into the work bench holster and remove the locator from on top of the parent material.

13. Use paper towels to wipe up any excess liquid from the specimen, making sure to dispose of the paper towels in the trash bin.

14. Next, take detailed pictures of the post cut specimen making sure that the eccentricity of the specimen is visible.

28. Use calipers to record detail measurements of the following in English units:

    28.1. Electrode ID and OD

    28.2. Length of the electrode

    28.4. ID and OD of cut

    28.7. Weight of electrode and of the parent material

29. Make sure that all measurements have been recorded and that the transportation cases are stored properly.

30. Repeat all steps, with a new specimen.

APPENDICES

APPENDIX C: CUT PHOTOGRAPHS

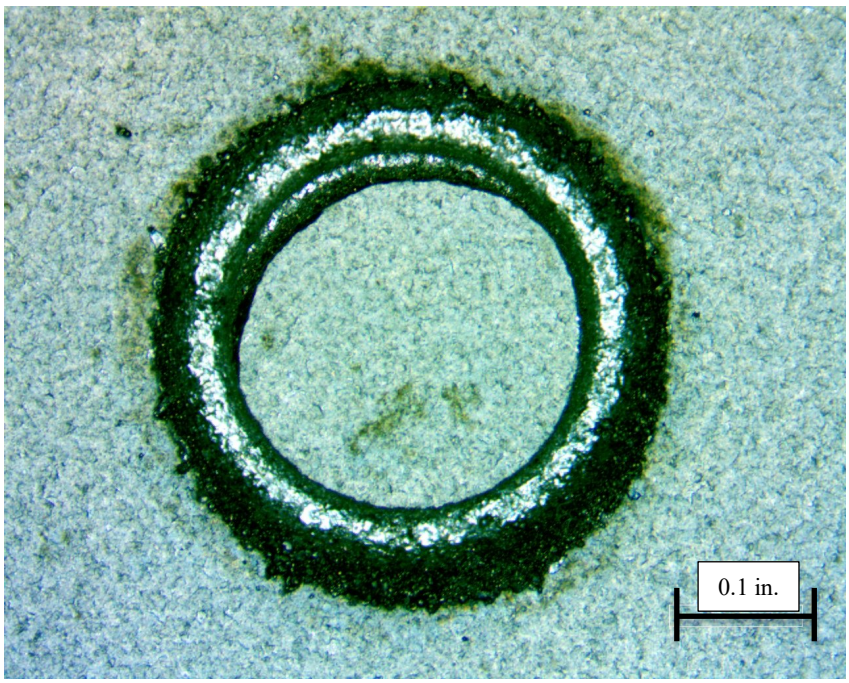

Figure 54: Task 1.1 Cut 1 with a Cut Depth of 0.05 in., an Electrode Diameter of 0.33 in., and a Fastener Material of Inconel

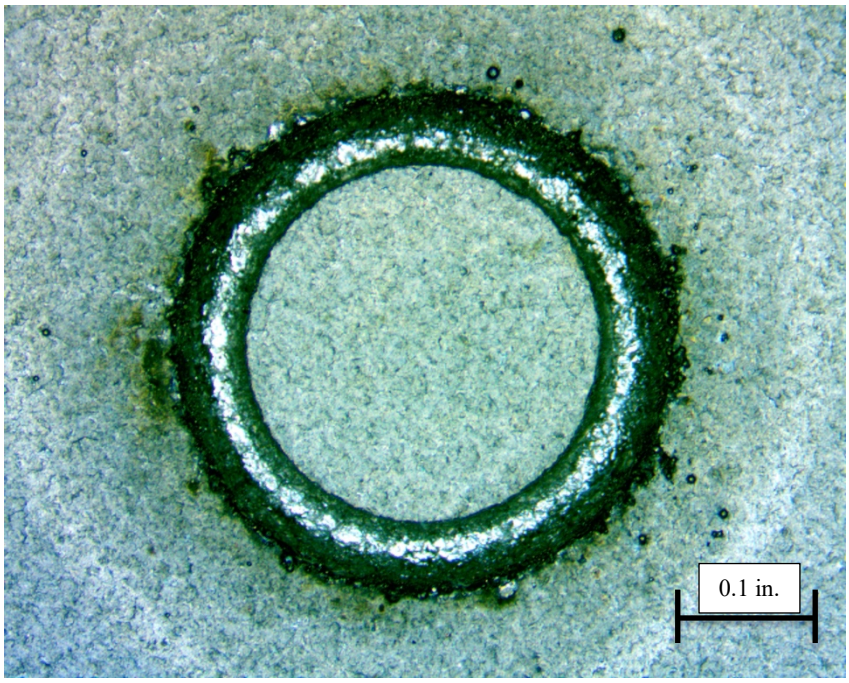

Figure 55: Task 1.1 Cut 2 with a Cut Depth of 0.05 in., an Electrode Diameter of 0.33 in., and a Fastener Material of Inconel

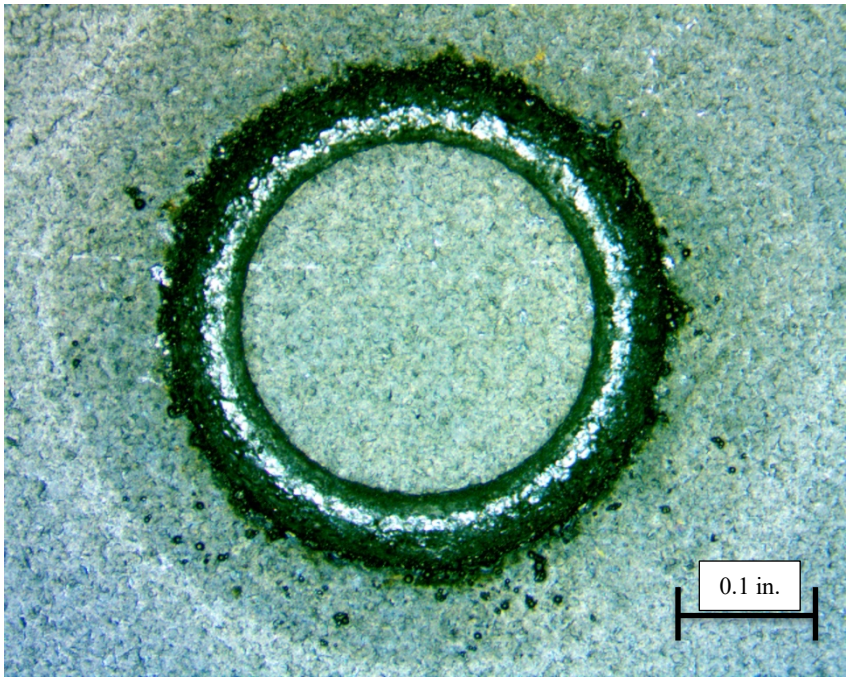

Figure 56: Task 1.1 Cut 3 with a Cut Depth of 0.05 in., an Electrode Diameter of 0.33 in., and a Fastener Material of Inconel

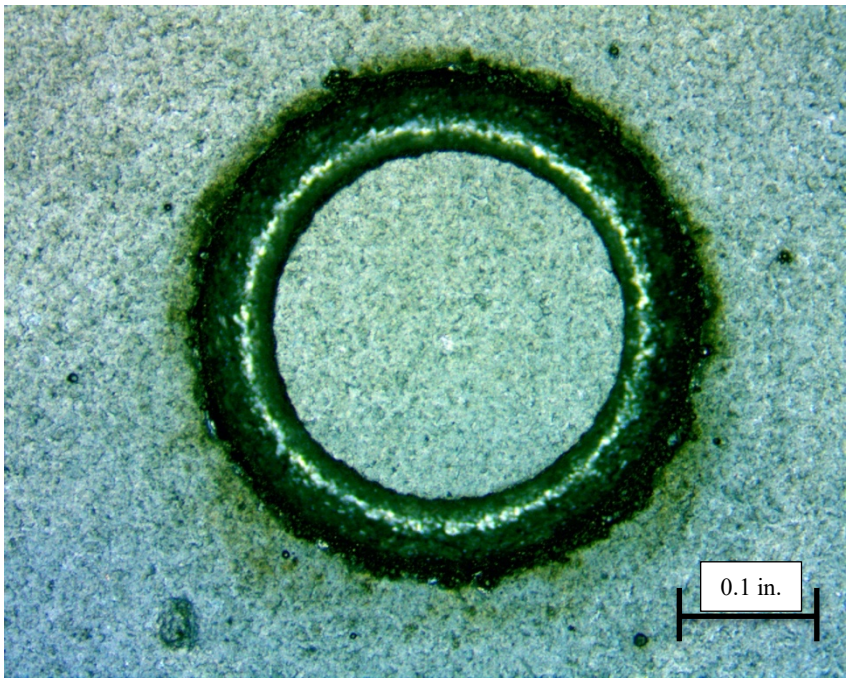

Figure 57: Task 1.2 Cut 1 with a Cut Depth of 0.1 in., an Electrode Diameter of 0.33 in., and a Fastener Material of Inconel

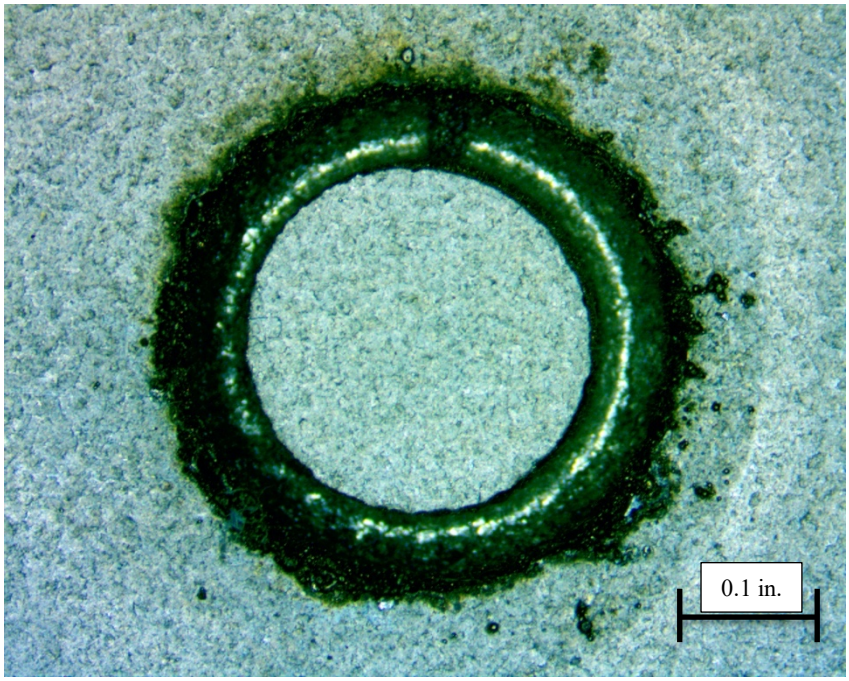

Figure 58: Task 1.2 Cut 2 with a Cut Depth of 0.1 in., an Electrode Diameter of 0.33 in., and a Fastener Material of Inconel

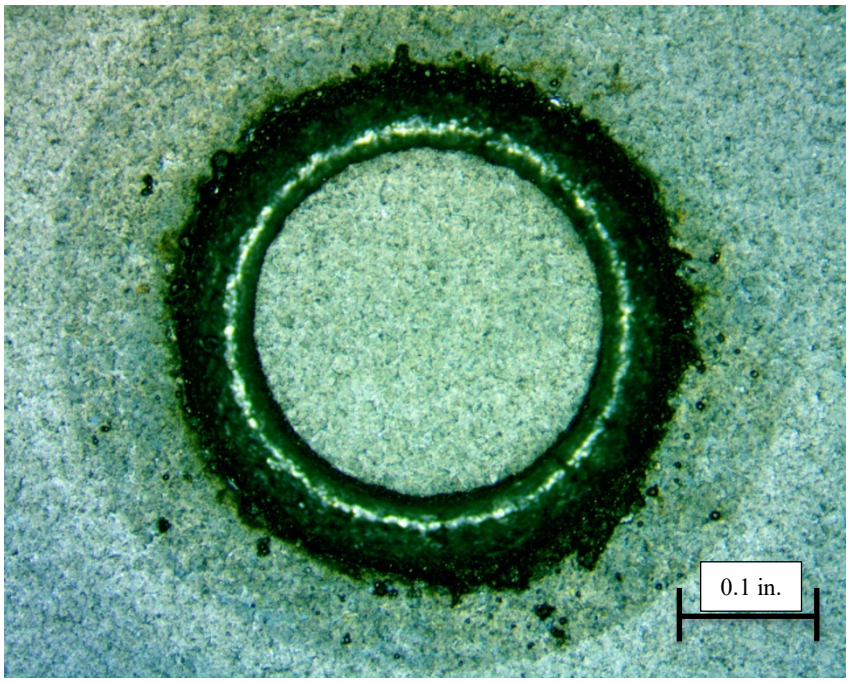

Figure 59: Task 1.2 Cut 3 with a Cut Depth of 0.1 in., an Electrode Diameter of 0.33 in., and a Fastener Material of Inconel

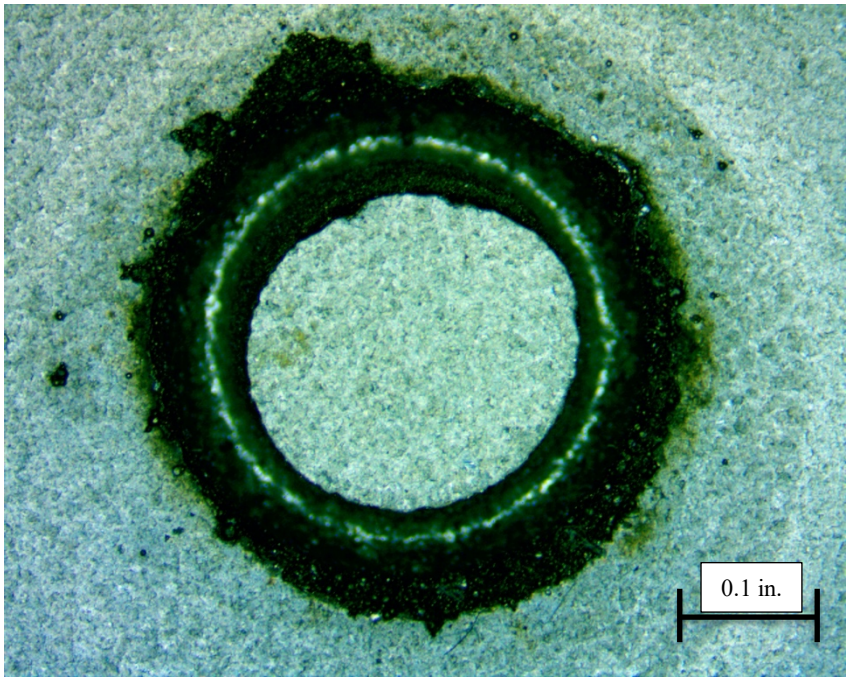

Figure 60: Task 1.3 Cut 1 with a Cut Depth of 0.15 in., an Electrode Diameter of 0.33 in., and a Fastener Material of Inconel

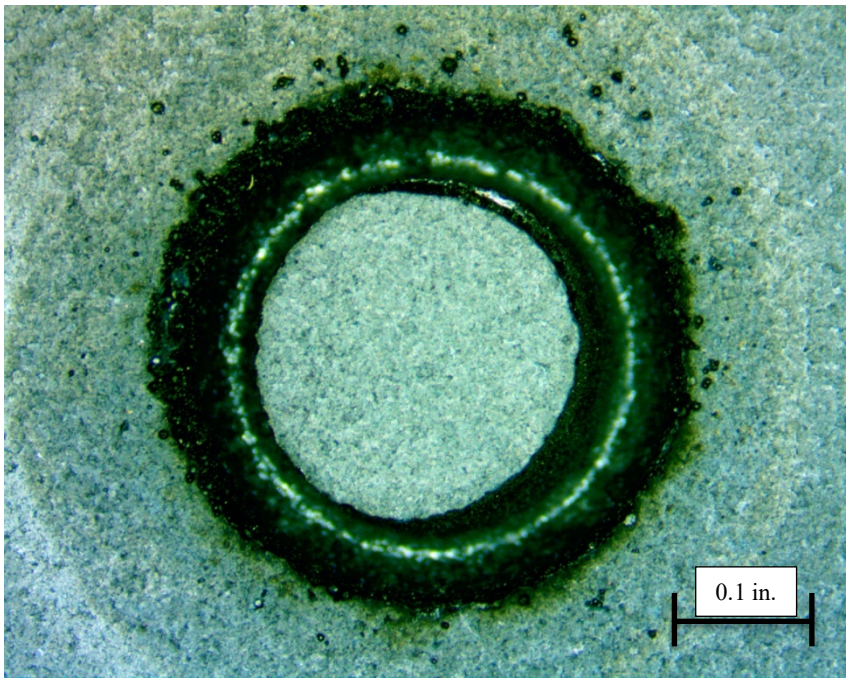

Figure 61: Task 1.3 Cut 2 with a Cut Depth of 0.15 in., an Electrode Diameter of 0.33 in., and a Fastener Material of Inconel

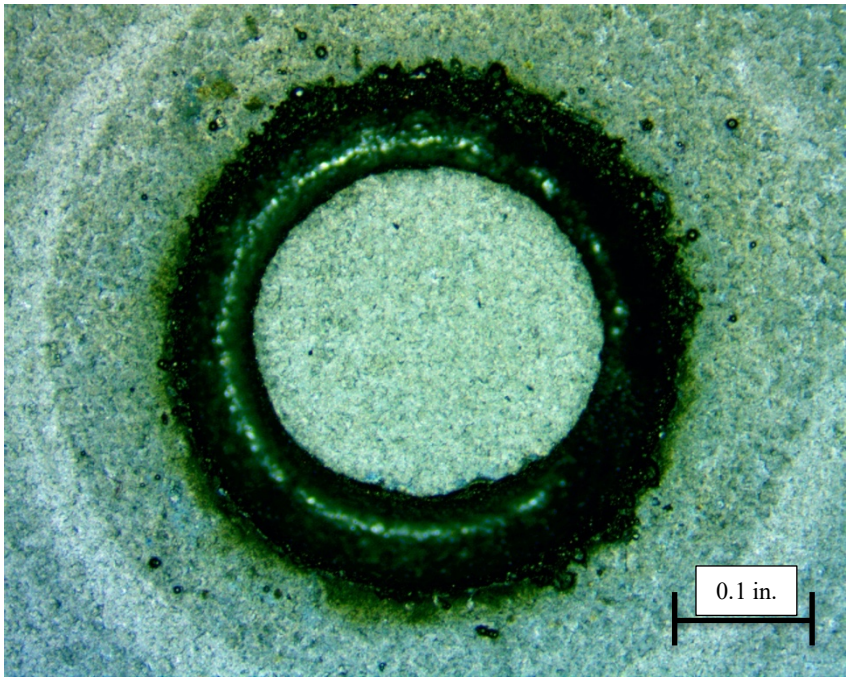

Figure 62: Task 1.3 Cut 3 with a Cut Depth of 0.15 in., an Electrode Diameter of 0.33 in., and a Fastener Material of Inconel

Figure 63: Task 2.1 Cut 1 with a Cut Depth of 0.05 in., an Electrode Diameter of 0.33 in., and a Fastener Material of Titanium

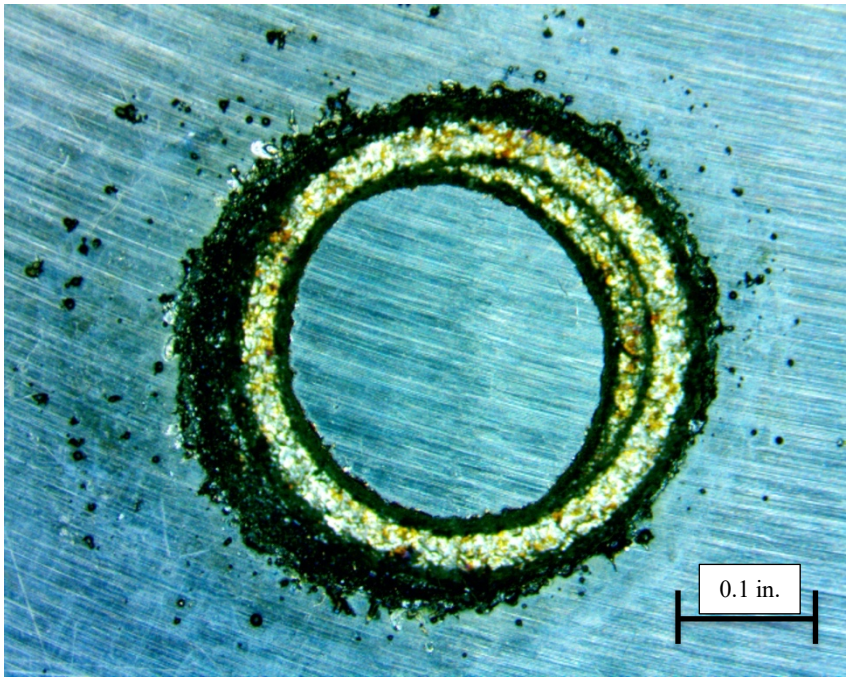

Figure 64: Task 2.1 Cut 2 with a Cut Depth of 0.05 in., an Electrode Diameter of 0.33 in., and a Fastener Material of Titanium

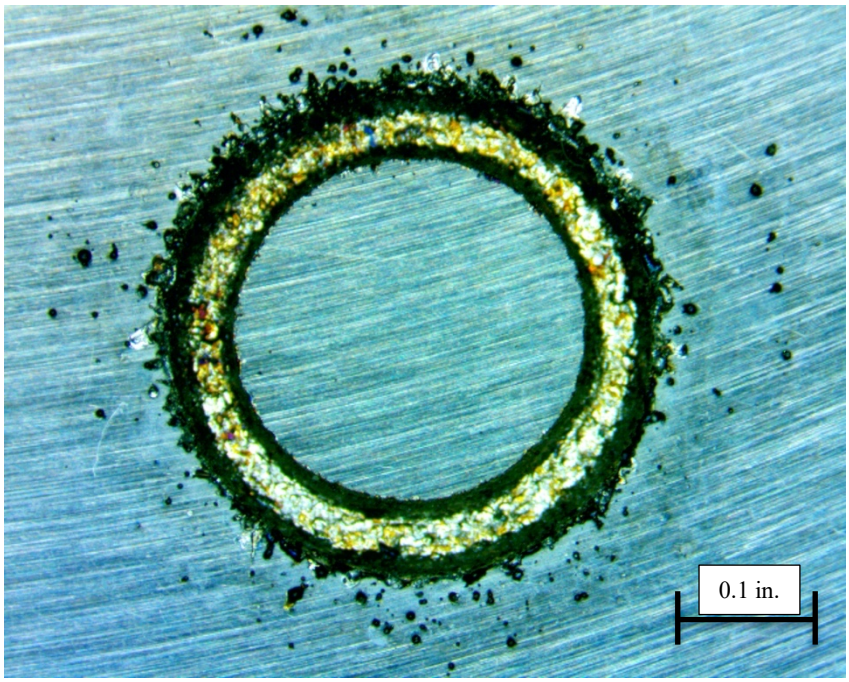

Figure 65: Task 2.1 Cut 3 with a Cut Depth of 0.05 in., an Electrode Diameter of 0.33 in., and a Fastener Material of Titanium

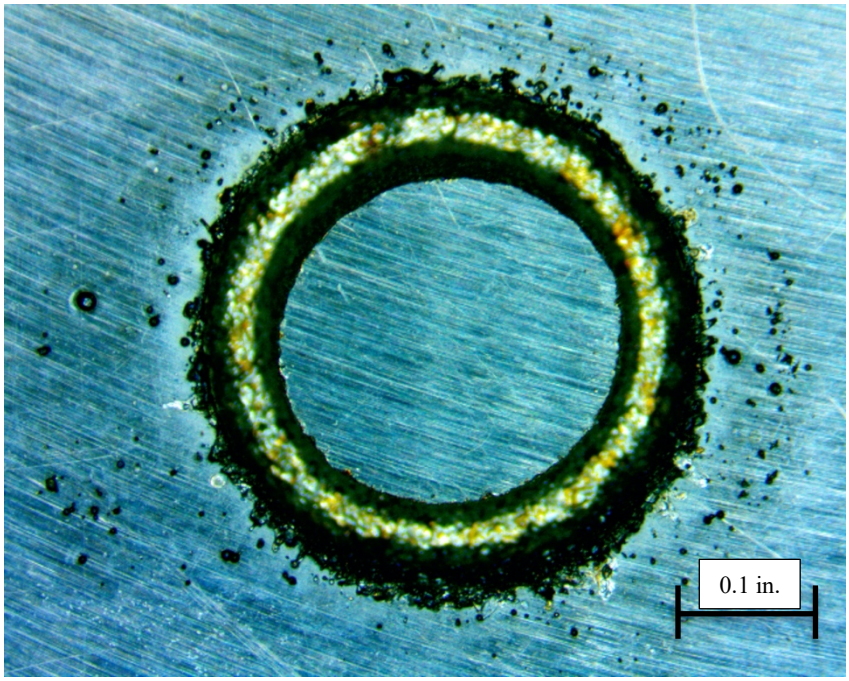

Figure 66: Task 2.2 Cut 1 with a Cut Depth of 0.1 in., an Electrode Diameter of 0.33 in., and a Fastener Material of Titanium

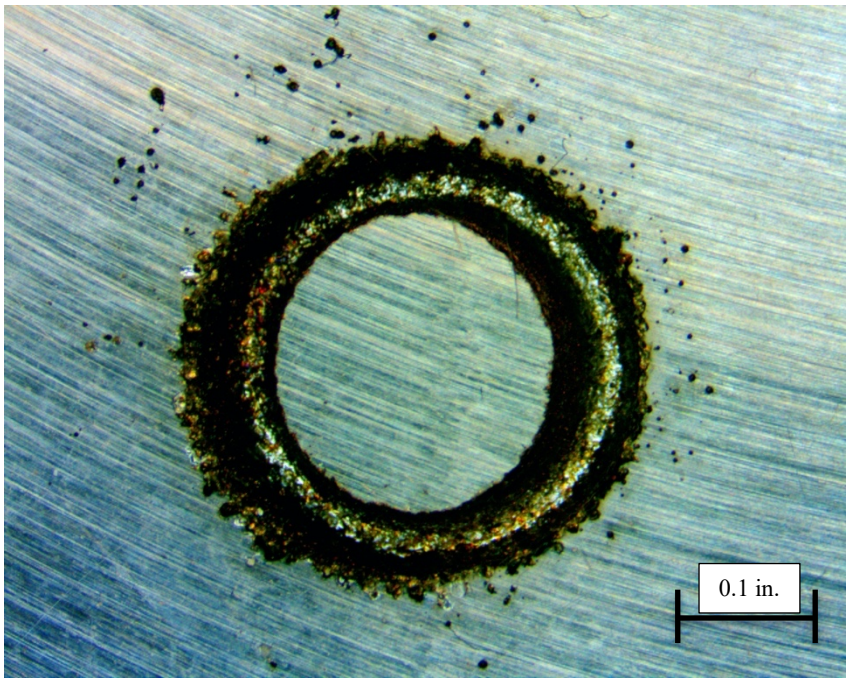

Figure 67: Task 2.2 Cut 2 with a Cut Depth of 0.1 in., an Electrode Diameter of 0.33 in., and a Fastener Material of Titanium

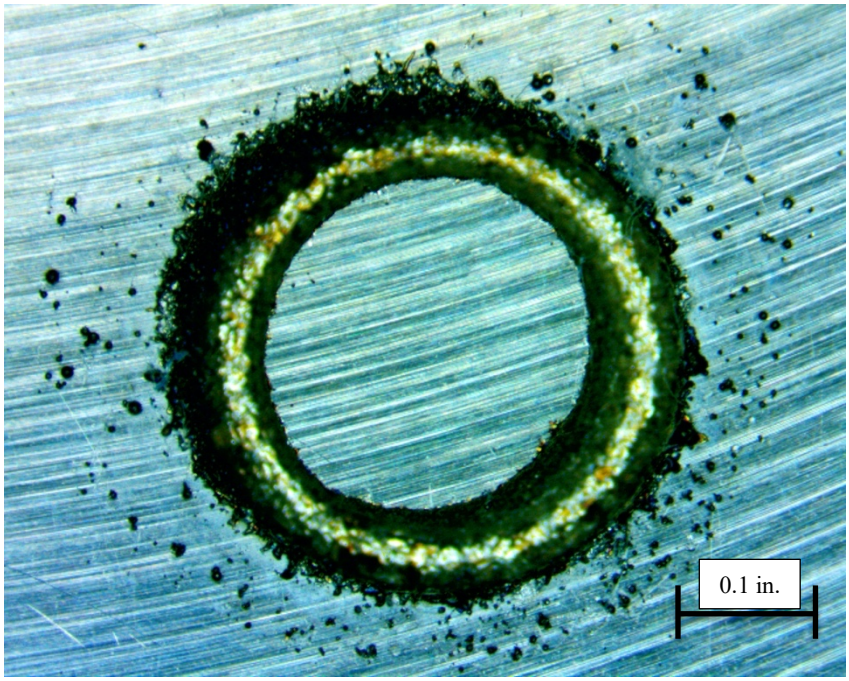

Figure 68: Task 2.2 Cut 3 with a Cut Depth of 0.1 in., an Electrode Diameter of 0.33 in., and a Fastener Material of Titanium

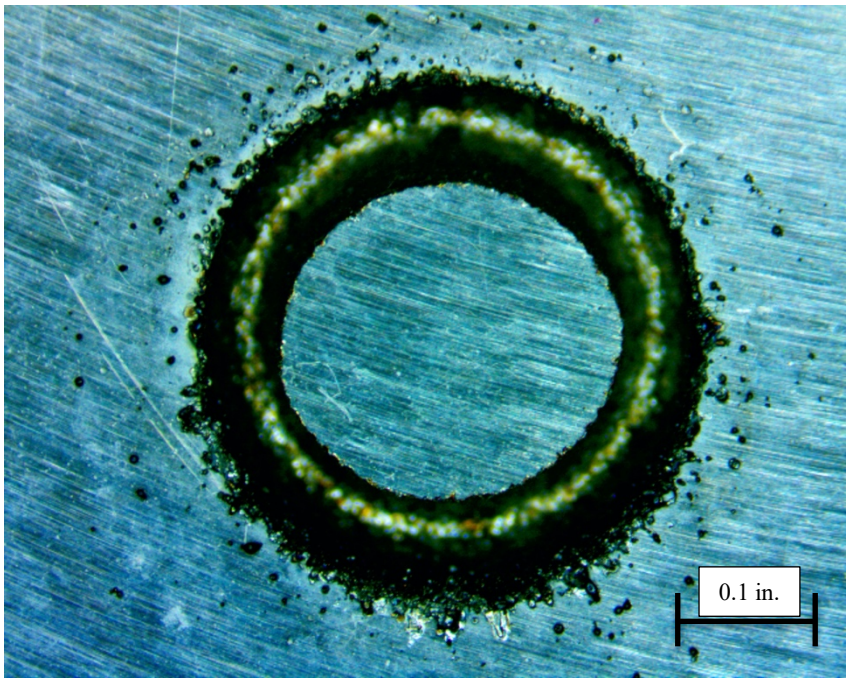

Figure 69: Task 2.3 Cut 1 with a Cut Depth of 0.15 in., an Electrode Diameter of 0.33 in., and a Fastener Material of Titanium

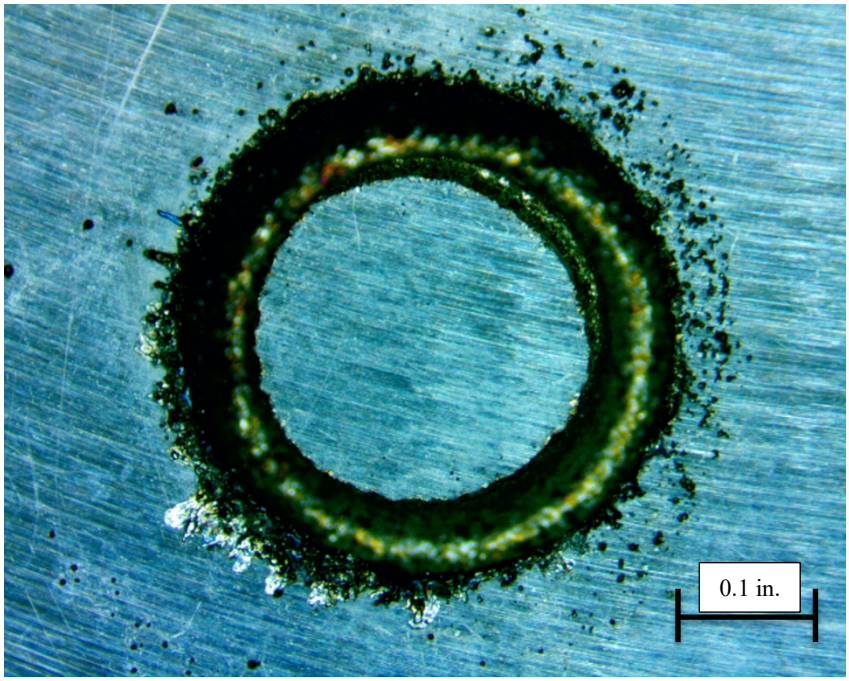

Figure 70: Task 2.3 Cut 2 with a Cut Depth of 0.15 in., an Electrode Diameter of 0.33 in., and a Fastener Material of Titanium

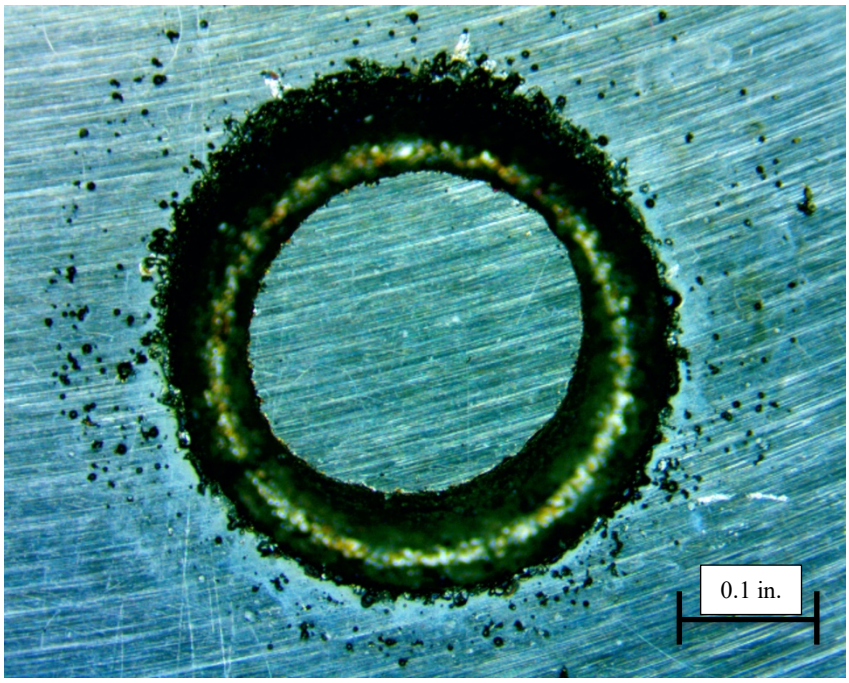

Figure 71: Task 2.3 Cut 3 with a Cut Depth of 0.15 in., an Electrode Diameter of 0.33 in., and a Fastener Material of Titanium

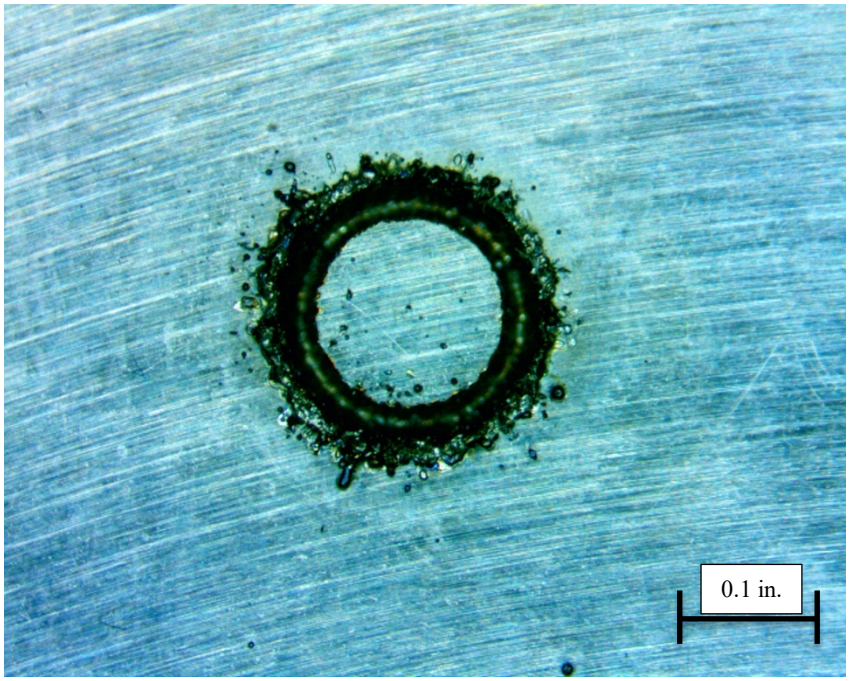

Figure 72: Task 3 Cut 1 with a Cut Depth of 0.1 in., an Electrode Diameter of 0.1875 in., and a Fastener Material of Titanium

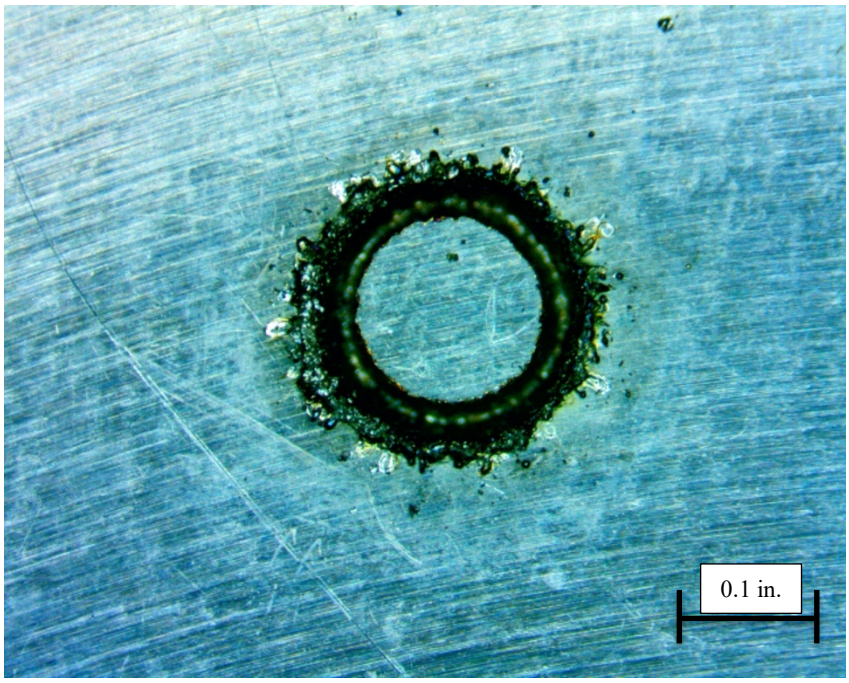

Figure 73: Task 3 Cut 2 with a Cut Depth of 0.1 in., an Electrode Diameter of 0.1875 in., and a Fastener Material of Titanium

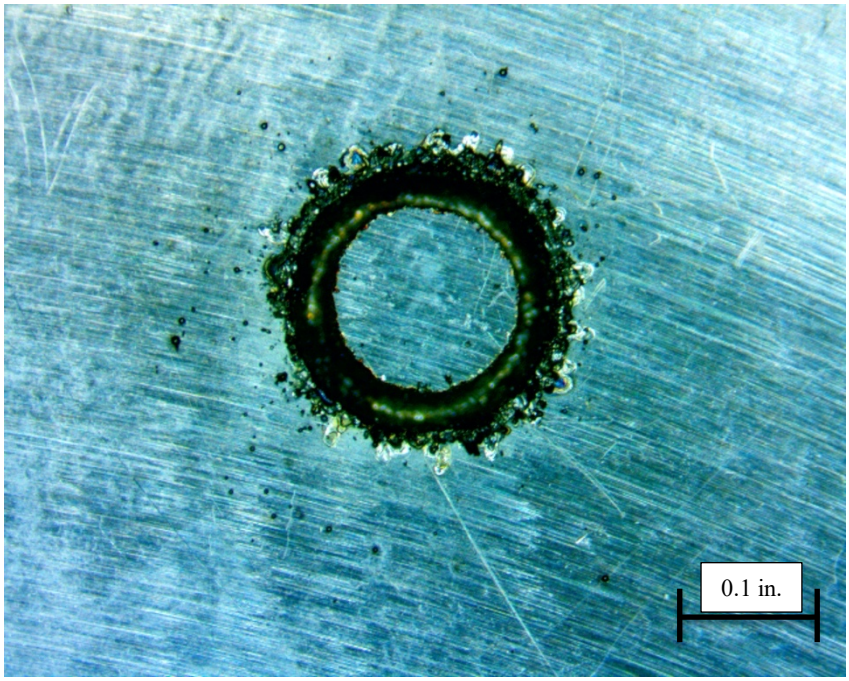

Figure 74: Task 3 Cut 3 with a Cut Depth of 0.1 in., an Electrode Diameter of 0.1875 in., and a Fastener Material of Titanium

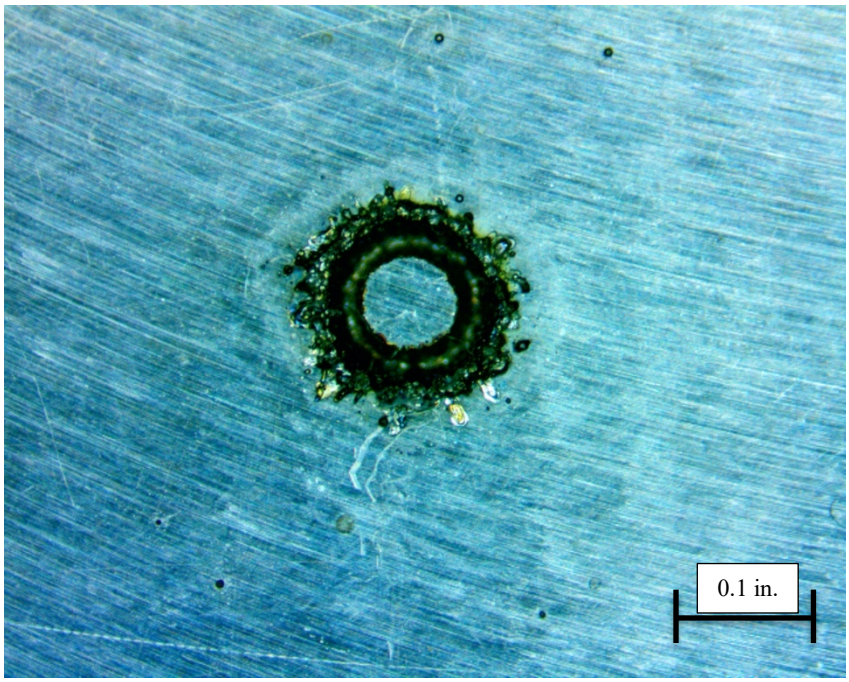

Figure 75: Task 4 Cut 1 with a Cut Depth of 0.1 in., an Electrode Diameter of 0.125 in., and a Fastener Material of Titanium

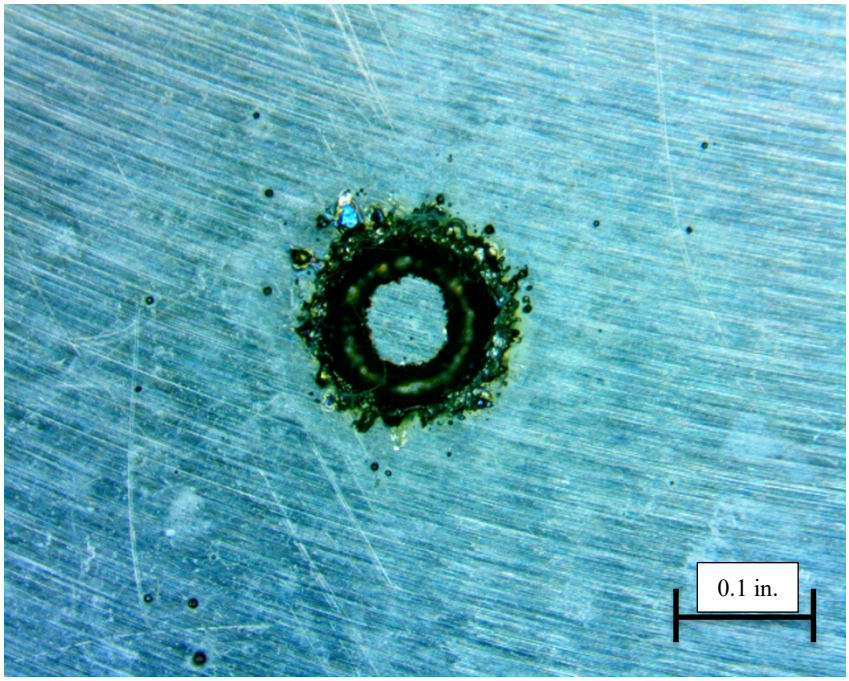

Figure 76: Task 4 Cut 2 with a Cut Depth of 0.1 in., an Electrode Diameter of 0.125 in., and a Fastener Material of Titanium

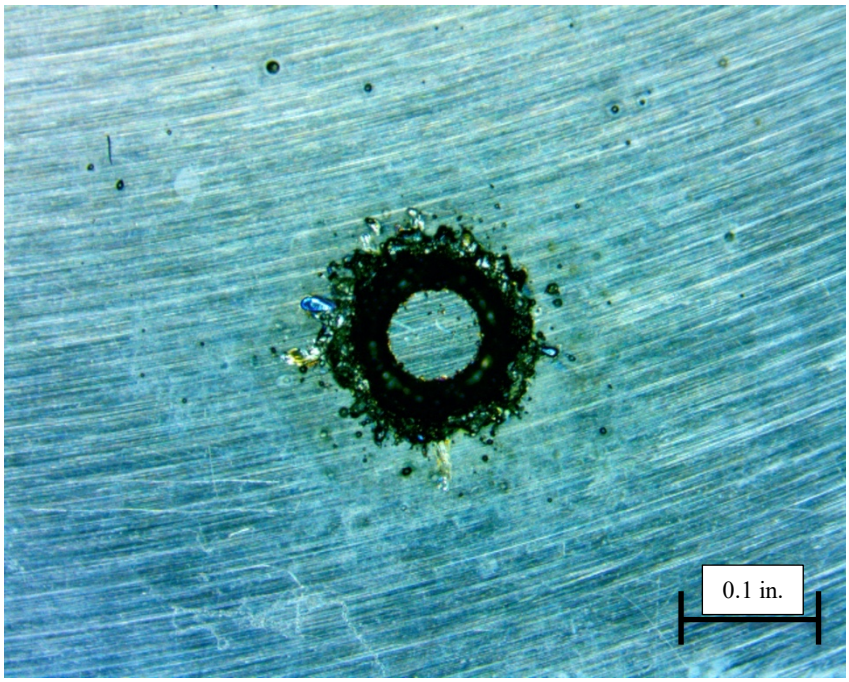

Figure 77: Task 4 Cut 3 with a Cut Depth of 0.1 in., an Electrode Diameter of 0.125 in., and a Fastener Material of Titanium

APPENDICES

APPENDIX D: COMPLETE DATA TABLES

Table 12: Electrode Wear Study

Task	Cut Depth (in.)	Electrode Diameter (in.)	Material	Cut Number
1.1	0.05	0.3300	Inconel (IN718)	T1.11
	0.05	0.3300	Inconel (IN718)	T1.12
	0.05	0.3300	Inconel (IN718)	T1.13
1.2	0.10	0.3300	Inconel (IN718)	T1.21
	0.10	0.3300	Inconel (IN718)	T1.22
	0.10	0.3300	Inconel (IN718)	T1.23
1.3	0.15	0.3300	Inconel (IN718)	T1.31
	0.15	0.3300	Inconel (IN718)	T1.32
	0.15	0.3300	Inconel (IN718)	T1.33
2.1	0.05	0.3300	Titanium (Ti64)	T2.11
	0.05	0.3300	Titanium (Ti64)	T2.12
	0.05	0.3300	Titanium (Ti64)	T2.13
2.2	0.10	0.3300	Titanium (Ti64)	T2.21
	0.10	0.3300	Titanium (Ti64)	T2.22
	0.10	0.3300	Titanium (Ti64)	T2.23
2.3	0.15	0.3300	Titanium (Ti64)	T2.31
	0.15	0.3300	Titanium (Ti64)	T2.32
	0.15	0.3300	Titanium (Ti64)	T2.33
3	0.10	0.1875	Titanium (Ti64)	T3.1
	0.10	0.1875	Titanium (Ti64)	T3.2
	0.10	0.1875	Titanium (Ti64)	T3.3
4	0.10	0.1250	Titanium (Ti64)	T4.1
	0.10	0.1250	Titanium (Ti64)	T4.2
	0.10	0.1250	Titanium (Ti64)	T4.3

Table 13: Electrode Data Before Cut

Task	Electrode Number	Mass Before Cut (g)	Length (in)	O.D. (in)	I.D. (in)
1.1	0.33" Box 1. Number 1	7.17	1.264	0.331	0.26
	0.33" Box 1. Number 1	7.2	1.261	0.331	0.258
	0.33" Box 1. Number 1	7.1	1.257	0.331	0.259
1.2	0.33" Box 1. Number 1	7.1	1.252	0.331	0.258
	0.33" Box 1. Number 1	7.06	1.245	0.331	0.258
	0.33" Box 1. Number 1	7	1.237	0.331	0.258
1.3	0.33" Box 1. Number 1	6.95	1.229	0.331	0.258
	0.33" Box 1. Number 1	6.85	1.213	0.331	0.259
	0.33" Box 1. Number 1	6.78	1.192	0.328	0.257
2.1	0.33" Box 1. Number 1	6.68	1.185	0.33	0.257
	0.33" Box 1. Number 2	7.12	1.257	0.331	0.256
	0.33" Box 1. Number 2	7.1	1.255	0.331	0.258
2.2	0.33" Box 1. Number 2	7.11	1.254	0.331	0.256
	0.33" Box 1. Number 2	7.1	1.255	0.331	0.257
	0.33" Box 1. Number 2	7.09	1.254	0.331	0.255
2.3	0.33" Box 1. Number 2	7.08	1.253	0.331	0.257
	0.33" Box 1. Number 2	7.08	1.251	0.331	0.258
	0.33" Box 1. Number 2	7.07	1.249	0.331	0.256
3	0.1875" Box 1, Number 1	3.86	1.261	0.173	0.141
	0.1875" Box 1, Number 1	3.85	1.258	0.174	0.138
	0.1875" Box 1, Number 1	3.84	1.256	0.175	0.14
4	0.125" Box, Number 1	3.64	1.266	0.104	0.07
	0.125" Box, Number 1	3.65	1.26	0.104	0.069
	0.125" Box, Number 1	3.65	1.256	0.106	0.069

Table 14: Electrode Data After Cut

Task	Electrode Number	Mass After Cut (g)	Length (in)	O.D. (in)	I.D. (in)
1.1	0.33" Box 1. Number 1	7.2	1.261	0.331	0.258
	0.33" Box 1. Number 1	7.1	1.257	0.331	0.259
	0.33" Box 1. Number 1	7.1	1.252	0.331	0.258
1.2	0.33" Box 1. Number 1	7.06	1.245	0.331	0.258
	0.33" Box 1. Number 1	7	1.237	0.331	0.258
	0.33" Box 1. Number 1	6.95	1.229	0.331	0.258
1.3	0.33" Box 1. Number 1	6.85	1.213	0.331	0.259
	0.33" Box 1. Number 1	6.78	1.192	0.328	0.257
	0.33" Box 1. Number 1	6.68	1.185	0.33	0.257
2.1	0.33" Box 1. Number 1	6.69	1.1855	0.331	0.258
	0.33" Box 1. Number 2	7.1	1.255	0.331	0.258
	0.33" Box 1. Number 2	7.11	1.254	0.331	0.256
2.2	0.33" Box 1. Number 2	7.1	1.255	0.331	0.257
	0.33" Box 1. Number 2	7.09	1.254	0.331	0.255
	0.33" Box 1. Number 2	7.08	1.253	0.331	0.257
2.3	0.33" Box 1. Number 2	7.08	1.251	0.331	0.258
	0.33" Box 1. Number 2	7.07	1.249	0.331	0.256
	0.33" Box 1. Number 2	7.06	1.248	0.331	0.258
3	0.1875" Box 1, Number 1	3.85	1.258	0.174	0.138
	0.1875" Box 1, Number 1	3.84	1.256	0.175	0.14
	0.1875" Box 1, Number 1	3.84	1.252	0.174	0.138
4	0.125" Box, Number 1	3.65	1.26	0.104	0.069
	0.125" Box, Number 1	3.65	1.256	0.106	0.069
	0.125" Box, Number 1	3.64	1.253	0.104	0.069

Table 15: Fastener Material Data

Task	Hole Depth (in)	Mass Before Cut (g)	Mass After Cut (g)	Hole O.D. (in)	Hole I.D. (in)
1.1	0.048	473.3	473	0.341	0.254
	0.041	473	472.7	0.343	0.251
	0.042	472.7	472.4	0.339	0.252
1.2	0.088	471.3	470.7	0.345	0.248
	0.091	470.7	470.1	0.344	0.251
	0.083	470.1	469.5	0.345	0.25
1.3	0.124	472	471.2	0.348	0.237
	0.113	471.2	470.3	0.343	0.245
	0.108	470.3	469.5	0.3525	0.241
2.1	0.02	226.28	226.25	0.326	0.2585
	0.035	226.25	226.1	0.361	0.254
	0.032	226.1	226	0.34	0.252
2.2	0.085	229.53	229.24	0.355	0.25
	0.083	229.24	228.94	0.346	0.25
	0.084	228.94	228.66	0.355	0.248
2.3	0.137	225.24	224.95	0.35	0.248
	0.117	224.95	224.48	0.345	0.248
	0.125	224.48	224.05	0.344	0.251
3	0.093	231.43	231.34	0.188	0.128
	0.091	231.34	231.29	0.185	0.133
	0.093	231.29	231.2	0.187	0.1245
4	0.115	229.36	229.31	0.117	0.066
	0.122	229.31	229.3	0.115	0.055
	0.108	229.3	229.26	0.122	0.065

Table 16: Post Cut Procedure Data

Task	Cut Time (s)	Picture Taken
1.1	9.8	x
	8.9	x
	8.3	x
1.2	22.2	x
	21	x
	20.3	x
1.3	38.7	x
	32.5	x
	34.3	x
2.1	9.4	x
	10.3	x
	8.5	x
2.2	27.7	x
	27.8	x
	29.3	x
2.3	48.5	x
	58.2	x
	38.3	x
3	5.8	x
	6.3	x
	6.5	x
4	6.2	x
	5.2	x
	4.2	x

VITA

Connor Aaron McCain

Candidate for the Degree of

Master of Science

Thesis: ELECTRODE EROSION OF AN ELECTRICAL DISCHARGE MACHINING DRILL FOR AEROSPACE FASTENER REMOVAL

Major Field: Mechanical and Aerospace Engineering

Biographical:

Education:

Completed the requirements for the Master of Science in Mechanical and Aerospace Engineering at Oklahoma State University, Stillwater, Oklahoma in May, 2020.

Completed the requirements for the Bachelor of Science in Engineering at Oral Roberts University, Tulsa, Oklahoma in 2018.

Experience:

Graduate Research Assistant – Oklahoma State University, Stillwater, OK
Graduate Teaching Assistant – Oklahoma State University, Stillwater, OK
Honors Research Assistant – Oral Roberts University, Tulsa, OK

Professional Memberships:

AIAA (American Institute of Aeronautics and Astronautics)
ASME (American Society of Mechanical Engineers)
ΣΓΤ (American Honor Society in Aerospace Engineering)